EROSION STUDIES ON NITRONIC STEELS FOR UNDERWATER PART APPLICATIONS

Ph.D. THESIS

by

ASHISH WAMANRAO SELOKAR

DEPARTMENT OF METALLURGICAL AND MATERIALS ENGINEERING
INDIAN INSTITUTE OF TECHNOLOGY ROORKEE
ROORKEE – 247667, INDIA
DECEMBER, 2014

EROSION STUDIES ON NITRONIC STEELS FOR UNDERWATER PART APPLICATIONS

A THESIS

Submitted in partial fulfilment of the
requirements for the award of the degree
of
DOCTOR OF PHILOSOPHY
in
METALLURGICAL AND MATERIALS ENGINEERING

by

ASHISH WAMANRAO SELOKAR

DEPARTMENT OF METALLURGICAL AND MATERIALS ENGINEERING
INDIAN INSTITUTE OF TECHNOLOGY ROORKEE
ROORKEE – 247667, INDIA
DECEMBER, 2014

INDIAN INSTITUTE OF TECHNOLOGY ROORKEE
ROORKEE

CANDIDATE’S DECLARATION

I hereby certify that the work which is being presented in the thesis, entitled **“Erosion Studies on Nitronic Steels for Underwater Part Applications”** in partial fulfilment of the requirements for the award of the degree of Doctor of Philosophy and submitted in the Department of Metallurgical and Materials Engineering, Indian Institute of Technology Roorkee, Roorkee is an authentic record of my own work carried out during the period from January, 2010 to December, 2014 under the supervision of **Dr. Ujjwal Prakash**, Associate Professor and **Dr. D. B. Goel**, Former Professor, Department of Metallurgical and Materials Engineering, Indian Institute of Technology Roorkee, Roorkee.

The matter presented in this thesis has not been submitted by me for the award of any other degree of this or any other institute.

(**ASHISH WAMANRAO SELOKAR**)

This is to certify that the above statement made by the candidate is correct to the best of our knowledge.

(Ujjwal Prakash) Supervisor	(D. B. Goel) Supervisor

The Ph. D. Viva-Voce Examination of Mr. Ashish Wamanrao Selokar Research Scholar, has been held on ....

Chairman, SRC **Signature of External Examiner**

This is to certify that the student has made all the corrections in the thesis.

Signature of Supervisor (s) **Head of the Department**
Dated:………………

Abstract

Energy is the primary requirement of economic development. Every sector needs input of energy. Power generation is mostly dependent on the nonrenewable fossils energy sources, these sources are fast depleting. The natural renewable power generation sectors like solar, wind and hydro sources needs to be developed for sustainable energy production. India is blessed with huge amount of hydroelectric potential. In the hydroelectric power plants, 13wt%Cr-4wt%Ni (all compositions in wt %) martensitic stainless steel (termed as 13/4 steel) is widely used as turbine blade material. Hydroelectric turbine blades are exposed to erosion by cavitation and by silt laden water. These environments lead to damage and failure of components resulting in decrease of turbine efficiency. It is difficult to sustain the long duration performance because of several repairs and maintenance related problems associated with 13/4 steel as the steel is difficult to weld. There is need to develop appropriate materials, which increase the efficiency and the life of hydroturbine underwater parts. The worn out/broken component of hydroturbine cannot be replaced so easily. Repair welding is the only solution to reduce the burden of replacing whole components.

Nitrogen containing steels exhibit excellent weldability and have promising wear resistance. In this research work attempts are made to develop an erosion resistant nitrogen alloyed austenitic stainless steels also called nitronic steels which have potential to replace the 13/4 steel. So far no investigation has been studied erosion behaviour comparative study of 23Cr-8Ni-N (23/8N) and 21Cr-12Ni-N (21/12N) steels. Nitrogen stabilizes the austenitic phase at room temperature. It enhances the strain hardening ability which results improved mechanical deformation. In the present work the weldability of 23/8N steel is studied and compared with suitable grade of austenitic stainless steel (309L). The solid particle erosion behavior as well as cavitation erosion of weld coating applied on the surface of 23/8N steel is also studied.

The nitrogen containing steels were received from M/S star Wire (India) Ltd. Ballabhgarh, Haryana, India in form of bar with 100x100 mm cross section. The heat treatment of 23/8N and 21/12N steels was carried out at various temperatures (1000^{o}C, 1050^{o}C, 1100^{o}C and 1150^{o}C) for 3 hrs followed by water quenching. 23/8N steel samples quenched from 1100^{o}C were aged at 700^{o}C for 20 hrs. Weld joining and weld overlay of 23/8N steel by 309L austenitic stainless steel has also been studied. For comparison 13/4 steel was also investigated. The microstructure of 13/4 steel consists of fine martensitic laths also exhibited with δ- ferrite. The microstructure of 23/8N and 21/12N steels made up of austenitic matrix with chromium carbides along the grain boundaries. High C and Cr in 23/8N (~ 6-9 %) steel compare to 21/12N (~ 2-4 %) steel possesses higher volume fraction of carbides. Different solution annealing heat treatment temperatures are used to dissolve most of the carbides in the austenitic matrix. Reprecipitation of carbides is observed in the microstructure after the aging heat treatment. 23/8N and 21/12N steels possess higher values of tensile toughness, ductility, strain hardening exponent and impact energy than 13/4 steel. The solution annealing heat treatment of 23/8N steel enhanced yield strength, ultimate tensile strength, ductility and the tensile toughness while decreased on aging heat treatment.

Cumulative weight loss (CWL) and mean depth of erosion (MDE) of as received, heat treated and weld coated steels were determined by means of cavitation using ultrasonic processor. A piezoelectric ultrasonic transducer was used to produce oscillations at a frequency of 20±0.5 kHz and peak to peak amplitude 50 µm in distilled water for the duration of 24 hrs. Water temperature was maintained in the range of 25±2 ^{o}C. Solid particle erosion test was performed using Air jet erosion tester. The abrasive alumina (Al_2O_3) particle of size 53-75 µm with velocity 32m/s and feed rate 3±0.3g/min has been employed. The tests were performed at various 30^{o}, 45^{o}, 60^{o} and 90^{o} impact angles at room temperature. The respective volume loss was calculated after every 3 min of testing. The ratio of volume loss to the weight of eroded particles (i.e. particle feed rate x testing time) causing the loss was then calculated as erosion rate in mm^3/g. The erosion test was repeated with each subsequent test of 3 min duration until a steady state in erosion rate was obtained. Scanning electron microscope was used to study the mechanism of erosion. The best results regarding the repair techniques applied to the cavitation affected areas of runner blades were obtained by overlay welding of work hardening austenitic steels. Weld coatings and joining was performed using filler metal austenitic AWS E309 stainless steel (SS 309L). Dye penetration and X-ray radiography tests were conducted to determine the weld defect. For the filler metal, the values for current and voltage during welding were 80A and 27.5V respectively. The result shows that weld coating by 309L steel provides good weldability as well as good erosion resistance.

The entire research work has been presented in six chapters in proposed thesis. **Chapter 1** presents a critical review of the available literature on nitrogen alloyed austenitic stainless steel, cavitation and solid particle erosion, erosion resistance materials and erosive wear of welded surface coating. **Chapter 2** consists of formulation of problem, objectives of present work based on literature review and planning of experimental works. **Chapter 3** deals with the experimental procedures employed for present work. Details of ultrasonic processor used for cavitation erosion, air jet erosion test rig has been described. Various heat treatments given to steels are described in details in this study. The techniques employed in the mechanical testing and metallographic study and instruments, machines used for welding are described in details. **Chapter 4** deals with characterization of microstructural and mechanical properties as well as the cavitation and solid particle erosion behaviour of 13/4, 23/8N and 21/12N steels have been analyzed as a function of microstructure, mechanical properties and alloying elements. Generally in power plant gray cast iron (GCI) and bronze were used as turbine materials for available impulse and reaction turbines. So, for cavitation erosion the grey cast iron (used in underwater parts as a pivot ring in the Mohhmadpur power plant, Uttarakhand, INDIA) is studied for the comparison purpose. **Chapter 5** is described the effect of heat treatment on cavitation and solid particle erosion behaviour of 23/8N and 21/12N. **Chapter 6** is deals with the weldability of 23/8N in terms of microstructural and mechanical properties. Also the erosion behaviour of the weld surface coating applied by 309L austenitic stainless steel has been studied**. Chapter 7** described the future directions in which these studies can be extended have been suggested at the end.

Acknowledgement

Every success which is a result of hard efforts never tastes that good if each and every one who participated in it is not acknowledged. First and foremost, I would like to express my gratitude and acknowledgement to almighty God who has given me enthusiasm and passion toward research work. My sincere thanks go to Dr. Ujjwal Prakash and Dr. D. B. Goel, Department of Metallurgical and Materials Engineering, Indian Institute of Technology Roorkee, my thesis supervisors for giving me the wonderful opportunity of doing research under them. Their enthusiasm on the problem and encouragement throughout the course of this work is very much appreciable. They have always been available for discussion and guided me to accomplish the objective of this study; they have been an inspiring and driving force during the course of this work. Without their timely help, intellectual input, constructive criticism and painstaking efforts, it would not have been possible for me to complete this thesis in the present form.

I would also like to thank Dr. S. K. Nath Professor & Head, and Dr. B.V. Manoj Kumar, Dr. Vikram Dabhade IIT Roorkee, Department of Metallurgical and Materials Engineering for their valuable suggestions.

The steels used in this investigation were received from M/S Star Wire (India) Ltd, Ballabhagarth, Haryana, India. I am great thankful to Mr. M. K. Gupta, Managing Director and Dr. S. K. Goel Executive Director of this organization as also the keen interest they took in this study.

I also wish to thank the whole staff of the Department of Metallurgical and Materials Engineering, Indian Institute of Technology Roorkee, in particular Mr. Kuldeep Sharma, Mr. Rajinder K. Sharma, Mr. Naresh Sharma, Mr. T. K. Sharma, Mr. R. K. Sharma, Mr. Shakti Gupta, Mr. S. M. Giri. Many thanks go to Mr. S. K. Saini, Mr. Shiv Kumar and Mr. Vaibhav Bajpayi of Institute Instrumentation Centre, IIT Roorkee for helping me in doing XRD, SEM and EDX work.

Thanks are also due to Mr. Ravi Kant without whom this thesis manuscript would not have been in the same format; in fact he has helped a lot. The discussions and interactions with the colleagues have been very fruitful. Many thank goes to Ph.D. fellows and friends, Mr.

Paritosh Dubey, Mr. Monu Verma, Mr. Amrendra H. J., Mr. V.N. Shukla, Mr. A. Malik, Mr. R. Sunil Kumar, Mr. Nageshwar Rao, Mr. S. Singh, Mr. Deepak, Mr. S. Rajput, Mr. Sandan Sharma, Mr. Abhay, Mr. Uday, Mr. Sidharth Jain, Mr. Ashvin Gaikwad, and Mr.Amit Kamble.

The author expresses his deepest esteem to his parents, Mr. Wamanrao Selokar and Mrs. Shalini Selokar and sisters (Archu and Bali) for keeping their blessing over me. You're waited for many years to see this moment. Thank you for all sacrifices that you're made. I know it was not easy. You will be always with me in memories. Without you I would never be where I am now. Thank for giving me strength and the spark of hope when everything looked hopeless. Author is highly appreciative to his brother in law Mr. Vaibhao Motghare for their encouragement throughout.

I also like to thank everyone who supported me for completing this work successfully and I express my apology that I could not mention everyone individually.

(Ashish Wamanrao Selokar)

Contents

List of Figures

List of Tables

List of Publications

In International Journals:

1) **Ashish Selokar**, D. B. Goel and U. Prakash, A comparative study of cavitation erosive behaviour of 23/8N Nitronic steel and 13/4 martensitic stainless steel, Advanced Materials Research, 585 (2012) 554-558.
2) **Ashish Selokar**, Ujjwal Prakash, D. B. Goel and A. Chaurasia, Erosion Behaviour of Fe-Alloys for Underwater Components of Hydroelectric Power Plant, Transaction of Indian Institute of Metals, 66(4) (2013) 425–428.
3) **Ashish Selokar**, Ravi Kant, D.B. Goel, Ujjwal Prakash, Solid particle erosion behaviour of martensitic and nitrogen alloyed austenitic stainless steel, Advanced Materials Research, 1043 (2014) 45-49.
4) **Ashish Selokar**, D. B. Goel and U. Prakash, B. V. Manoj Kumar, The cavitation erosion and air jet erosion behavior of a nitrogen alloyed austenitic stainless steel, ISIJ International 55 (2015) 1123–1130.

In conferences:

1) **Ashish Selokar**, Ujjwal Prakash, D. B. Goel and A. Chaurasia, International Symposium "International Symposium for Research Scholars (ISRS-2012)" 20-22 Dec.2012, Department of Metallurgical and Materials engineering. Indian Institute of Technology Madras, Chennai, India.
2) **Ashish Selokar**, D. B. Goel and U. Prakash, National Seminar on Metallurgical Problems in Power Projects in India, 22-23, Feb.2013, Malaviya National Institute of Technology Jaipur, Jaipur, Rajasthan, India.
3) **Ashish Selokar**, D. B. Goel and U. Prakash National conference "Recent Trends in Materials Engg. (RTME-2013)", Mechanical Engineering Society, 4-5 Oct.2013, BRCM College of Engineering & Technology, Bahal, Haryana India.

Chapter 1

Literature review

1.1 Introduction

Erosion of underwater parts is a serious problem encountered in hydro power plants. This problem of erosion in hydraulic machinery is not limited to hydroelectric plant. Similar, problems are also encountered in mining industries, dredging work, and waste disposals. There is increasing demand for electric power in the developing countries leading to promote renewable and non-fissile fuel energy source. Considerable amount of power production is done from hydroelectric power plants in Asian countries. At present, India is generating nearly 176 GW of electricity from various installed sources such as 66% thermal, 26% hydro, 3% nuclear and 5% through other renewable sources. Himalayan rivers are the main source of hydropower potential and the estimate potential is about 325GW.The Himalayan Region Rivers which contribute to a large portion of the hydropower potential available in the country bring more than 20,000 ppm of quartz of hard silt particles during rainy session. The underwater components of hydro turbine operating in silt laden water suffer from extensive erosion. Due to high amount of silt damage it becomes impossible to run the unit for longer time thus, incurring heavy loss of power generation as well as replacement / repair cost. Welding is the only option for repair of worn out under water parts and to extract maximum life in their operation.

Damage concerning water turbines (10-12 mm per year) is caused mainly by cavitations problem, silt erosion and material defect. Synergetic effect of cavitation and silt erosion cause enhanced erosion rate. As cast steel (13Cr-4Ni) has conventionally been used as material for water turbine runner, guide vane, and stay vane. Water turbine elements are used towards high head (water level) for high output and in such conditions erosion becomes more severe by silt and lower head erosion is more severe by cavitation.

Erosion is progressive loss of target materials from the surface as a result of interaction between that surface and fluid, multi component fluid or impinging liquid or solid particles [Naidu 2001]. Materials are exposed to erosive environments in a large number of applications. The impact of sand particles suspended in water or entrant into airflow on the surfaces of various components of materials cause erosion damage. Various studies may be found from the literature of specific erosion and practical formulation. Finnie has proposed the first model to predicting the removal of material by solid particle erosion as a result of cutting action of a single particle plunged against ductile target material [Mann 1987]. Erosive wear depends upon the number of mechanisms such as angle of impingement, nature of abrasive particle, impact velocity, size and shape of abrasive particle. The ductile material is mainly removed through the impacting particles cutting chips from the surface of target material as in machining process (micro-machining) [Sakhujja 1987]. The impacting particle goes deep inside the target material by small amount, removing surface of material ahead of particle in machining mode and finally departs the surface. At low angle particle tends to track across the worn surface erosive wear process nearly same to abrasion. For ductile materials, material losses are by the process of cutting and ploughing while for brittle, material losses by atomization and removal of chips [Li 2006]. Erosion rate is maximum at lower angle and minimum at normal impact of abrasive particle. Hutching predicted Fatigue wear equation for erosive wear by vertical impact of solid particles [Zheng 1995]. Bitter proposed analysis of the problem in which wear of ductile materials is by cutting wear and is followed by plastic deformation of surface material [ASTM G76 2003, ASTM G40 2003]. The repeated blows caused the deformation wear of the specimen and which finally lead to cracking and spalling of surface material.

Various techniques have been reported to reduce the loss of material due to erosion [Mann 1987, Zheng 1995, Li 2006]. Cavitation erosion and solid particle erosion often co-exist causing severe damage. According to ASTM standard, erosion is the progressive loss of target material from surface because of mechanical interaction between that surface and a fluid, a multi-component fluid, or impinging liquid or solid particles [ASTM G76 2007]. In cavitation there is the formation of cavities or bubbles and subsequent collapse, within a liquid, that comprise of gas or vapor or both. Cavitation erosion is progressive loss of original material from a surface due to continued exposure to cavitation [ASTM G40 2011]. Cavitation erosion is one of wear process in which target material comes into contact with a flowing fluid, e.g. ship propellers, hydro turbines etc [Kwok 2000, Wu 2002]. The bubble burst during cavitation and produces very high and temporary stresses, which strains the materials in a particular way [Karimi 1986]. The bubbles or cavities in cavitation nucleate from a local reduction in hydrostatic pressure in the fluid; it is also generated by velocity of the fluid i.e. decrease in static pressure induced by changes in velocity of a flowing fluid or cavitation caused by the pressure variations within a fluid, produced by the vibration of a solid surface plunged in the liquid [ASTM G32 2010].

Initially the cavitation erosion is not too dangerous for the hydro turbine under water parts, but in presence of silt erosion damage, cavitation enhances the erosion damages. This is called synergetic erosion i.e. erosion due to silt as well as cavitation [Li 2006, Thapa 2015]. Hydro turbine must have specific shape and contour in order to improve its efficiency. Cavitation erosion has created pits or cavities which alter these contours, producing obstacles to fluent flow of water through the turbine. As a result of this, the overall operating efficiency of turbine decreases. By keeping the cost of electrical energy in mind, even a small change in the operating efficiency of turbine can be a matter of concern [Zheng 1995].

Cast martensitic stainless steel having 13%Cr and 4%Ni recently used as structural material in number of applications in hydro turbine and other industrial applications which undergo damages due to erosion [Mann 1997, Kishor B 2014]. At present various attempts are concentrated on techniques to minimize the erosion damages namely, reduce the silt content by sedimentation, providing hard surface coatings and development of erosion resistant materials. Sedimentation techniques suffer from the limitation that concentration of particles below 300 ppm cannot be eliminated [Panwar 2000]. The erosion resistance of materials can be improved by understanding the mechanism of material removal due to erosion. In brittle materials the material removal is through flake fragmentation and removal of flakes while ductile materials, it through cutting and ploughing [Deng 2001, Lindsley 1999, Burnett 1999, Divakar 2005]. Work hardening of the material also plays significant role in reducing the erosion. The erosion of copper, nickel and 304 stainless steel by using sharp alumina particles has been reported [Goretta 1991]. It was also reported that work hardening of copper results in improvement in the erosion resistance. Higher hardness also contributes to the erosion resistance of the material if it retains sufficient ductility. The role of ductility, which facilitates plastic flow of the target material by the impingement of abrasive particles, becomes very important. Poor ductility leads to tendency for localization of strains and development of cracks. As far as cavitation erosion is concerned, the characteristic of a ductile material exposed to cavitation is to be progressively hardened by the successive collapses of water bubbles. So any measure to allow some plastic deformation in the target material is expected to improve its erosion resistance. It is predicted that the erosion resistance can be increased by any treatment which improves the ductility. It has been theoretically predicted [Hutchings 1981] in maraging steel that erosion increases with the increasing hardness at constant ductility [Naim 1985], which is in conflict with the results of [Finnie 1958] that erosion decreases with increase in the hardness. An increase in erosion rate increases as the ductility was reduced by cold working essentially at high strength [Naim 1985].

Ductile failure mechanism is observed during erosion for most engineering metallic materials which are not very sensitive to strain rate. Metals having FCC lattice structure are in general not sensitive to strain rate. The response of FCC materials to cavitation erosion is generally similar to their static mechanical behaviour [Chen 2005]. Metals with BCC lattice structure are generally strain rate sensitive. Thus, cavitation is always a competition between flow and fracture. Brittle materials show often brittle failure behaviour due to poor capability of energy absorption during the impact. The more the impact energy of particle utilized to crack formation, the more frequent is removal of the target material. The absorption of energy required to remove fraction of material by cracking is much less than the same volume of material by plastic deformation. Tensile toughness measures the ability of a target material to absorb the energy of the abrasive particles to be impacted. Levin [1999] have reported that a material with higher toughness shows good erosion resistance.

Coatings provide an alternative way of using the materials at the upper end of their performance capabilities protecting against erosion wear, by allowing without any change in the mechanical properties of the substrate materials [Amirhaghi 1999, Sidky 1999, Xu 2014]. Coating technology is one of the most recent growing technologies in field of materials [Raju 2014, 2011]. A combination of development of materials specifically erosion resistance and the appropriate technique for the application of these materials, as a coating would be the optimum solution. Suitable coating technique also allow for regeneration of parts that have been rendered unusable by erosion. Coatings are primarily used to restrict surface damage of components in practice [Matthews 2014 a, b, Rudrakshi 2007]. Erosive damage arises to components are depend on the working environment/medium and conditions. Mechanical distruction and corrosion are modes of failure in hydraulic components. The mechanical damage under erosion–corrosion is due to the strike of solid particle. It under cavitation erosion is from the continuous collapse of cavities. The synergies of the mechanical and electrochemical processes contributed to the total mass loss [Wood 1990, Neville 2010]. Therefore, only the material with both good mechanical property and good corrosion resistance may serve well under hydraulic condition. In industrial applications the corrosion-reducing coatings are sprayed on hydraulic components. But it is questionable whether such products actually do help under wear or cavitation loads or not. In last few decades, extensive works have been carried out to improve the erosion resistance of surface coating deposited on steel [Cheng 2001, Krella 2006]. The coatings can be easily formed on the surface of steel, which can exhibit smooth surface and good mechanical properties, such as high hardness, high elastic modulus or high oxidation resistance [Oliver 1992]. Many fluid machinery components are supplied with coatings to prolong their lifespan and to improve their work efficiency. However, when bubble collapses on the coating's surface, a high temperature may be achieved, which could influence the coatings' properties, for example makes coatings more ductile [Watanabe 2006]. Thousands of pressure pulses act on the surface when bubbles collapse. The coating may undergo local thermal softening, which has an essential influence on the coatings deformation. The thermal mismatch between the coating and substrate may also result in adhesion failure [Shuji 2013]. Coatings with weak adhesion could soon be peeled off. If the coatings can avoid adhesive fracture, they protect the substrate from corrosive fluid. Adhesion plays an important role in the incubation period and ensures the protection of the substrate material against mass loss. The outstanding results observed in any given coating can be attributed to the strong adhesive connection. When a coating is very ductile, it is easy to cause the dislocation movement and peeling off of the coating [Thiruvengadam 1963]. In addition, cavitation erosion investigations proved that the cavitation erosion resistance of conventional materials (stainless steel, etc.) depends on their mechanical parameters (hardness, Young's modulus, tensile strength, and fatigue strength) [Krella 2009, Shuji 2011]. More energy is needed to be absorbed before fracture, if the hardness and Young modulus are high. Delamination may also happen due to the large difference in hardness and Young's modulus between the substrate and coating. It has been reported earlier that thermal spray coating is a useful technique to produce wide range of materials for diverse applications [Barber 2005, Wood 1999, Berger 2015]. Among the commercially available thermal spray coating techniques, high velocity oxy fuel (HVOF) spray and detonation spray are the best alternatives to obtain dense, hard and wear resistant coatings [Barbezat 1993, Wang c 1993, Semenov 2002, Liu 2014].

Welding is one of the most commonly used fabrication process employed for joining of such material with varied section size in normal as well as in critical applications. Depending upon application, the integrity of weld joint is largely adjudged by its relevant properties. The worn out parts of power generation industries can be repaired only by the in site welding process. Today’s repair welding procedures in India are not standardized as well as not satisfactory. Different power plants used different welding procedures for same kind of repairs on worn out component [Goel 1993, Panthee 2015].Since the repair welding in Indian hydroelectric projects is currentely being using austenitic stainless steel electrode as its good weldability characteristics [Goel 1996].

1.2 Hydro turbine steels

The stainless revolution began when it was observed that addition of 12% Cr imparts good corrosion resistance and avoids the rust formation over steels. There are many grades of stainless steel, of which fifteen are most common. The AISI (American Iron and Steel Institute) defines the following grades among others:

- 200 Series—austenitic Fe-Cr-Ni-Mn alloys
- 300 Series—austenitic Fe-Cr-Ni alloys
    - Type 301—highly ductile, for formed products. Also hardens rapidly during mechanical working.
    - Type 303— addition of sulfur- free machining version of 304
    - Type 304 — the most common; the classic 18Cr/8Ni stainless steel
    - Type 316— Addition of Mo to specific form of corrosion protection
- 400 Series—ferritic and martensitic alloys

Selection of proper stainless steel for hydro turbine underwater parts operating in silt laden water is important for ensuring their longer life. The material should be erosion resistant and should be weldable quality to enable repair at site. The most commonly used 13/4 Martensitic stainless steels for critical hydro turbine components exhibits resisatance against cavitation erosion as well as erosion due to silt laden water [Naidu 2001, Sharma 1996, McCaul 2007] . Based on Indian experience, following materials are recommended for critical turbine components.

1.2.1 13/4 martensitic stainless steel

CA6NM is a 13Cr-4Ni cast grade of martensitic stainless steel that is widely used throughout the hydro turbine and pump industry [Sharma 1996, McCaul 2007]. CA6NM is the result of material development efforts conducted at a Swiss foundry in the early 1960’s, with the following aims:

- Increase impact strength and improve weldability by lowering carbon content
- Attain a microstructure free of delta ferrite by increasing the nickel content
- Suppress temper embrittlement and improve corrosion resistance by suitable molybdenum content

Conventionally produced CA6NM has a carbon content of 0.06% maximum. In fact, foundries employing argon-oxygen-decarburization (AOD) refining routinely produce CA6NM castings with even lower carbon content in the vicinity of 0.03% or less. The relatively low level of carbon in CA6NM facilitates welding in several ways. Low carbon retards the formation of a brittle heat affected zone consisting of untempered martensite. Preheat is usually only 200°F, compared with 400°F minimum for CA-15. Postweld heat treat temperature is also some 250°F lower and minor repairs can be made without postweld heat treatment, a distinct advantage for finish machined castings.

Despite its weldability, CA6NM repair welds made with matching filler metal have been consistently harder than the base metal. The higher hardness can cause machining difficulties. In addition, many CA6NM pump castings are used in oil industry applications where exposure to hydrogen sulfide and the potential for sulfide stress corrosion cracking dictate that the weld and heat affected zone not exceed 255 BHN in hardness [McCaul 2007]. In practice, it has proven difficult to consistently meet this 255 BHN hardness requirement in welds. In fact, the lowest attainable hardness of repair welds is near this 255 BHN limit.

1.2.2 Nitronic steels

Nitronic steel is basically the austenitic stainless steel which contains nitrogen as alloying element. This is also known as high nitrogen austenitic stainless steels. Various steels are contemplated high nitrogen varieties if they contain N content well above that present in conventional steels and stainless steels. For example, steels having 0.1 mass % of N are used as creep resistance varieties [Srinivasan 1999, Bose 2008] while those with 0.9 mass% N are used in the normal grades Steels containing 2 mass% N in tool steels are considered high nitrogen steels (HNS). If the content of N exceeds than 0.08 wt% N in a martensitic matrix or more than 0.4 wt% N in austenitic matrix are designated as high nitrogen alloyed stainless steels [Speidel 1990]. According to Mudali [2004], steel can be high nitrogen alloyed where N added to steels or stainless steels attains properties different in comparison to alloy without N. The development of HNS alloys resulted in improvement in mechanical properties as well as corrosion resistance.

Table 1.1 Selection of material for critical turbine components [Naidu 2001].

Si. No.	**Component**	**Material**
1	Runner	13%Cr, 4% Ni stainless steel
2	Labyrinth seals	13%Cr, 4%Ni or 18%Cr, 10%Ni stainless steel
3	Guide vane	13%Cr, 4% Ni stainless steel
4	Guide vane bush housing	Cast steel
5	Liners for top cover and pivot ring	18%Cr, 10%Ni stainless steel
6	Fasteners in water path	Stainless steel
7	Tubes for bearing coolers	Cupro-Nickel (80% Cu-20%Ni)
8	Rubber seals	Neoprene synthetic rubber

The yield strength (YS) and ultimate tensile strength (UTS) of HNS alloys can exceed those of conventional AISI 200 and 300 series by 200% to 350% in the annealed condition without any loss in toughness. High strain hardening potential and cold deformation could further enhance yield strength (YS) above 2 GPa. The combination of fracture toughness and yield strength which can be achieved at room temperature in case of HNS than any other steel [Mudali 2004].

According to Mudali [2004]**,** addition of nitrogen to steel was never popular because of incredulity associated with it resulting in decrease in ductility in ferritic steels and the problems involved in adding nitrogen into steel during casting. The benefits of nitrogen addition to steel were realized only in the beginning of twentieth century. In late 1930s and 1940s, the lack of Ni during world war inspired researcher on the possible substitution of Ni with nitrogen to stabilize austenite. The interest was due to two factors: focus on decreasing supplies of alloying element such as Ni and the unsuccessful dream of a high strength FCC steels [Malakondaiah 1997].

In United States, addition of nitrogen to stainless steels became common when it was realized that introduction of nitrogen as gas instead of different alloy systems was possible with the argon oxygen decarburization (AOD) process. Replacing nickel (Ni) with a combination of nitrogen (N) and Manganese (Mn) had lead to the additional advantage of increasing solubility of nitrogen and this research resulted in standardized new alloy of AISI 200 series. In the late 1960s, the first commercial introduction of N-bearing stainless steels “Nitronic” with 0.18N and German grade 1.4439 (AISI 317LMN stainless steel) were introduced in steel market [Katada 2007]. The nitronic steels contain high Mn and N (21Cr-9Mn-7Ni-0.32N) and exhibit high strength and toughness at low temperatures as well as good corrosion resistance.

The scientific community of HNS alloys evolved series of International conferences on the topic since the first conference at Lillie, France in 1988 (HNS 88), followed by HNS 90 in Germany, HNS 93 in Ukrain, HNS 95 in Japan, HNS 98 in Finland and Sweden, HNS 2001 in India and HNS 2003 in Switzerland. Mudali [2004] has reported that high nitrogen steels are being transformed into high interstitial alloys with addition of C to HNS alloys. Addition of C probably would avoid steel making HNS with very high N contents (about 0.9 wt %) and the possibility of having new class of alloys with C (0.4 wt %) and N (0.4 wt %) together. The high nitrogen contents in the austenitic stainless steels decreases the stacking fault energy and stabilize austenitic structure so that no strain induced transformation to α-martensite and ε-martensite occurs [Schramm 1975, Mullner 1994, Hanninen 2001]. The best known application of HNS alloys is retaining rings for power generating sector, but many other application exist (bolts, spring, turbine blades, washing troughs, protective liners etc). The largest use for N-alloyed stainless steels is for replacement of Ni and this area will probably grow with time, because Ni is a potential allergic and carcinogenic element that is restricted for biomedical applications, and the developments and applications of HNS alloys in this area will be more attractive too [Sumita 2004].

1.2.3 Solubility of nitrogen in austenitic stainless steels

Iron in pure form shows low solubility of nitrogen (0.044% N) in the solid as well as in the liquid state. The solubility of nitrogen goes on increasing with increase in the Cr content as shown in Fig. 1.1 [Balachandran 2001]. When there is δ-ferrite formation during solidification, the solubility of nitrogen diminishes to a value far below the equilibrium solubility in the liquid state. However, in the solid state, further lowering of temperatures results in the formation of austenite phase, in which nitrogen solubility increases remarkably to values well above that in the liquid state. Like Cr, the presence of Mn has also been reported to increase the

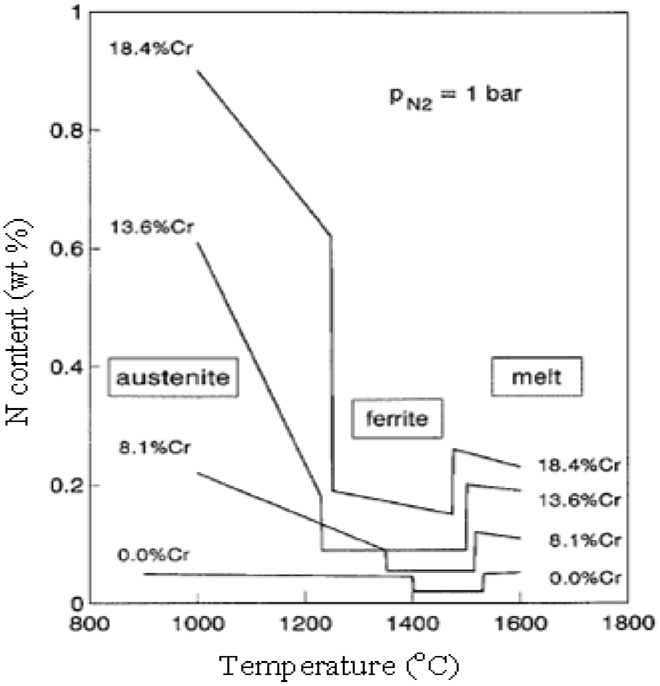

Fig. 1.1 Nitrogen solubility in steel as a function of temperature and Cr content [Balachandran 2001].

solubility of nitrogen. Nitrogen solubility in the presence of both Cr and Mn in steel shows deviation from Sievert's law [Balachandran 2001]. Thus, it is understood that to achieve high nitrogen content in steels, the presence of large amounts of Cr and Mn is required.

Steels are generally reported to acquire corrosion resistance, when Cr content is greater than 12%. Conventional austenitic stainless steels have metastable austenite phase [Pickering 1978]. Nickel in these steels expands the austenite phase field and promote sluggishness of phase transformation. Other economically viable austenite stabilizers are carbon, copper, manganese and nitrogen. Among these, carbon has a tendency to sensitize the steel, copper leads to hot shortness and manganese alone cannot totally replace Ni to form austenite phase. This leads to nitrogen as the best alloying additive.

Thermodynamics of Fe–Cr–N system [Hertzman 1987] show that for 12% Cr content, the austenite phase exists in a narrow range of nitrogen composition, which increases with increasing Cr content. Beyond the range, Cr_2N and CrN phases are formed. At high Cr levels, there is the formation of ferrite, austenite and Cr_2N type nitrides. The problem with this system is that the nitride can precipitate out readily at lower temperature aging [Uggovitzor 1996] and they are not stable against martensitic transformation [Burns 1996]. Hence, one of the alternatives was to have Mn in the Fe–Cr–N system. Then, it is necessary to know the minimum limits of N and Mn contents required to make stable austenitic stainless steel. Analysis of the Fe–Cr–Mn phase diagram at temperatures of 800 to 1200°C shows that, when Cr is greater than 13%, Mn alone cannot produce a fully austenitic structure. At Cr contents greater than 15 %, there is the formation of sigma phase. This necessitates addition of other austenite stabilizers such as Ni or N or both. Thus, an 18% Cr steel with 0.1% C and 8% Mn requires 4 to 5% Ni and 0.15% N for getting stable austenitic microstructure at room temperature. Each 0.05% N is found to be equivalent to 1% Ni in its austenite stabilizing effect. In steels with 10 to 35% Cr and 2 to 23% Mn, increasing nitrogen content expanded the austenite field and shifted the sigma phase to higher Cr contents.

There are several advantages of nitrogen alloying stainless steel over alloying with carbon:

(1) Nitrogen addition causes more effective solid-solution strengthening than carbon and also increases grain size (Hall-Petch) strengthening.

(2) Nitrogen reduces the tendency to form ferrite and deformation-induced and ε martensites.

(3) Nitrogen serve as strong austenite stabilizer thereby decreasing the amount of nickel needed for stabilization.

(4) Nitrogen has greater solid-solubility than carbon, thus decreasing the tendency for precipitation at a given level of strengthening.

1.3 Solid particle erosion

Erosion wear is due to impact of particles against a solid surface. Erosion is speedy and severe forms of wear and can results in considerable costs if not controlled. Erosive wear takes place in a large number of machineries for examples, the deterioration to gas turbine blades when aircraft flies through dust clouds, hydro turbine under water parts when silt laden water flows through it and the damage of pump impellers in mineral slurry processing systems. As compared to other forms of wear, mechanical strength is not deciding the wear resistance and a detailed study of material properties is needed for reducing wear damage. The properties of the impacting particle are also important. Erosion of metallic components occurs by various mechanisms depending upon type of material, operating conditions as well as environment and geometry of the wearing bodies. These can be classified as those dominated mainly by the mechanical and physical behaviour of solids and those controlled by chemical behaviour of materials.

1.3.1 Mechanisms of solid particle erosion

In erosion, the detailed process that cause material removal is still poorly understood [Gee 2003]. Finnie's [1960] analysis of the cutting action of a single particle proposed against a ductile material was the first model of the solid particle erosion capable of predicting erosion rate. Ruff and Wiederhorn [1979] developed two models for erosion of brittle materials: one is the based on assumption that erosion occurs entirely by crack propagation and chipping and the other is based on the assumption that plastic deformation contributes to the process of crack formation and surface chipping.

Material removal is mainly the result of particle impacts as the jet delivers abrasive particles at high velocities to the target surface. Fig. 1.2 shows the hierarchy of this process. These mechanisms are cutting, brittle fracture, fatigue and melting. Clearly, these mechanisms generally do not act individually, but in combination. Their significance for the erosion process depends on various factors, such as the particle kinetic energy, impact angle, the particle shape, properties of target-material, and most importantly environmental conditions [Meng 1995].

In order to compare solid particle erosion, a non-dimensional erosion number, $E_{N,}$ is defined by Equation (1.1).

$$E_N = \frac{m_M}{m_P} \qquad \text{…..(1.1)}$$

Here m_M is the mass of the material removed and m_P is the mass of the abrasive particle. Thus, removed volume of the material is

$$V_M = \frac{E_N \cdot m_P}{\rho_M} \qquad \text{..(1.2)}$$

The term 'erosive wear' refers to an unspecified number of wear mechanisms which occur when relatively small particles impact against mechanical components. This definition is empirical by nature and relates more to practical considerations than to any fundamental understanding of wear. The known mechanisms of erosive wear are illustrated in Fig. 1.3 [Stachowiak 2006]. The angle of impingement is the angle between the eroded surface and the trajectory of the particle immediately before impact. A low angle of impingement favors wear processes similar to abrasion because the particles tend to track across the worn surface after impact. At high angle of impingement wear mechanisms are typical of erosion.

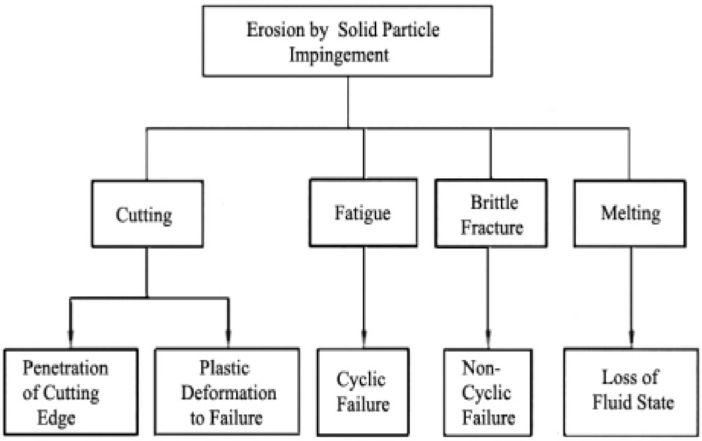

Fig. 1.2 Mechanisms of material removal by solid particle erosion [Stachowiak 2006].

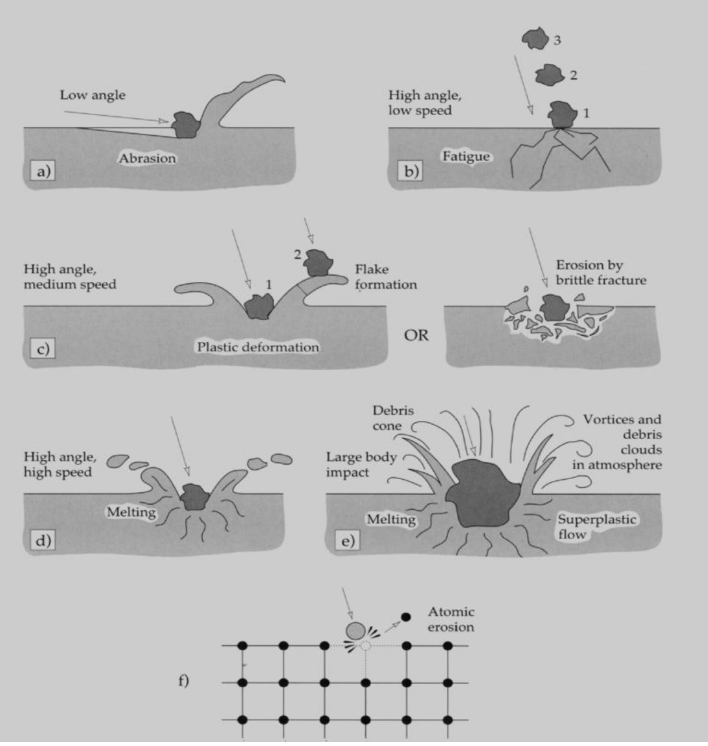

Fig. 1.3 Different observed mechanisms during the erosion (a) abrasion at low impact angles, (b) surface fatigue during high impact angle and low speed (c) multiple plastic deformation or brittle fracture during medium speed and large impact angle, (d) melting of surface at high impact speeds, (e) macroscopic erosion with secondary effects and (f) degradation of crystal lattice from impact by atoms [Stachowiak 2006].

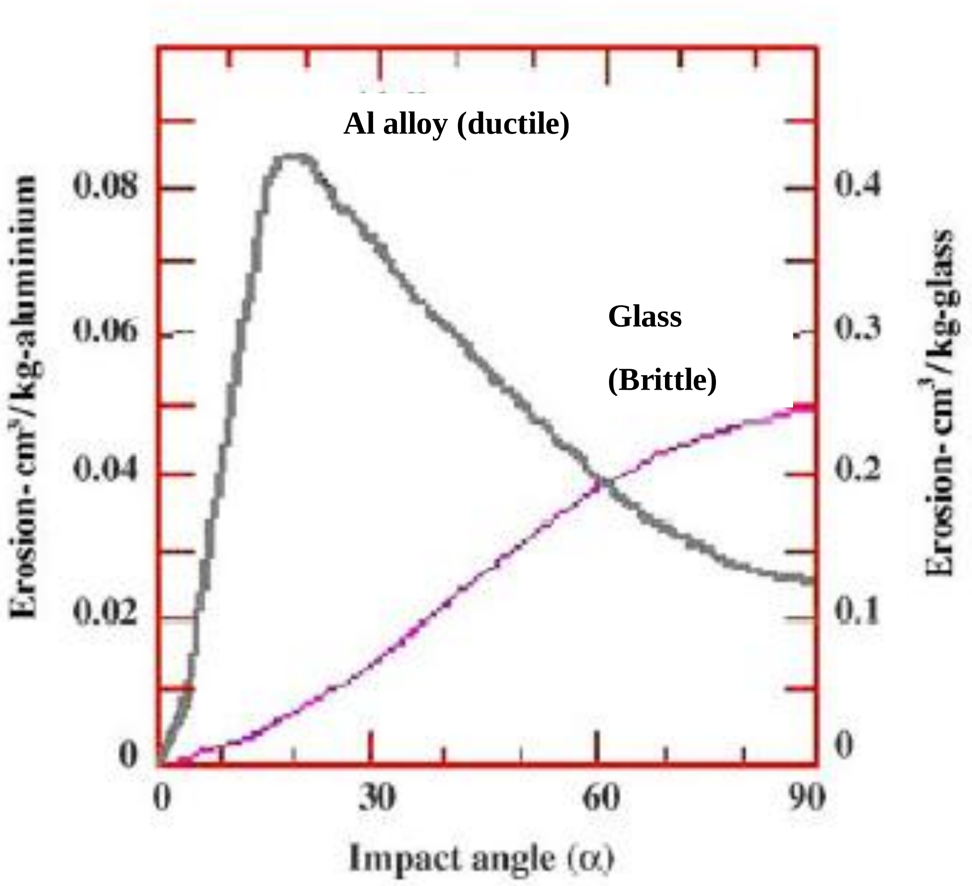

Fig. 1.4 Erosion behaviour of brittle and ductile materials [Divakar 2005].

Erosive wear includes various wear mechanisms which are affected by material of particle, the impact angle, the impact velocity and the size and shape of particle. In erosion, the erosion behavior of the material is mainly defined two different modes of erosion: brittle and ductile. These two modes differ from each other by a manner in which the erosion rate changes with the impact angle. For brittle materials, the maximum erosion takes place at normal impact angle but in case of ductile materials maximum at glancing angles. The failure is primarily because of large plastic deformation of surface material. The erosion rate vs impact angle for brittle and ductile materials is shown in Fig. 1.4 [Divakar 2005].

1.3.2 Erosion mechanisms of ductile materials

For ductile materials, a model for the erosion was first developed by Finnie [1960]. He handled the problem by assigning a plastic response property to the material through a flow stress σ_F. He calculated the trajectory of an erodent particle cutting and removing the target material, and determined the volume loss (V_M) given by the expression:

$$V_M = (mv^2/\sigma_f Kd)\ g(\theta) \qquad \text{……(1.3)}$$

Where m is mass of the particle,

v is velocity of impacted particle,

K is the ratio of vertical force to horizontal force on the particle,

d is depth of cut, and

$g(\theta)$ is a function describing the effect of attack angle θ.

But this model could not be suitable for attack angle $\theta = 90^0$ and also quantitative discrepancies arise relating to the effect of flow stress and the velocity exponent. Hutchings [1986] developed a model to describe erosion at various attacking angles. He believed erosion to comprise of two simultaneous processes, cutting wear for impact at low angles and indentation deformation wear for high angle impact. This theory demands experimentally determined parameters for complete applications [Bitter 1993 a, b]. Tilly [1973] proposed another model consisting of two-stage mechanism of erosion recognizing explicitly that the normal incidence of impacting particles may fragment and these fragments may cause for erosion of exposed surface.

Levy [1981] has reported the variation of erosion against the microstructures of steel; he used an erosion weight loss curve that occurred due to micro cutting mechanism. In order to understand the mechanism more about the initiation of erosion that occurred the erosion was performed on steel; increasing gradually 60 gm of particles at a time and weight loss was measured caused by each 60 gm increment and plotted as shown in Fig. 1.5.

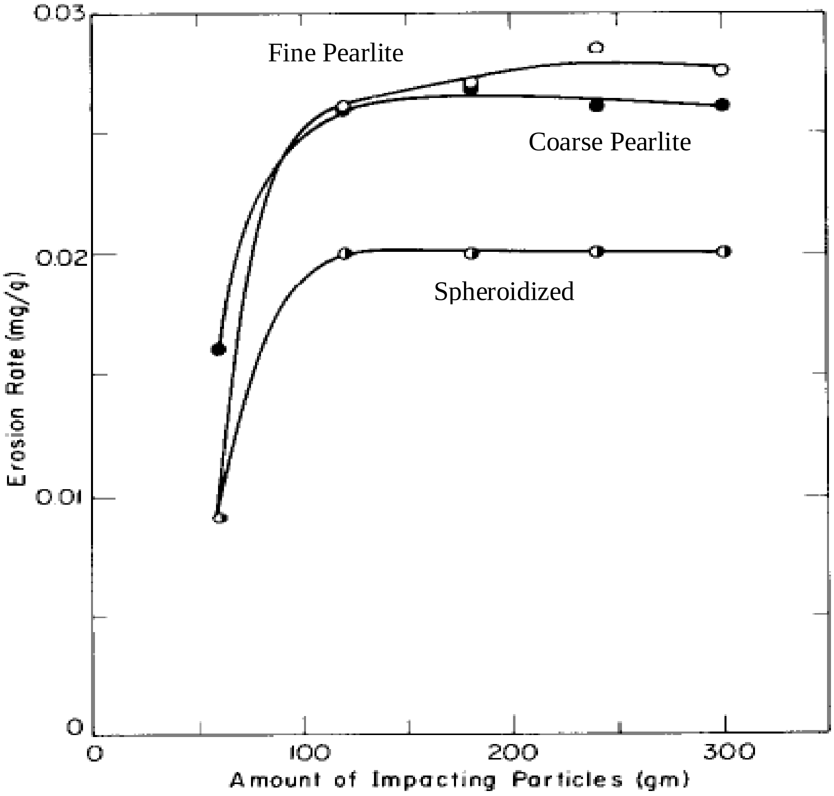

Fig. 1.5 Plot of erosion rate verses mass of impacting particles for 1075 steel (SiC particles 240 µm in diameter; v = 30.5 m s^{-1}; θ = 30^{o}) [Levy 1981].

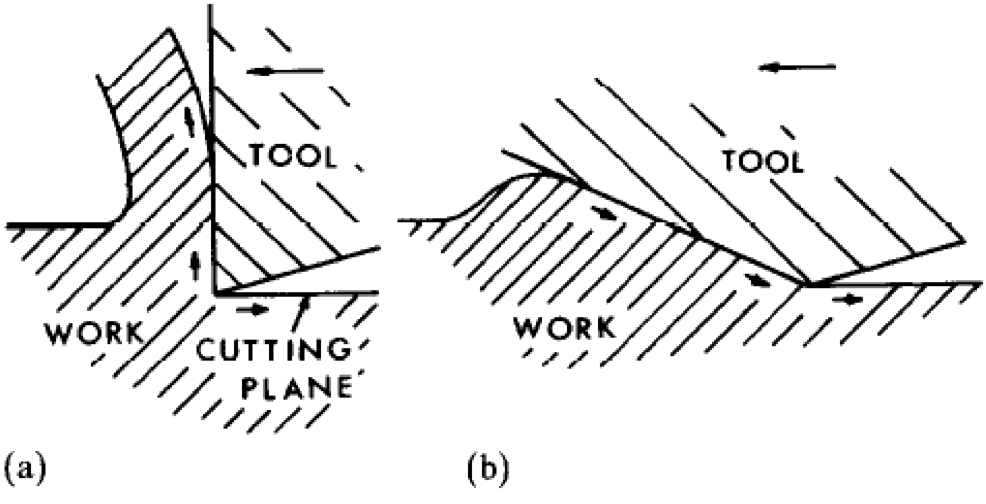

Fig. 1.6 The two modes of surface deformation considered (a) cutting, in which the metal flow bifurcates at the cutting edge, (b) ploughing, in which the metal flows continuously past the cutting edge [Winter 1974].

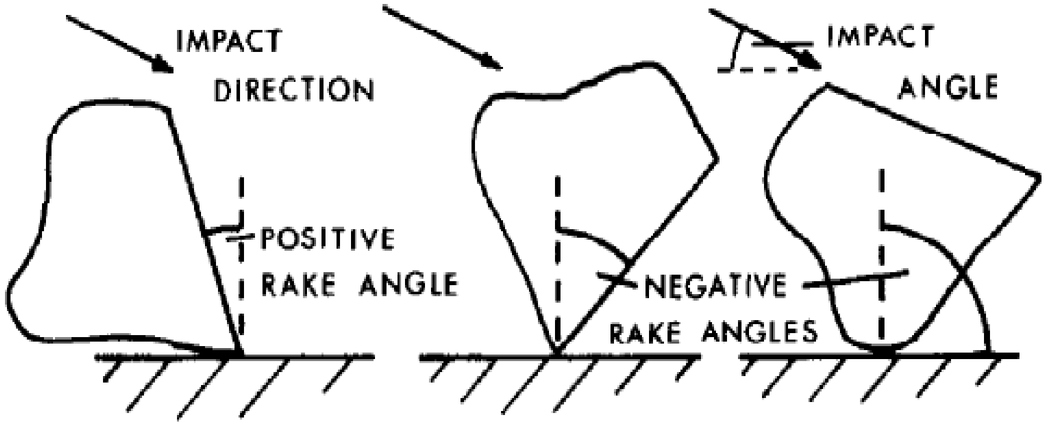

Fig. 1.7 A typical sand grain striking a surface at different orientations. The rake angle as defined here varies with particle orientation [Winter 1974].

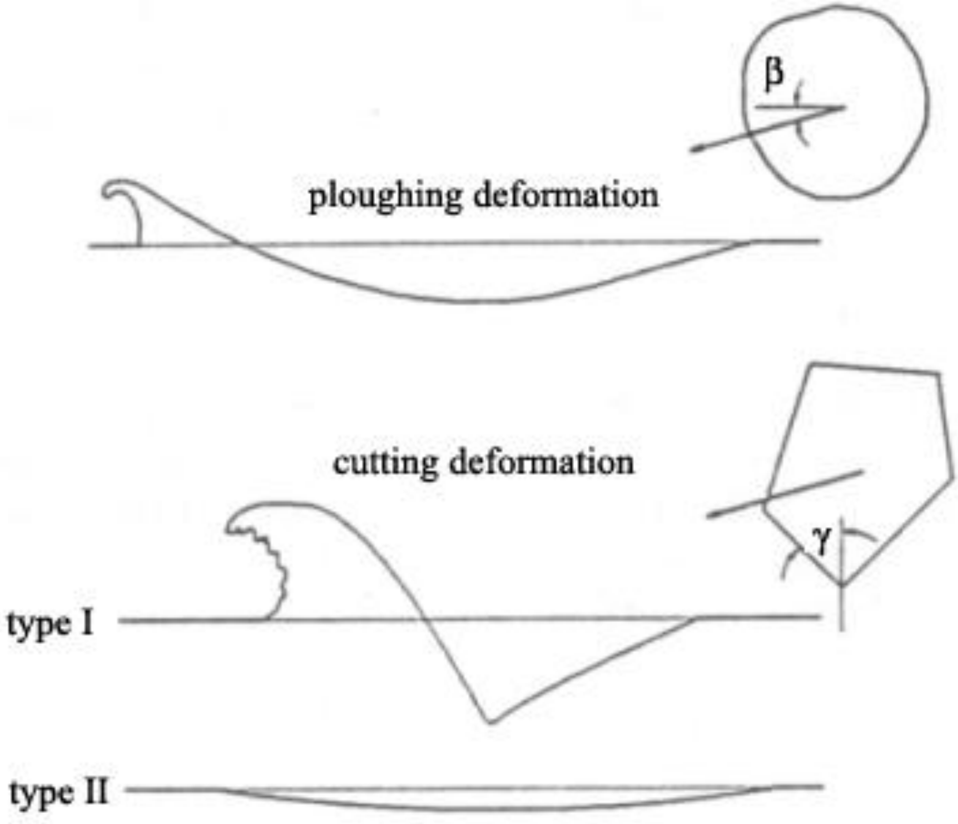

Fig. 1.8 Cutting and ploughing by solid particles at oblique impact angles [Hutchings 1979].

The initial erosion rate due to impact of SiC particles was much lower than that of subsequent 60g SiC batches of erodent particles. Also, extrapolating the curves down to zero erosion reveals that number of SiC particles have hit the surface before erosion losses began. With subsequent increases of erodent particles, the material loss rate enhanced until it attained steady state conditions. Levy [1981] further reported that if micro cutting was the main mechanism of erosion, the initial erosion rate, uneroded surface should be higher than subsequent incremental erosion rates. This is due to the fact that the work hardening of the surface of the material due to machining action would have decrease the machinability of the surface and the thus, the amount of material loss.

Some researchers [Sheldon 1972, Hutchings 1974, Winter1974, 1975, Christman 1979] have used the large single particle, millimeter in diameter, and impacted them individually at the target surface to study the mechanism of erosion from a physical standpoint. Winter [1974] have identified the two different regimes of deformation ploughing and cutting (Fig.1.6). According to them at rake angles more positive than a critical angle, cutting occurs; material flows up the rake face of the tool and the flow of metal bifurcates at the cutting edge of the tool producing a cutting plane. On the other hand, at rake angles more negative than this critical angle, ploughing dominates; in this case material probably flows down the tool face and the flow of metal is continuous over the cutting edge. Fig. 1.7 shows the rake angles for a typical sand particle hitting a material surface at different angles. The material is taken out by ploughing when a critical impact speed is exceeded except other conditions remain constant. They further added that ploughing deformation is, however, decreased if the particle carries out a rolling type rotation during contact with the material surface instead of sliding along it.

A model has been developed for volume removal due to the action of the abrasive water jet which is based on observations obtained by high-speed photography and SEM [Hutchings 1979]. He also defined two modes of cutting. One is cutting deformation and the other is ploughing deformation as shown in Fig. 1.8. As can be seen the ploughing deformation mode works best with blunt shaped abrasive particles. It is noticed that as the abrasive particle interacts with the target material, a lip of material is formed. However, not every abrasive particle will "plough" into the material. Some may rotate in the opposite direction in which case the Type II cutting profile is valid.

A theoretical model which tells about the weight loss as well as degree of lip formation using the single impact experiments [Sundararajan 1983a]. The model presumes that the lip formation occurs due to deformation in the localized regions near the surface of the target and lip is taken out either by inertial-stress-induced tensile fracture or by separation across adiabatic shear bands formed at the base of the lip. He used the single impact data's for brass, copper, nickel and thoria dispersed nickel targets. Sundararajan [1983b] had proposed another theoretical model which implies the erosion by normal incidence of the impact which uses a criterion for critical plastic strain to determine when the material will be removed. The term critical plastic strain is characterized as the strain at which the deformation in the target material localizes and causes in the lip formation. Brach developed an analytical model for the energy loss experienced by rigid particle impacting the target surface at any impinging angle [Brach 1997]. He assumed that the energy loss by the solid particle during impact is proportional to erosion rate and demonstrated that the erosion effect will be brittle (highest erosion rate at normal incident of particle) or ductile (highest erosion rate at glancing impact angles of particles) depending on angle of impact.

Hutchings and Levy [1989] have discussed the mechanisms of erosion in ductile metals undergoing impingement of solid particles and studied the various changes arising due to local rise in temperature. They observed that heat conduction plays a significant role in decreasing the maximum temperature rise. They described the observed erosion mechanisms in three different phases, which happened sequentially at any location. According to them, in the steady state condition all phases take place simultaneously at different points over surface of target. In the starting phase a crater is formed by an impacting particle and target material undergoes extrusion or displaced from the crater and ultimately forms lip. In the second phase the subsequent impacts of particles lead to deformation of the displaced metal; this may cause lateral displacement of the material and can be accompanied by some ductile fracture in localized region with heavily strained. Finally when the impact rate is very high, the displaced material undergoes so severely strained and then detached from the surface of target material.

They reported this type of erosion mechanism as the platelet mechanism defined by Levy [1981] and differs from the micro cutting model proposed by Finnie [1960]. He postulated that in many times the striking of most of the particles is essential in order to take out a fragment from the surface of metal [Brach 1988].

Sundararajan [1991] developed a model which is applicable for all impacts angles as an extension of previous model [Sundararajan 1983] suggested specifically for erosion due to normal impact of particles. The model [Sundararajan 1991] is based on the assumption that plastic flow in the localized region below the particle impact is accountable for lip formation and thus erosion. He reported that it is capable of justifying the various observations during the experiment related to erosion, namely the effects of impact velocity, impact angle, material properties and particle shape and size. Sundararajan and Shewmon [1987] developed a model for the oblique impact of hard ball to ductile target material. The model correctly estimates the dimension and volume of the crater, and also their variation with velocity and impact angle. It also enables prediction of the energy absorbed per impact.

1.3.3 Erosion mechanisms of brittle materials

In case of brittle fracture caused by the impact of an erodent particle, the loss of the material is done by the formation and intersection of cracks. If the mechanism responsible for material removal by brittle fracture, there is also be some deformation of the material around the point of contact of the erodent particle. The magnitude of cracking done by impact of particle is most intense when the particle impacts normal to the surface and erosion rate is more rapidly increased (Fig. 1.4). Erosion rate drops monotonically when the impact of the particle deviates from 90^o, in contrast to the behaviour when erosion occurs by cutting and ploughing mechanisms (curve for ductile material in Fig. 1.4).

Sheldon and Finnie [1996] have proposed another model which is based on the assumption that erosion take places due to Hertzian contact stresses during impact. They considered that the surface and particle experienced a dynamic force between them that resulted in removal of volume of material. They also concluded that the fracture at the surface is depending on volume of material constrained in the primary erosion zone in relation to the surface and volume flows. The theory by Evans [1976] explains erosion occurs due to crack behavior during single particle impact events, and leads to lateral crack formation during erosion. It also assumes that the amount of material removed by each impact gives the erosion rate.

Zambelli and Levy [1981] investigated he erosion behaviour of brittle oxide layer on ductile substrates. They interpreted the damage of the NiO layer using assumptions based on the concepts of fracture propagation. The removal of NiO duplex layer in a two step mechanism. The first step of mechanism involves the indentation of plastic flow and lateral crack growth in the columnar outer layer [Zambelli 1981]. While, pits are produced from Hertzian cone fractures formed in the inner layers, which enlarges the pits in the second step. The greater velocities, impact angles and particle sizes result in removal of the thinner oxide layer and bare Ni within few seconds. It is suggested that the bond strengths between the two scale layers i.e. oxide layer and metal substrate are proportional to the erosion behaviour.

It was pointed out that the angular dependence of erosion is not a characteristic of the material alone, but depends also on the conditions of erosion [Hutchings 1992]. For example, although most metals eroded by angular particles do show typical ductile behaviour of erosion (Fig.1.4), erosion by spherical particles, even of a ductile metal such as mild steel, can lead to apparently brittle angular dependence, although wear still occurs by purely plastic processes. Alloys which exhibit low ductility and high hardness may also show maximum erosion rate at normal incidence; an example, for a low alloy bearing steel after different heat treatments, is shown in Fig.1.9. At comparatively low hardness and high ductility, the steel shows characteristic ductile behaviour, while with high hardness it shows apparently brittle behaviour, although microscopic observation shows no sign of brittle fracture.

1.3.4 Erosive wear resistance of materials

Material characteristics exert a strong effect on erosive wear and have been extensively studied [Gahr 1988]. In a similar manner to abrasive wear, it is found that improvements in mechanical properties do not always coincide with superior erosive wear resistance. For example, erosive wear rates may increase when a material is deliberately hardened. An illustration of this rule is provided by the comparison of the relative erosion resistance of metals as a function of impingement angle. When the impingement angle is shallow, hardened steel shows lower erosion than a soft steel; the converse is true at high impingement angles. This is illustrated in Fig. 1.10, where the erosive wear rate, at two different impingement angles of 15^o and 90^o, is shown as a function of material hardness for various metals and grades of steel hardness. The abrasive used was silicon carbide of diameter about 1 mm impinging at a velocity of 30 (m/s).

Heat treatment of steel to increase hardness improves erosive wear resistance at low impact angles but lessens the erosive wear resistance at high impact angles. There is no general recipe for a high level of erosive wear resistance. Because of the two different erosive wear protection mechanisms that can take place, high wear resistance can be achieved by more than one type of material. In some cases the material can be extremely hard and tough so that the impacting particle is unable to make any impression on the surface. Alternatively, the material can be tough but with an extremely low elastic modulus so that the kinetic energy of the particles is harmlessly dissipated. These contrasting wear protection mechanisms are illustrated in Fig. 1.11 [Meng 1995]. Rubber is generally believed to provide good erosion resistance by elastic absorption of particle energy although this has not been demonstrated experimentally. It has been shown that the first particle impact causes no visible damage to a rubber surface and that wear depends on slow fatigue processes [Arnold 1990].

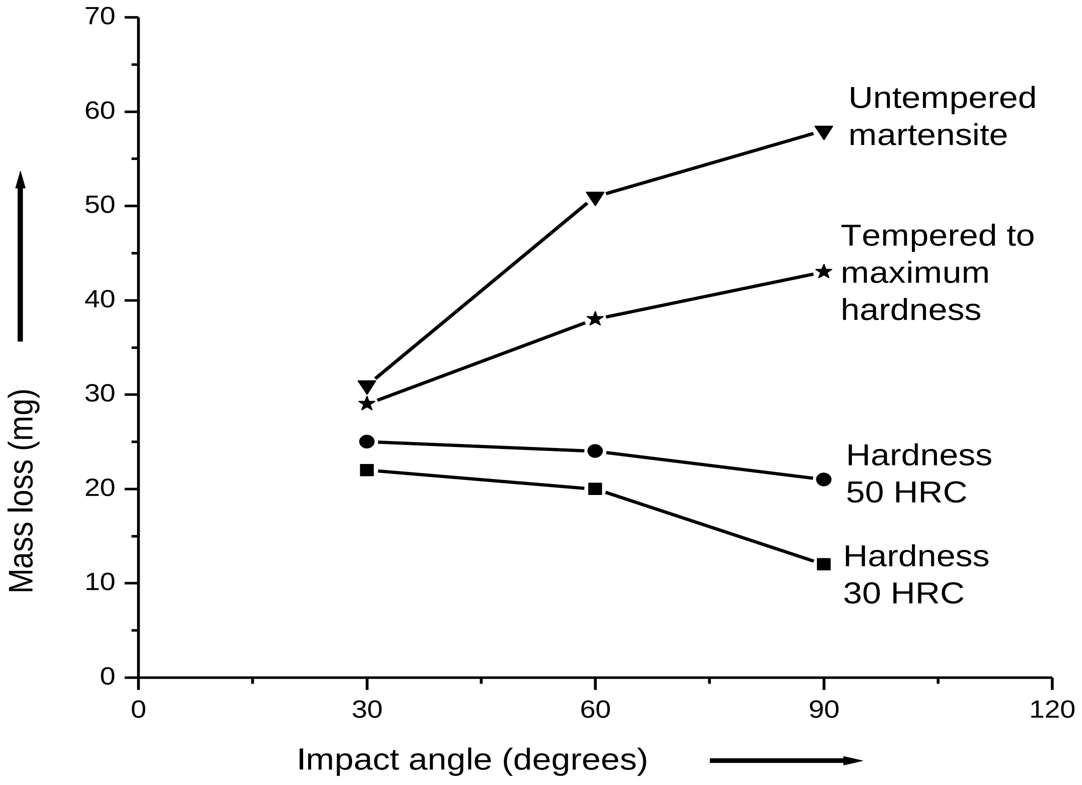

Fig. 1.9 Erosion rate of AISI 52100 steel samples (1%C, 1.5%Cr) with different microstructures as a function of impact angle. Silica particles were used at 153 ms^{-1} [Arnold 1990]

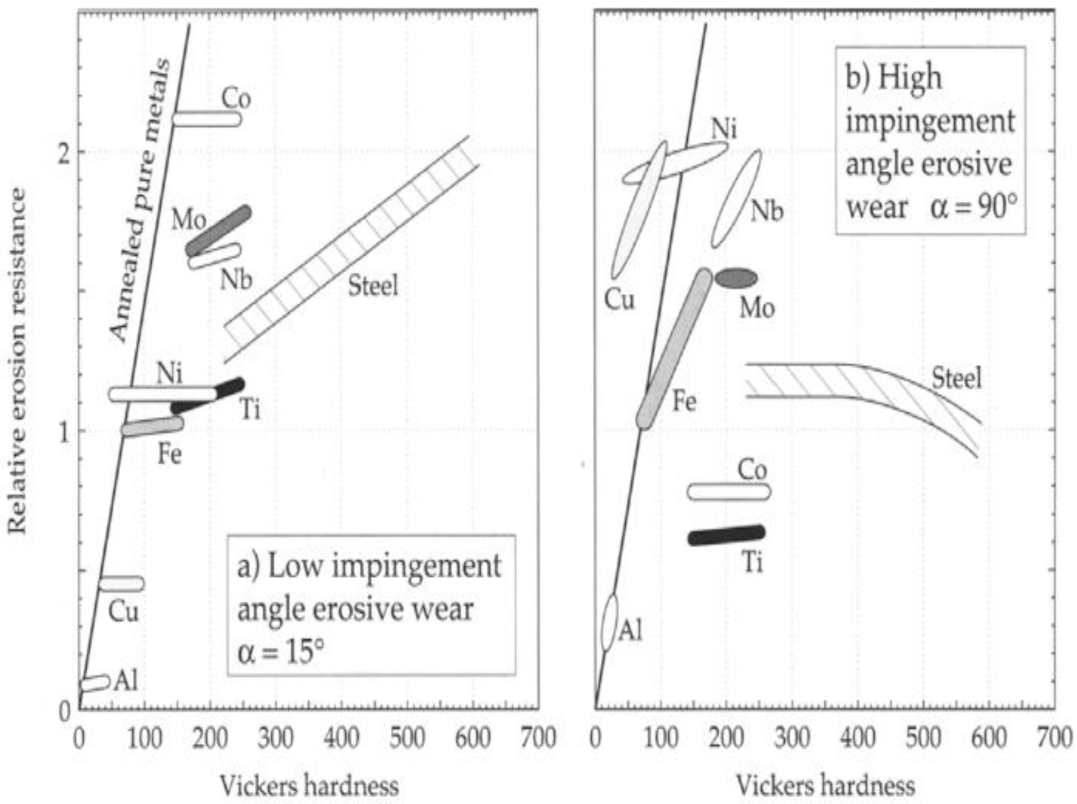

Fig. 1.10 Effect of primary material characteristics and erosion parameters on erosion rate [Gahr 1988].

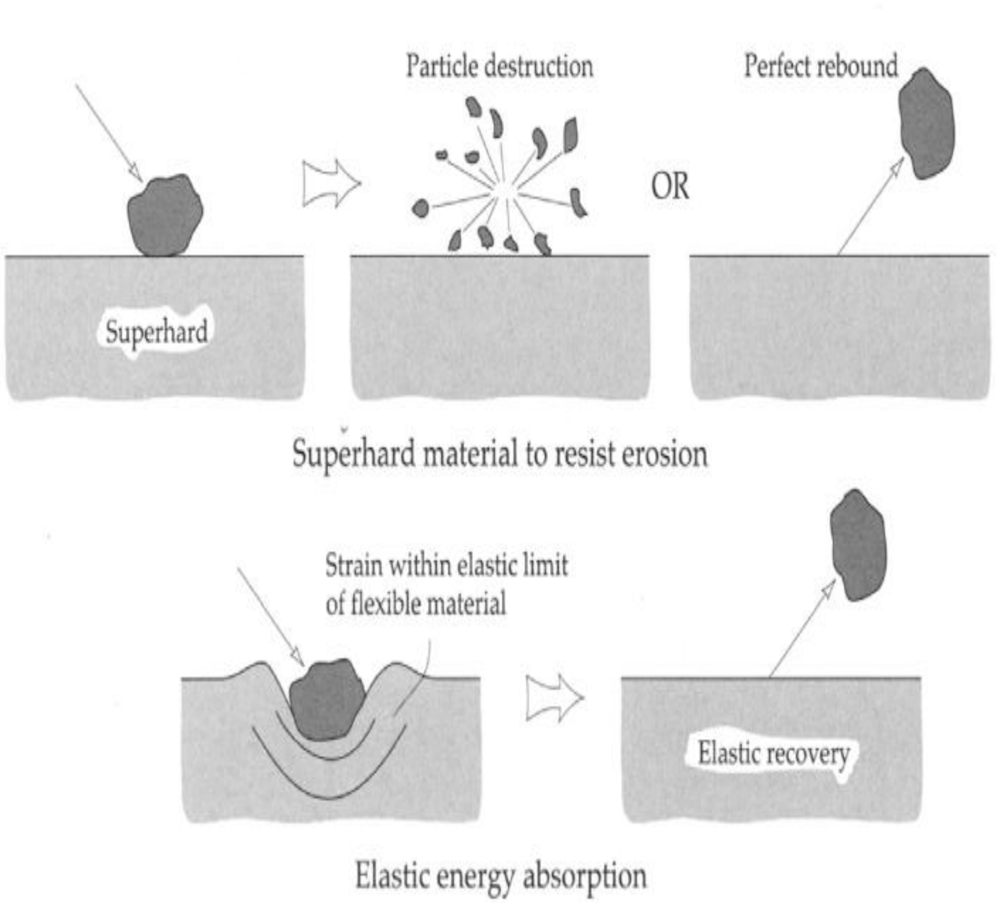

Fig. 1.11 Comparison of the high and low elastic modulus modes of erosive wear protection [Stachowiak 2006].

The choice of erosion resistant material may also be compromised by other considerations such as operating temperature or material transparency. Clearly, temperatures in excess of 200°C preclude polymers from service, but if a transparent material is required for a specific application then metals are not particularly useful. For example, materials for aircraft windscreens, apart from being transparent, are required to be resistant to high speed erosion by sand, dust and rain. Rao and Buckley [1986] found that polymethylmethacrylate is the best candidate for this application since it is both tough and shows a minimum of transparency loss by erosion damage.

1.3.5 Erosive wear resistance of steels

The literature available on the effect of steel microstructure on erosive wear rates suggests that ductile steel is the most wear resistant. Hardening of steel to form martensite offers little improvement except at very low impingement angles, and the formation of massive or lamellar carbides reduces erosive wear resistance. The selection of steel for erosive wear minimization is therefore different from the case of abrasive wear. For low alloy carbon steels, the ferritic phase with sufficient spheroidal carbide inclusions to induce strengthening is very effective against erosive wear [Levy 1981]. Pearlitic steels show inferior wear resistance to spheroidized steels. The erosive wear of steels shows the classical ductile erosion characteristics, i.e., a maximum wear rate at low impingement angles with subsurface and surface cracking [Levy 1981]. This suggests that the erosive wear resistance of steels is limited by a lack of ductility. For very soft erosive particles such as coal, the inclusion of carbides promotes wear resistance slightly [Sargent 1986]. Alloying of steel or cast iron to obtain a microstructure containing a significant amount of retained austenite is an effective means of reducing erosive wear. Adding about 2.5 wt% of silicon to 0.7 wt% carbon steel or about 0.45 wt% of silicon to 2.54 wt% cast iron results in good erosive wear resistance [Shah 1986a, 1986b]. The optimum heat treatment of this steel or cast iron includes a relatively long austempering time where all the martensite is removed and only retained austenite and bainitic ferrite are present. As a general rule, however, ductility rather than hardness should be enhanced in steels for improved erosive wear resistance.

1.4 Cavitation erosion

Cavitation is defined by Dular et al as the condition when a liquid reaches a state at which vapour cavities are formed and grow due to dynamic-pressure reductions to the vapour pressure of the liquid at constant temperature [Dular 2006]. In a flowing liquid, these cavities are subjected to a pressure increase that stops and reverses their growth, collapsing implosively and disappearing. The violent process of cavity collapse takes place in a very short time of about several nanoseconds and results in the emission of large amplitude shock-waves [Avellan 1989]. A high-speed reentrant liquid micro-jet directed towards the boundary can also occur for cavities collapsing close to a solid surface [Philipp 1998]**.** If the amplitude of the resulting pressure pulse is larger than the limit of the material mechanical strength, a hollow or indentation of several micrometers called ‘‘pit’’ will be formed on the surface. If an accumulation of pits takes place in a narrow area, the material is finally eroded and mass loss occurs due to the repetitive action of the cavity collapses. In a flowing liquid, these cavities can take different forms that can be described as travelling bubbles, attached cavities or cavitating vortices. Cavitation erosion is usual damage phenomenon in flow handling parts of hydraulic turbines, and service life and capability of such parts are reduced by the damage [Karimi 1986]**.**

1.4.1 Mechanism of cavitation erosion

The characteristic feature of cavitation is the cyclic formation and collapse of bubbles on a solid surface in contact with a fluid. Bubble formation is caused by the release of dissolved gas from the liquid where it sustains a near-zero or negative pressure. Negative pressures are likely to occur when flow of liquid enters a diverging geometry, i.e., emerging from a small diameter pipe to a large diameter pipe. The down-stream face of a sharp sided object moving in liquids, e.g., ship propeller, is particularly prone to cavitation. The ideal method of preventing cavitation is to avoid negative pressures close to surfaces, but in practice this is usually impossible[Dular 2015].

When a bubble collapses on a surface, the liquid adjacent to the bubble is at first accelerated and then suddenly decelerated as it collides with the surface. The collision between liquid and solid generates large stresses which can damage the solid. Transient pressures as high as 1.5 GPa are possible. The process of bubble collapse together with experimental evidence of a hole formed in a metal surface by bubble collapse are shown in Fig. 1.12 [Karimi 1986]. The cavitation crater, shown in Fig. 1.12, was produced on the surface of indium which is soft. Harder materials such as ceramics are unlikely to form a deep hole under the same conditions. Cracking and spallation are the predominant modes of wear for hard brittle materials. Almost all materials suffer some kind of subsurface damage by cavitation erosion; and accumulated work hardening and crack formation are commonly observed [Trethewey 1988]. In some cases when the cavitation is intense, the density of holes may be sufficient to reduce the worn material to a porous matrix or 'sponge'. Although cavitation involves a similar process of collision between a liquid and a solid as occurs in erosion by liquids, however, there are some significant differences. Cavitation erosion is a much milder process than erosive wear. In cavitation wear particles are detached per millions of cavitations whereas only a few thousand impacts by droplets are enough to cause erosive wear [Preece 1980]. Cavitation wear has an 'incubation period' like erosive wear but the weight gain found in erosive wear is not possible unless the cavitated material absorbs liquid.

Cavitation wear can be accelerated by the simultaneous occurrence of erosive wear, in other words synergetic interaction between these two wear mechanisms is possible. If the cavitating fluid contains erosive particles, then the collapsing bubbles cause the particles to hit the worn surface at high velocity. The rate of wear in synergetic erosion is higher than either cavitation or erosion alone. For example, this phenomenon takes place in hydraulic turbines operating in sandy water [Jin 1986]. The turbine, operating at a head of 900 m and utilizing water containing fine silt (<0.060 mm), undergoes mild erosion damage at the needle tip after 300 hrs of operation, as shown by Fig. 1.13(a). It was because of the strong turbulence near the tip.

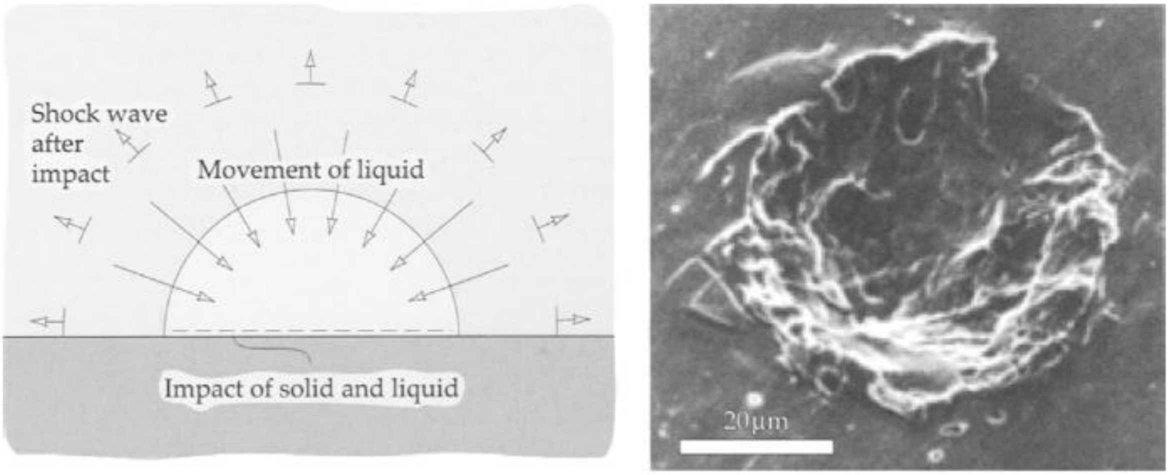

Fig. 1.12 Mechanisms of cavitation wear (a) mechanism of bubble collapse and (b) experimental evidence of damage by cavitation to a metallic (indium) surface [Karimi 1986].

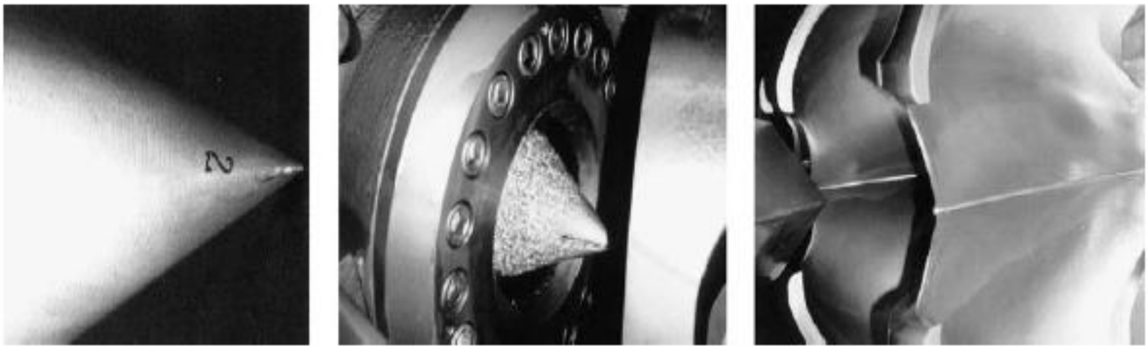

Fig. 1.13 Synergetic erosion in a Pelton turbine (a) (left) Initial stage: silt erosion on needle tip (300 h), (b) (middle) subsequent synergetic erosion (600 h) on needle tip, (c) (right) no noticeable erosion on buckets. Material: stainless steel (13Cr -4Ni) [Li 2006].

However, owing to the initial damage to the very streamlined and smooth surface, subsequent cavitation set in, which acted in concert with the silt erosion process, significantly enhancing the damage rate. Only after a similar time interval of operation, did the resultant damage to the tip become very severe such that the needle had to be replaced, as shown by Fig. 1.13(b) [Li 2006].

Taking the components of a turbine working in silt-laden water as an example, in most cases there are stagnation points (lines) on the bodies immersed in the flow. These stagnation points will be severely eroded owing to the impingement of particles at large angles ($\approx 90^{\circ}$). This might be the initial cause of erosion, following which cavitation usually sets in owing to the deterioration of the streamlined profile. Then the synergetic erosion starts, such as in the example shown above, referring to Fig.1.13. Alternatively, when cavitation already exists, the synergetic erosion starts from the very beginning. However, whether it is a subsequent phenomenon or not, the synergism mechanism is virtually the same [Li 2006].

1.4.2 Cavitation erosion resistant materials

A basic determinant in the choice of material for protection against cavitation erosion is the physical scale of the device where the cavitation takes place. Cavitation can occur in components ranging from propellers to dam spillways. For large-scale structures, concrete based materials are often used, e.g., concrete reinforced with chopped steel fibres, polymer impregnated concrete or concrete coated with epoxy resin. More information on these materials can be found elsewhere [Hattori 2008, Rao 1988]. A material with good cavitation wear resistance is rubber since its low modulus of elasticity allows the bubble collapse energy to be dissipated harmlessly.

A basic feature of cavitation is its preferential attack on the weakest phase of a material. An example of this is found in the significance of graphite inclusions on the cavitation wear of cast iron. The graphite regions provide the weak phase for crack initiation and increase the erosion wear by brittle fracture [Okada 1983]**.** A similar process affects cermets which often contain a hard material such as tungsten carbide particles surrounded by a softer metallic matrix. Cavitation can dislodge the tungsten carbide by gradual removal of the surrounding matrix. Heathcock et al have observed the improvement in cavitation erosion resistance, which is dependent on the properties of the binder rather than the tungsten carbide [Heathcock 1981]. The material which exhibits good erosion resistance should have uniform microstructure without much difference in the mechanical behavior of the phases. The mechanism of cavitation wear in multi-phase materials is schematically illustrated in Fig. 1.14.

Of the ferrous metals, stainless steels exhibit better cavitation resistance than cast iron. Plain carbon steels are not often considered as materials providing protection against cavitation erosion. With stainless steels, the ferrite phase is inferior to the austenite phase and the martensitic phase has the best resistance. Austenitic chromium-manganese-nitrogen stainless steels (Cr-Mn-N) shows better resistance to cavitation than conventional chromium-nickel-molybdenum stainless steels. The additional benefit of this steel is the substitution of manganese and nitrogen as alloying elements reduces the cost of the stainless steel. It is believed that the pronounced work hardening characteristics of the austenitic (but not ferritic) Cr-Mn-N stainless steels helps in improving the resistance to cavitation wear [Liu 2003]. Hadfield steel or the manganese steels offer the more resistance to cavitation wear of the austenitic steels. High nitrogen austenitic steels (HNAS) provide excellent cavitation erosion resistance among the recently developed materials. HNAS composed of nitrogen content more than 0.4% and low carbon contents, shows good combination of yield strength with toughness and good ductility. During the impact of bubble, the high work hardening ability of these steel is attributed to its high resistance to cavitation by HNAS [Fu 2001].

Cobalt alloys like 'stellite' are especially useful in more severe cavitation problems. Karimi and Martin have pointed out that cobalt shows more resistance to cavitation erosion as compared to solid particle erosion. During cavitation the ductile material experiences plastic deformation and dynamic recovery and work-hardening are key characteristics of plastic deformations [Karimi 1986]. Materials which have more stacking fault energy (SFE) show fast dynamic recovery and poor strain-hardening. For alpha aluminum bronzes, the stacking fault energy is inversely related to resistance to cavitation erosion [Zhang 2002]. Thus, for alpha aluminum bronzes it is clear that, plastic deformation due to bubble impact is important and that the energy of impact of bubble is not entirely consumed by plastic deformation.

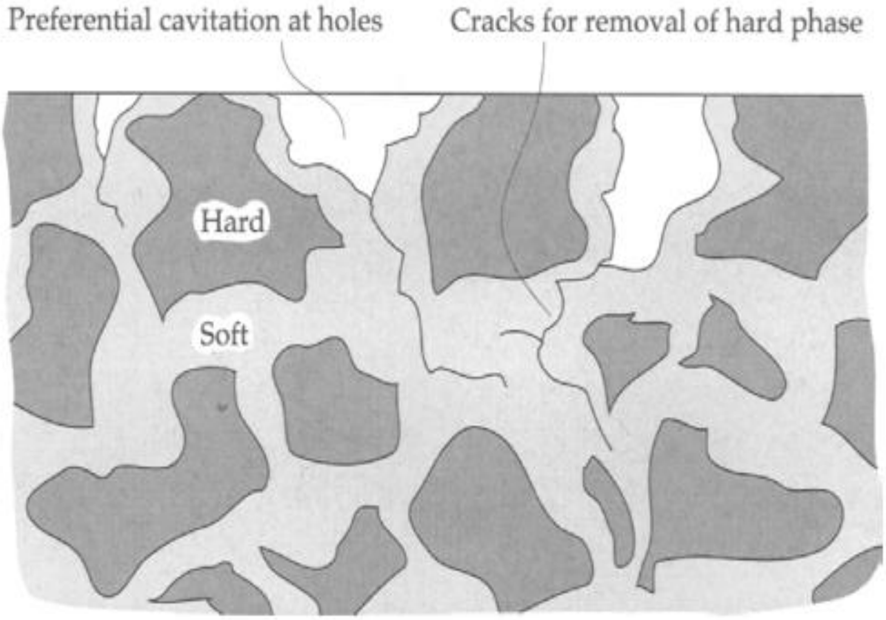

Fig. 1.14 Preferential attack by cavitation of the weaker phase in a microstructure [Stachowiak 2006].

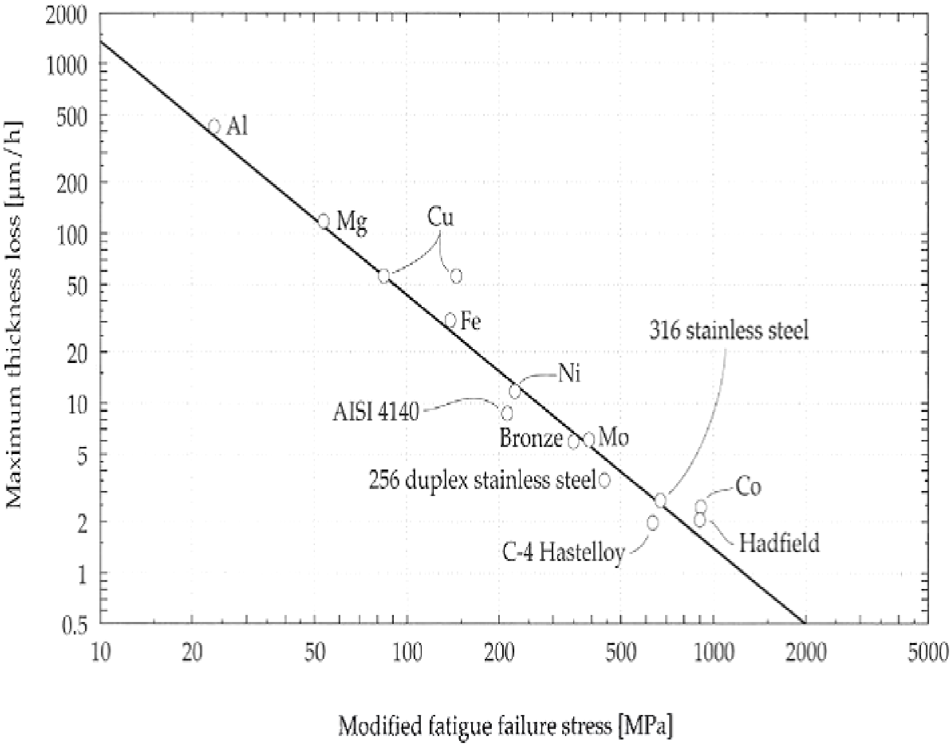

Fig.1.15 Relationship between the cavitation wear resistances expressed in terms of modified fatigue failure stress and maximum thickness loss [Head 1970].

Cavitation erosion is fundamentally a fatigue-type damage process which permits some useful comparisons of the relative wear resistances of metals based on metal fatigue theory [Head 1970]. It is found that the erosion rates in cavitation testing of different pure metals correlate well with a fatigue strength parameter which is defined as the product of the exponent of stress increase during cyclic plastic strain and the nominal fatigue failure stress at zero cycles. The relationship between the cavitation erosion resistances (in terms of maximum thickness loss) and modified fatigue failure stress is shown in Fig. 1.15.

1.5 Factors affecting erosion

The loss of the material during erosion is dependent on many factors that include metallurgical as well as operating parameters [Naim 1986, Goretta 1993, Richman 1990, Hutchings 1992, Jiang 1995, Zhou 2005]. The main metallurgical factors affecting erosion are mechanical properties and microstructure of target material.

1.5.1 Mechanical properties

Metal hardness and impact strength are among the most important characteristic to consider when selecting the metals for minimum erosion. Hardness appears to be a dominant factor governing the erosion resistance of various materials in specific applications [Richman 1990, O’Flynn 2001]. In general wear resistance tends to increase with hardness and it decreases as impact strength increases [Sharma 2015]. But in case of erosion, high hardness increases the erosion rate and it decreases as impact strength increases. This is an important relationship in application that requires both wear resistance and impact resistance. If the material is sufficiently hard, it will have more resistance to erosion and also resistance to crack propagation. The material having higher impact strength poses more resistance to erosion. The impact strength of metals is closely related to the crack propagation rate, which also affects the rate of erosion.

Goretta et al analyzed the solid particle erosion behaviour of AISI 4140 heat treated steel which results in the improvement in hardness of 288-650 HV [Goretta 1993]. They concluded that erosion rate was not dependent on hardness for HV ≤ 365, but increased with HV ≥ 365. Divakar et al have studied the surface hardness effect on the erosion behaviour of AIAI 316 steel. They reported that hardness improvement results higher erosion resistance of AIAI 316 steel due to compressive stresses, which is induced in to the target material by the cold rolling [Divakar 2005].

The work hardening behaviour of the target material during solid particle impact also plays a significant role. The work hardening characteristics of austenitic grades of steels is usually responsible for their wear resistance [Goretta 2001]. For example, the development of wear resistant Hadfield steel is mainly based on its strain hardening characteristics. Richmann and McNaughton have described the cavitation erosion behavior of metals and their relation with the mechanical properties. They observed that the fatigue strength coefficient (σ_f) is most important property to determine the cavitation erosion resistance which leads to differences among materials. These correlations are further enhanced by adding the work hardening exponent ‘n’ in a combined parameter “$\sigma_f n$” [Richman 1990].

Levin et al have reported that tensile toughness is indicative of the ability of a material to absorb energy of the abrasive particles impacted and have shown that a material having higher tensile toughness possesses higher erosion resistance [Levin 1999]. O’Flynn et al have reported that increase in the erosion rate as $1/U_T\varepsilon_u$ increases; where U_T is tensile toughness and ε_u is uniform strain. Thus, the erosion resistance increases as the product of uniform strain (strain up to UTS) and tensile toughness increases [O’Flynn 2001].

1.5.2 Microstructures

Metallurgically hardness and microstructures are commonly interrelated and both have importance as factors in resistance to erosion. Increasing the carbon content of steel results in change in microstructure that increases hardness and decreases ductility, impact strength and tensile toughness. The maximum hardness depends on amount of carbon in the steel and the amount of martensite. Carbon content also affects erosion resistance through formation of various carbides [Sharma 1996].

Effect of microstructure on erosion has been studied by various authors [L´opez 2005, Levy 1981, Kishore 2005, Hodgson 1996]. The effects of the microstructure of two ductile steels on their behavior under solid particle erosion were determined by Levy. He presented that the erosion rate is directly related to the distribution of soft, ductile and hard, brittle phases. He again emphasized that within limits, the erosion rate is low for more continuous the ductile matrix. However, when the ductile matrix turns into the main phase and the strength of the steel is notably decreased, and becomes the dominant factor in erosion [Levy 1981]. Wang et al have investigated the corrosion- erosion resistance of 1018 plain carbon steel and 2.25Cr-1Mo steel, two most commonly used boiler tubing steels in various conditions, i.e. hot rolled, quenched-tempered, annealed, normalized and cold rolled at room and elevated temperatures using SiO, particles at velocity $V = 20\ ms^{-1}$ and impact angle $\theta = 30^o$ [Wang 1991]. They presented the similar observations reported by Levy that the effect of microstructure on erosion at room temperature depends on the distribution of soft, ductile and hard, brittle phases present in the steel, which determined their combination of strength and ductility [Levy 1981].

The microstructure of target material plays a significant role in the solid particle erosion. In solid particle erosion, the austenite phase is believed to be suitable component because (i) the high strength at the interface between austenite and carbide [Xi 1993], (ii) austenite is plastic and tough and (iii) localized strength of austenite increases with strain hardening [Soussan 1991]. In case of 21Cr-4Ni-N steel when hot rolled, the austenitic matrix becomes continuous and the strength raises, which play supporting role in erosion resistance [Tilly 1973].

Kwok et al have studied the cavitation erosion behaviour of alloys having duplex structures such as super duplex stainless steel (UNS S32760) and α + β brass (Cu–40%Zn) in 3.5% NaCl solution at 23°C using a 20 kHz ultrasonic vibrator operating at peak-to-peak amplitude of 50 µm and compared with that of austenitic stainless steel (UNS S30400). They concluded that cavitation erosion behaviour of α + β brass, S32760 and S30400 is significantly affected by the microstructure and the deformation mechanism of the alloys. They explained that for alloys with duplex structure such as super duplex stainless steel S32760 and α + β brass, the weaker phase is attacked preferentially. For α + β brass, α phase exhibit lower hardness than β phase, is attacked preferentially, whereas for S32760, ferritic (α) phase which shows strain rate sensitivity is attacked preferentially by brittle fracture mechanism. The interface boundary between the two different phases becomes the initiation locations for cavitation erosion and the damage covers the entire weaker phase. For austenitic stainless steel S30400, the starting point of the damage due to cavitation is at the twin boundaries by ductile fracture mechanism [Kwok 1998].

Bregliozzia et al have studied the cavitation erosion mechanisms of two austenitic stainless steels i.e. high nitrogen steel and AISI 304, in water at room temperature using a 20-kHz ultrasonic vibrator operating at peak-to-peak amplitude of 40 µm. They reported that the cavitation attack occurs preferentially at the grain boundaries and slip bands and leads to development of surface undulations. During cavitation erosion, the cracks generally initiate from these defects, which are characterized as the stress concentration sites. They explained that the material is primarily removed by ductile fracture mechanism. The high nitrogen steel, due to superior mechanical properties than AISI 304 steel, shows better cavitation erosion resistance [Bregliozzia 2005].

1.5.3 Operating variables

1.5.3.1 Effect of erodent velocity

The velocity of the erosive particle plays a significant role in the wear process. If the velocity is very low, the impact results weak stresses which are not sufficient for plastic deformation and wear occurs by surface fatigue [Stachowiak 2006]. When the velocity raises to higher value, the eroded material may plastically deform upon impact of particle. In this way, wear is caused by repetitive plastic deformation. At brittle wear response, the wear proceeds by subsurface cracking. The melting of the impacted region may occur for very high velocity (Fig. 1.3).

From medium to high velocities, a power law [Stachowiak 2006], can describe the relationship between wear rate and impact velocity:

$$dm/dt = kv^{n'} \qquad \text{…..(1.4)}$$

where m is the mass of the worn specimen, t is the duration of the process, k is an empirical constant, n’ is a velocity exponent. The characteristics of the erodent and target material determine the value of the exponent n’. It has been stated that ‘n’ varies in the range of 2–3 for polymers behaving in a ductile manner, while for composites of polymers which show brittle character, the value of ‘n’ lies in the range of 3–5 [Roy 1994].

1.5.3.2 Effect of impact angle

The impact angle (θ) also has significant effect in solid particle erosion and is categorized as below [Divakar 2005]:

- Erosive wear at normal impact angles ($\theta \approx 90^o$)
- Erosive wear at oblique impact angles ($0^o < \theta < 90^o$)

The erosive wear behaves similar to abrasion at low angle because the particles have the tendency to across the worn surface after impact. A high angle of impact results erosive wear mechanisms as shown in Fig. 1.4 [Divakar 2005]. It can be seen in Fig. 1.4 that in ductile mode of erosion the removal of the materials is maximum at low impact angles whereas maximum erosion takes place at high impact angles due to brittle mode of erosion.

1.5.3.3 Effect of erodent characteristics

The main key factor of the erosion problem is related to the erodent characteristics. Variations in particle size and shape can lead to fundamental variations in the erosion response. In case of blunt or spherical erodent particles the plastic deformation is favourble, if the particles are sharp then brittle fragmentation and cutting are more likely to occur. A blunt particle has nearly spherical shape while a sharp particle has flat areas connected by corners having very small radii leading to erosive wear mechanism [Stachowiak 2006].

It is assumed that the erosion rate does not dependent on the particle size more than the critical value [Stack 1999]. This critical value is observed between 100–200 μm, however, it depends on the exposure conditions and interactions between the particle and target [Stack 1999]. Up to this critical value, experimental results showed that with increasing size of the erodent also the erosion rate increases. The existence of this critical value has been attributed to various factors [Stack 1999]. These factors are:

(i) Strain rate effects: It has been noted that strain rates are lower for larger than for smaller particles. This indicates that the target material stresses are increased when attacked with small particles.

(ii) Differential work hardening due to erodents of various particle sizes: It has been observed that a surface scale of range of 50–100 μm “hardens” more as compare to the bulk material. Hence, small particles will encounter a layer which is characterized by significantly higher flow stress in comparison to bulk material. For larger particles, it is easier to penetrate this thin layer. When the particle size is above the critical size, the effect of this layer should be negligible.

The influence of erodent hardness depends mainly on the mode of erosion mechanism occurring e.g. brittle or ductile. In the brittle mode the hardness of the particle has pronounced effect as compare to the ductile mode. It is usually believed that harder particle leads to higher wear rates than softer one, but it is not possible to detach hardness completely from other characteristics of the particle (e.g., shape). Even if the particle is hard, but relatively blunt, then it is unlikely to cause severe erosive wear [Stachowiak 2006].

With respect to the size and type of the erodent material, two trends may hold for harder and/or more brittle material. The erosive wear increases the higher the hardness of the erodent and the larger the erosive particle size are (until a level of saturation is reached in both cases) [Friedrich 1986]. In ductile polymers, however, the situation may be quite different. Due to the relatively low hardness no pronounced effects of changes in the hardness of the usually much harder erodent materials should be expected [Friedrich 1986].

1.6 Welding

Welding is one of the most commonly used fabrication process employed for joining of such material with varied section size in normal as well as in critical applications. Depending upon application, the integrity of weld joint is largely adjudged by its relevant properties. Weldability is in-built characteristics of material refers to its ability to be welded. Many metals can be welded, but some metals can easily weld as compare to others. It greatly influences the weld quality and is an important factor in choosing which welding process is used.

The cavitation and silt erosion damage the some areas of hydroturbines and the repair work is done by welding. Traditionally, on site repair work has been done by martensitic stainless steel filler metal whose chemical composition matches to base metal. These alloys have no longer erosion life. Frequently repair work ultimately leads to time consumption and increases repair cost [Li 2000]. The use of cavitation resistant surfacing (both as a preventative measure and to repair cavitation damage) remains one of the best and most economical ways to control cavitation on carbon steel and stainless steel, the predominant base materials used for turbine runners. The surface overlay of austenitic stainless steels is good option for erosion resistant. Due to its good weldability and mechanical properties [Santa 2002], the weld overlay hardface coating shows good abrasion resistance but the not appropriate resistance to erosive condition [Feliskovich 1994]. Feliskovich has also reported that hardness is not only responsible factor to improve erosion resistance. Weld overlay coating of 316L austenitic stainless steel shows good erosion resistance. Toughness, ductility and strain hardenability of the material also play significant role in erosion process [Ninham 1987, Hutching 1986, Levin 1998].

The development of different grades of austenitic stainless steel (ASS) by appropriate designing of chemical composition including minor alloying have resulted in applications in chemical, pharmaceutical, petrochemical and nuclear power industries [Padilha 2002, Basak 1995]. This has primarily happened due to its good mechanical and fracture mechanics properties over a long temperature range from -80^0 to 450^0 C. It has also superior resistance to corrosion in variety of environments in comparison to that of structural steel [Covert 2000, Peckner 1977, Folkhard 1984]. These unique properties are primarily achieved by keeping the carbon content at a significantly lower level and through substantial additions of chromium and nickel to iron, along with addition of other elements such as manganese, molybdenum and nitrogen [Padilha and Rios 2002, Hertzman 2001]. However, the acceptance of ASS in critical applications has been often questioned by its sensitivity to carbide precipitation ($M_{23}C_6$, $M_{11}(CN)_2$) [Harris 1975, Gill 1982, Cieslak,1984, Padilha 2002].

1.6.1 Nitrogen Added Austenitic Stainless Steel

Nitrogen alloyed austenitic stainless steels show several notable features like better mechanical properties at ambient as well as high temperatures, excellent corrosion resistance in various media, wear resistance and are promising materials to replace other more expensive materials [Basak 1995, Baldev Raj 2002,]. Alloying with nitrogen increases mechanism of strengthening due to lowering of the stacking fault energy and thus increases the yield strength of austenitic stainless steels, without any substantial loss of toughness [Vanderschaeve 1995].

1.6.2 Effect of chemical composition

Nitrogen behaves as a strong austenite stabilizer in the weld metal. Its marked influence through modified Schaffler diagram on different phase formation is as shown in Fig. 1.16. Through the addition of 1% N, a purely ferritic stainless steel is rendered completely austenitic as marked by arrow in the Fig. 1.16. This prediction was not fulfilling in the weld metal contain a higher amount of nitrogen and or manganese. Such predictions were found to be inaccurate. Thus the influence of nitrogen on weld metal was further evaluated by the researchers based on its influence on the δ ferrite content [Woo 2002]. Nitrogen coefficient (multiplication factor of N for the Ni equivalent in modified schaffler diagram) developed by various studies is shown in Table 1.2 [Okagawa 1983, Woo 2002, Shankar 2003].

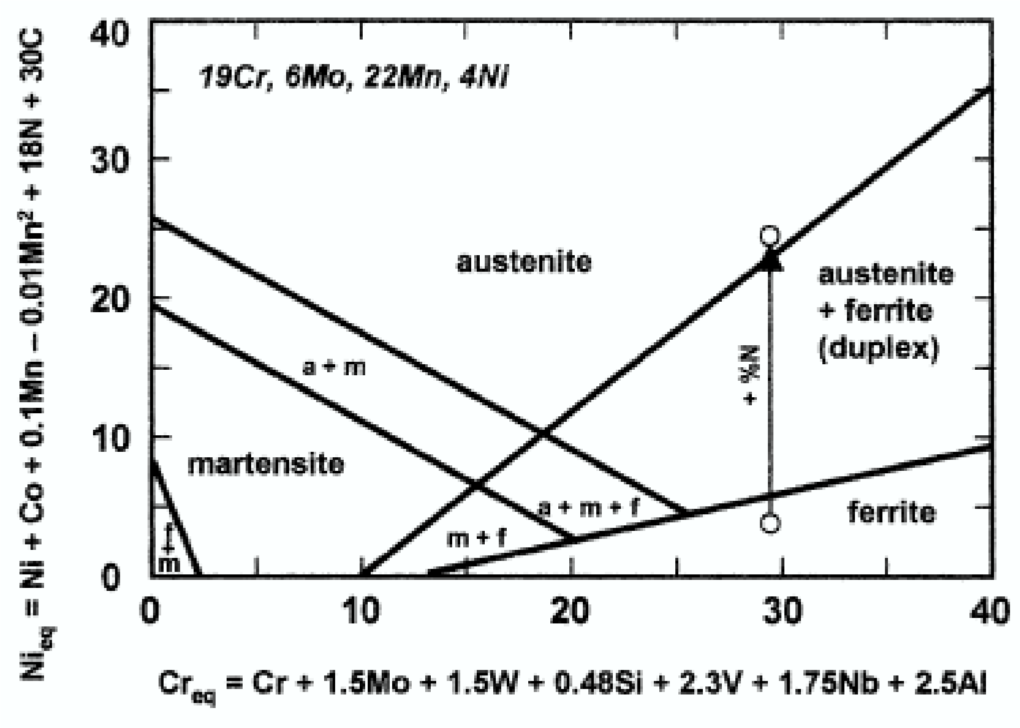

Fig. 1.16: Modified schaffler diagram for stainless steel weld metal [Woo and Kikuchi 2002].

Table-1.2: Various nitrogen coefficients determined in previous studies.

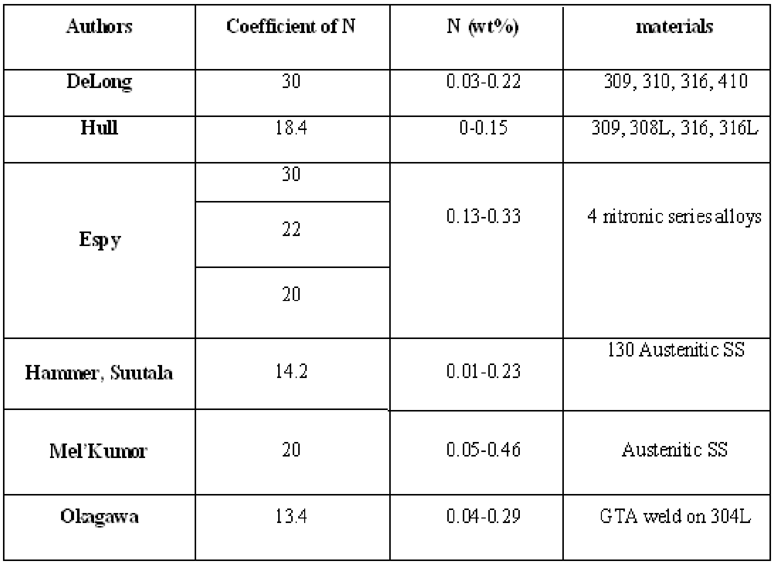

Authors	Coefficient of N	N (wt%)	materials
DeLong	30	0.03-0.22	309, 310, 316, 410
Hull	18.4	0-0.15	309, 308L, 316, 316L
Espy	30	0.13-0.33	4 nitronic series alloys
	22		
	20		
Hammer, Suutala	14.2	0.01-0.23	130 Austenitic SS
Mel'Kumor	20	0.05-0.46	Austenitic SS
Okagawa	13.4	0.04-0.29	GTA weld on 304L

Suutala has mentioned that the solidification mode of austenitic stainless steel weld metal containing up to 0.23% nitrogen can be described by using Hammer's equivalents. In this contrast, Okagawa reported that in nitrogen added type 304 welds, the nitrogen effect on ferrite content was smaller than that predicted by DeLong. He estimated that the nitrogen coefficient for nickel equivalent expressed as 13.4, which was considerably lower than the coefficient of 30 determined by DeLong. Espy reported that the nitrogen effect as an austenite stabilizer decreased as nitrogen content increased, and proposed the modified Schaffler diagram, in which the nitrogen coefficient varied from 30 to 20 with nitrogen content. The discrepancies in the nitrogen effect results in a serious drawback in developing proper weld compositions to obtain the desired ferrite content and its distribution. Hence, more systematic work is necessary to verify the nitrogen effect on solidification behaviours of stainless steel welds [Woo and Kikuchi 2002, Shankar 2003a]. Another drawback of non equilibrium diagram is that it does not take into consideration the influence of the cooling rate and aging heat treatments [Padilha and Rios 2002].

In weld joints precipitation of all the phases not capable of dissolving nitrogen are shifted towards longer times. This means that nitrogen shifts the beginning of sigma phase formation to higher chromium contents and to longer time [Folkhard 1984]. Secondly precipitation of M_6C will be favoured to the detriment of $M_{23}C_6$, because the former is able to dissolve more nitrogen than the latter. Nitrogen addition also sometimes favours formation of nitrides. In general nitrogen depletion of the matrix due to precipitation of nitrides can make austenite unstable. It can also make possible the formation of ferrite and sigma phase at aging temperatures [Padilha and Rios 2002]. On the other hand amount of δ ferrite in the weld metal is decreased by nitrogen addition in high nitrogen containing austenitic stainless steel resulting in increase in its susceptibility to solidification cracking [Shankar 2003b].

The addition of nitrogen affects not only the composition of the weld but also the kinetics of solid-state transformation characteristics of delta ferrite. This is expected to help in obtaining weld with low residual delta ferrite content without encouraging solidification cracking incidences [Hertzman 2001, Okagawa 1983]. Thus the solidification mode in unstabilised ASS can be controlled by nitrogen addition. However its level in weld metal depends on welding parameters, compositions of filler metal and base metal and other metallurgical factors.

1.6.3 Weld deposit

In weld metal, the desired phase ratio is obtained by combination of nitrogen and increased nickel content. Nitrogen resides in weld metal in the following forms (i) interstitial nitrogen dissolved in the lattice structure – may collect around lattice defects, (ii) combined nitrogen present as nitrides, and (iii) blocked nitrogen in pores. It is the first two forms of nitrogen that affect the metallurgical behaviour of the weld metal [Ogawa 2002]. It has been commonly observed that 18-8 type stainless steel weld metal which maintains the $\delta + \gamma$ dual phase at 0.16 % nitrogen content shows very good weldability with no porosity or loss of nitrogen along with increase in mechanical properties. It is primarily caused by localized deformation through minimized segregation as well as reduction in secondary dendrite arm spacing resulting the microstructure finer [Ogawa 1984]. Nitrogen is essential in order to obtain good weldability in these steels.

It has also been reported that dissolved nitrogen in the weld metal is significantly influenced by welding variables. Under certain conditions, it can reduce the amount of δ-ferrite in a reheated weld metal microstructure below that adequate to prevent liquation cracking. In summary, it appears that the effect of nitrogen in weld metal containing ferrite (or ferritic solidification mode) has better weld properties as well as susceptibility to liquation cracking. The shielded metal arc welding has maximum flexibility and can weld many metals in all positions. There is definite relationship amongst the welding current, size of welding electrode and welding position.

Chemistry of weld metal primarily depends upon proper selection of filler metal. The filler metal should not only provide good weldability, but also produce weldments having mechanical and corrosion properties equivalent to those of the base metal [Han and Sun 1999]. To produce the sound weld joints, microfissuring tendency should also be controlled by maintaining purity of consumable composition such that amounts of ferrite in the weld metal vary ferrite number (FN) from 3 to 8 [Cui 2004]. A higher nominal ferrite content does not ensure uniform distribution throughout the weld metal [Brooks 1983]. Filler metals in general for austenitic stainless steels should either match or exceed the alloy content of the base metal. If a filler material of the correct match is not available, filler with higher alloy content being normally should be used.

The design, prediction of performance and safety analysis of austenitic stainless steel welded components generally require a complete knowledge of their physical and mechanical properties. In particular, it would be useful to have at one's disposal more information on the mechanical properties of the weld deposited metal as influenced by its material variability. This is characterized by microstructural variations between the parent metal (usually fully austenitic) and the weld metal (containing various amounts of δ-ferrite retained at room temperature). The presence of δ-ferrite in the austenite matrix is necessary to prevent cracking during welding according to a well-established practice [Piatti 1990].

Chapter 2

Formulation of the problem

In order to meet ever increasing demands of electrical power in India, it is essential to improve the working life of hydro electric power plants. Himalayan region has huge amount of hydro potential but silt concentration is reported to be higher. It is observed that in hydro electric power plants, underwater components get severe damages due to higher cavitation and silt laden water. Cavitation erosion occurs at high velocity and low pressure areas which damage the flow handling parts of hydro turbine. The erosion due to silt particles is a result of mechanical wear of components on account of dynamic interaction of silt with wearing surface. Extensive research has been carried out in last decade to understand the mechanism of material removal by cavitation erosion and silt laden water. It is reported that synergetic effects of cavitation erosion and silt laden produce severe damages in underwater parts of hydroturbine.

Most of the hydroelectric power plants in Himalyan region are trapped in silting problem which faces regularly damages due to excessive silt in water. Silt particles settle down in a reservoir by sedimentation technique. Sedimentation techniques have not provided satisfactory results. Silt particle size below 300 µm is major constituent in silt laden water and complete elimination of this constituent is not possible. Furthermore, deposition of this constituent in reservoirs reduces the storage capacity. The technology of silt elimination by sedimentation now appears saturated and no further benefit is expected from sedimentation control technique. So the sedimentation management is a big challenge especially in Himalayan region.

Austenitic stainless steels have great potential to replace the currently used 13/4 martensitic stainless steel due to its good mechanical properties, corrosion resistance, weldability, and in-situ strain hardenability. The addition of nitrogen in these steels further improves mechanical properties and leads to cost reduction. Nitronic steels may be suitable alternative to presently used 13Cr-4Ni martensitic (hereafter called13/4) steel.

Extensive work has been carried out to develop repair welding of 13/4 steels under water parts. For 13/4 martensitic steels, pre (avoid crack formation) and post (elimination of stresses) weld heat treatment are required to avoid the formation of carbides and intermetallic compounds. The weldability of this steel is, however, poor and cracks are invariably formed in the weld metal and heat affected zone (HAZ). The welded parts are very sensitive to silt laden water attack and also act as point of stress concentration resulting in acceleration in erosion rate in the HAZ portion. Thus repair of worn out martensitic steel components is very difficult.

Objectives

1. Development of erosion resistance Nitronic steel.
2. To study the effect of heat treatment on microstructure and mechanical properties of Nitronic steel.
3. Identification of the formation of different phases in the system by X-ray diffraction
4. Characterization of mechanical properties (such as tensile, impact, hardness) of heat treated steels.
5. Comparative erosive wear study of heat treated of 13/4, 23/8N and 21/12N steel.
6. To optimize the processing time and temperature which makes feasible mechanical
7. Properties and wear rate.
8. Weldability of Nitronic steel: the microstructural features, mechanical and wear Properties.

In this research attempts are made to evaluate 23Cr-8Ni-0.31N and 21Cr-12Ni-0.19N (henceforth called 23/8N and 21/12N) steels for erosion resistance purpose. Comparative study of erosion behaviour of 13/4, 23/8N and 21/12N steels has not been reported till now. In 23/8N nitrogen alloyed austenitic stainless steel, nitrogen improves mechanical properties, corrosion resistance, and reduces the amount of chromium carbides at grain boundaries. Nitrogen also improves austenitic stability by solid solution hardening and decreases stacking fault energy which results improves work hardening ability of steel. In literature it has been reported that austenitic stainless steel may have good erosion resistance than martensitic stainless steel due to its high work hardening ability.

Planning of experiments

The samples of 13/4 and 23/8N steels were obtained from M/S Star Wire (INDIA) Ltd. Ballabhgargh (Haryana). The samples were heat treated and rolled to have modification in microstructure and mechanical properties. For microstrctural studies, the section of various samples were ground to 1500 grit emery paper and polished with alumina powder 0.5µm finish and observed under optical microscope and scanning electron microscope equipped with EDS. The mechanical testing of the samples were performed using tensile test, cavitation and solid particle erosion. The tensile toughness and strain hardening exponent were measured and correlated with the erosion behavior of the material. In solid particle erosion test, a high speed air blast erosion rig was used at impingement angles 30^o and 90^o. The alumina powder with particle size 53-75µm and angular shape was used as erodent. The erosion behavior was studied by analyzing the morphologically changes occurred at different angles. The same studies were repeated for heat treated, rolled samples of both the steels. The cavitation erosion tests were performed to study the erosion behavior of the underwater parts. The specimen of as received, heat treated, rolled and weld overlay conditions was tested under an ultrasonic processor with peak to peak amplitude 50µm at frequency 20±0.5 KHz was used to study the cavitation erosion.

Besides development of erosion resistant nitronic steel, the effect of weld overlay and weldability by 309L SS on erosion behaviour has also been studied. SMA welding process has been used for welding. According to scheffler diagram Cr_{eq} and Ni_{eq} 309SS matches with the 23/8N steel result. So far no investigation has been reported on the erosion of weld overlay on 23/8N steel. For this purpose weld overlay coated on 23/8N steel cavitation and solid particle erosion were performed under erosive environment has been studied.

Chapter 3

Experimental Procedure

This chapter presents the experimental techniques and procedures employed for heat treatment, weld coating deposition and joining, and characterization. A detailed description of cavitation and solid particle erosion tests of specimens are given in this chapter.

3.1 Material selection

The Gray Cast Iron (hereafter GCI), 13/4, 21/12N and 23/8N steels were used in the present study. Bars of 10 × 10 cm specimens of 13/4, 21/12/N and 23/8/N steels were supplied by M/S Star Wire (India) Ltd., Ballabhgarh, Haryana, India. GCI was received from Mohhmadpur hydropower plant, Uttrakhand, India. The chemical compositions of as received steels were measured by atomic emission spectrometer. These are reported in Table 3.1. Specimens for metallographic examination, hardness test, impact test, XRD analysis, surface roughness test and erosion tests were machined from these specimens.

Table 3.1 Chemical composition of GCI, 13/4, 23/8N and 21/12N steels in wt %

Steel	C	Si	Mn	Cr	Ni	N	S	Cu	Co	P	Mo	Fe
GCI	3.24	2.09	0.58	-	-	-	0.116	0.072	-	0.147	-	**Bal.**
13/4	0.06	0.74	1.16	13.14	3.9	-	0.014	0.088	0.035	0.015	0.56	**Bal.**
23/8N	0.31	0.765	2.05	22.48	7.45	0.285	In traces				0.12	**Bal.**
21/12N	0.195	1.06	1.15	20.92	10.65	0.20	In traces				0.17	**Bal.**

3.2 Heat Treatment

The heat treatments for 23/8N and 21/12N austenitic stainless steels are described below. The heat treatments were carried out in a laboratory type electrically heated muffle furnace with the proper attachment of temperature controller duly calibrated. The sample surface was properly protected to avoid any oxidation in heating.

3.2.1 Solution annealing treatment of 23/8N and 21/12N steels

Unlike conventional austenitic stainless steels, 23/8N and 21/12N steels cannot be hardened by heat treatment but will harden as a result of cold working. The heat treatment of nitronic steels consists of heating the steel upto austenitizing temperature, holding there for some time to allow the dissolution of carbides and then quenching in water to prevent the carbide precipitations. During annealing, chromium carbides were dissolved. Since carbide precipitation can occur at temperatures between 425^{o}C and 900^{o}C, it is desirable that the solution annealing temperature should be above this limit. The annealing temperatures of 1000^{o}C, 1050^{o}C, 1100^{o}C and 1150^{o}C were selected for the solution annealing treatment of 23/8N and 21/12N steels. The 23/8N and 21/12N steels specimens were there for 3 hrs to ensure the dissolution of carbides. The specimens were then quenched in water.

3.2.2 Aging of 23/8N steel

The aging of solution annealed (1100^{o}C for 3 hrs) 23/8N steel was carried out at 700^{o}C for 24 hrs to achieve a uniform carbide distribution (reprecipitation of carbides) and to improve mechanical properties of 23/8N steel.

3.3 Manual metal arc welding

The repairs of the components of Kaplan turbines made from 13/4 steels affected by erosion are made usually by weld overlays [Hart 2007]. Up to now the best results regarding the repair techniques applied to the cavitation affected areas of runner blades were obtained by overlay welding of cold hardening austenitic steels. Welded coatings and joining by shield metal arc welding (SMAW) with commercial filler metal austenitic AWS E309 stainless steel (SS 309L) was used to repair hydraulic turbines.

In present work, direct current with positive electrode polarity was used. Chemical composition of base metal (23/8N steel) is given in Table 3.1 and the chemistry of filler metal SS 309L is summarized given in Table 3.2. Filler electrode conforming to AWS/SF 5.4 was manufactured by ESAB Aristo 2000 – LUD 450 UW. To removal of moisture, filler electrodes dried in furnace at 250°C. Welding parameter for joining and weld coating are given in Table 3.3. 23/8N steel plate 20 mm thick was welded with SS 309L filler metal. Two layers of thickness 7 mm was deposited uniformly over the surface of plate in flat position. Slag was remade after each weld bead deposited and penning was done by hammer after each pass. Dye penetration and X-ray radiography test conducted for any weld defect. For the filler metal, the welding current and voltage during welding were 80 A and 27.5 V respectively.

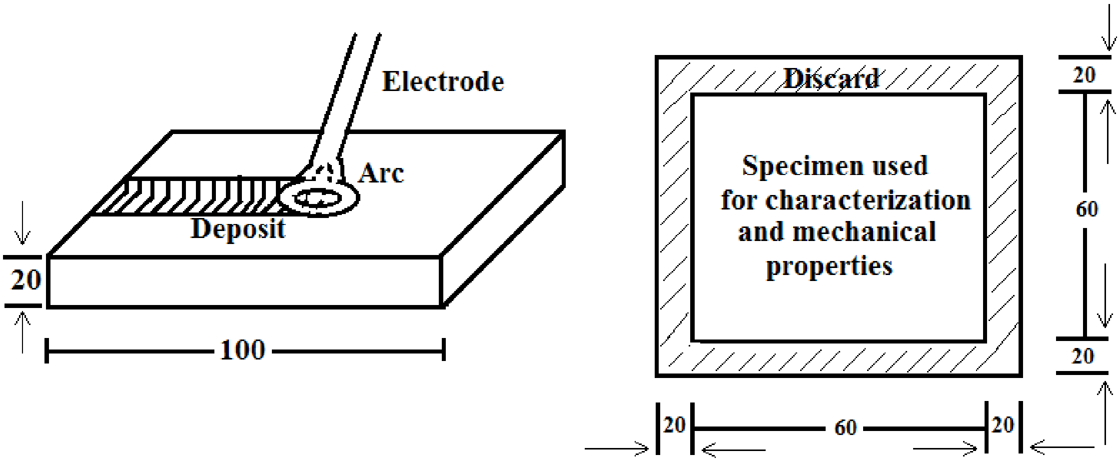

Fig. 3.1 Schematic diagram of weld overlay on steel surface at flat position (all dimensions in mm).

Table 3.2 Chemical composition of AWS 309 austenitic stainless steel in wt %

Filler metal	C	Si	Mn	Cr	Ni	V	S	Cu	P	Mo	Fe
309L SS	0.045	0.053	1.25	22.03	11.81	0.07	0.013	0.19	0.025	0.045	Bal

Table 3.3 welding parameter used for weld coating deposition

Filler metal	**Dia. (mm)**	**Length (mm)**	**Current (Amp)**	**Voltage (Volt)**	**Welding speed(mm/min)**
309L SS	2.5	350	80	27.5	25

Specimen collection for different studies

Sectioning of the weld joints for fabrication of various test specimens was made with the help of EDM wire cut machine. The collection of schematics of specimens for mechanical testing, metallography and fracture toughness test from different locations of the weld joint is schematically shown in Fig. 3.2.

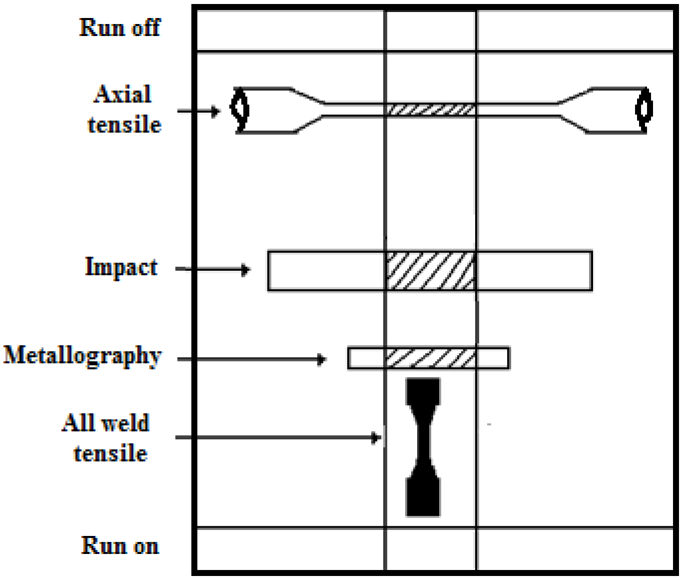

Fig.3.2 Schematic diagram of collection of test specimens from the weld joint.

3.4 Mechanical Testing

3.4.1 Tensile Test

The tension specimens (as-received and processed) of round shape (Fig. 3.3) were prepared as per ASTM standard specifications [ASTM E8M-09 2011] with a gauge length of 20 mm and a diameter of 4 mm. Tensile tests were carried out at constant strain rate (10^{-3} s^{-1}) using a computer controlled Hounsfield H25K materials testing machine. The data from the machine was recorded by the computer and a load-elongation curve generated. This is converted into engineering stress-strain curve for further analysis. The tensile tests provided the properties such as yield strength (YS), ultimate tensile strength (UTS) and elongation percentage of all processed specimens. The tensile toughness and strain hardening exponent (η) was determined by measuring the area under the engineering stress-strain curve.

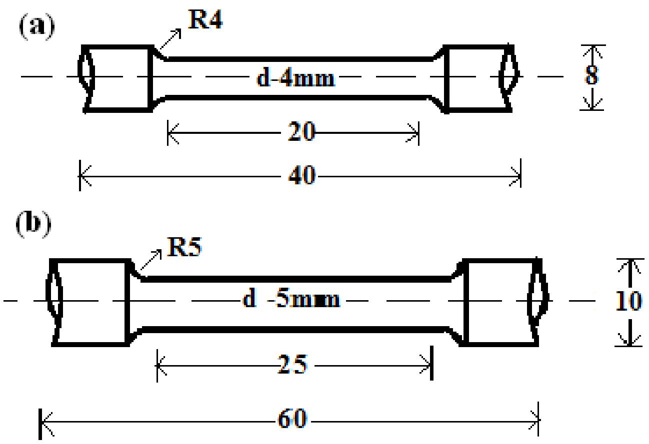

Fig. 3.3 Schematic diagram of the tensile specimens sample (a) base metal as well as processed specimens and (b) all weld metal at different locations of weld metal(all dimensions in mm) [ASTM E8M-09 2011].

3.4.2 Impact test

Samples of (as-received and processed) steels were prepared for measuring the impact strength using the charpy method at room temperature. The tests were performed as per ASTM standard [ASTM E-23-07 2011]. The Charpy sample is shown in Fig. 3.4. The samples were set in a horizontal position with notch being vertical and facing opposite direction of the impact. The value of energy absorbed before fracture was noted.

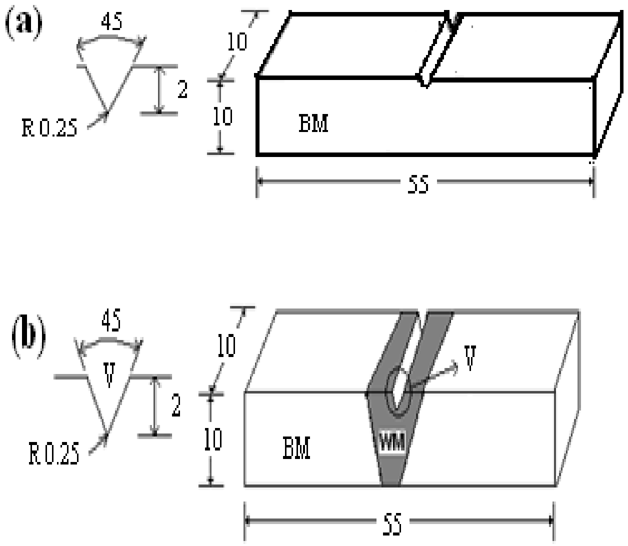

Fig. 3.4 Dimensions of Charpy V- notch impact test specimen (a) base metal as well as processed specimens and (b) from weld joint (all dimensions in mm).

3.4.3 Hardness Measurement

3.4.3.1 Bulk Hardness

A section of 10 x 10 mm was cut from all specimens and then polished to 0.5 µm finish. Hardness measurements were performed on FIE-VM50 PC Vickers hardness tester at load of 30 kg for dwell time 20 sec. Each specimen was tested for 5 different readings and final value was reported as an average of these values.

3.4.3.2 Microhardness

The steel specimens (13/4, 23/8N and 21/12N steels) were cut and polished as explained in section 3.5. The micro hardness of the specimens was measured by using Micro hardness Tester (VHM-002 Walter UHL, Germany) using 25 g of load applied for a dwell time of 15 sec. Each reported value of the microhardness is the average value of five measurements. These microhardness values are incorporated in Chapter 4, 5, and 6 of the present study.

3.5 Metallographic examination

For metallographic examination, steel specimens (as-received and processed) were prepared according to standard metallographic practice. Steel specimens were mechanically polished to 1 µm finish by alumina suspension. The polished surfaces of steel specimens were subsequently etched using aquaregia ($3HCl{:}1HNO_3+H_2O$) for observation using a Leica DMI 5000M optical microscope attached with digital imaging via computer system. The typical microstructural features of steel specimens were examined and digitally photographed.

The microstructure of etched samples, the fracture surfaces of Charpy impact and tensile samples and the eroded surfaces of cavitation and particle erosion test samples were studied by FE-SEM. A LEO 435 VP scanning electron microscope and FEI Quanta 2000 field emission scanning electron microscope (Fig. 3.5) were used in this study.

3.6 X-Ray Diffraction (XRD) Analysis

XRD analysis was used to indentify various phases present in the specimens. A section of the specimens were polished upto cloth polishing to minimize the distortion in X-ray diffraction patterns. A Bruker AXS D-8 (Fig. 3.6) Advance Diffractometer (Germany) with Cu K_α radiation and nickel (Ni) filter at 30 mA under a voltage of 40 kV was used to obtain XRD data. The specimens were scanned at a speed of 1^o/min in the angle range between 20^o to 100^o. The peaks of phases were indexed by using Expert High Score software which has inbuilt JCPDS X-ray diffraction data.

3.7 Erosion test

3.7.1 Cavitation Erosion Test

The cavitation erosion (CE) tests for the steel samples (as-received and processed) were conducted using the vibratory test method (Fig. 3.7), as per ASTM standard G-32-10. The sample size dimensions were 20 × 20 × 4 mm for cavitation. The schematic diagram of ultrasonic processor is given in Fig. 3.7. A piezoelectric ultrasonic transducer was used to produce oscillations at a frequency of 20±0.5 kHz and peak to peak amplitude of 50 µm in distilled water. Water temperature was maintained in the range of 25±2 ^{o}C. The samples were placed in distilled water next to the transducer. A distance of 0.5 mm was maintained between the tip of the ultrasonic probe (horn) and the specimen during the test. The processor was stopped after every 3 hrs cycle. The specimen was cleaned by acetone using ultrasonic cleaner and subsequently weighed with an accuracy of 10^{-4} g. After weighing, surface roughness was measured by Mitutoyo SJ-400 surface profilometer. The cavitation erosion test cycle was repeated after every three hr up to 24 hrs. Primary result of CE test was cumulative weight loss which was further converted into mean depth of erosion (MDE) using the following formula:

$$\text{MDE } (\mu\text{m}) = \frac{10\ X\ \Delta W}{\rho\ X\ A} \qquad \text{........ (1)}$$

Where, ΔW (mg) is the weight loss, ρ (g /cm^3) is the density of steel and A (cm^2) is the eroded area.

3.7.2 Solid Particle Erosion Test

The solid particle erosion (SPE) test was performed on (as-received and processed) steels by air jet erosion tester TR 470, Ducom made (Fig. 3.8), as per ASTM G76-10 standard [ASTM G76-10 2011]. A nozzle diameter of 3 mm was used. The test was performed using alumina (Al_2O_3) erodent powders having particle size range between 53 and 75 µm with operating eroding particle velocity of 32±1 m/sec which was calibrated using double disc method. Typical SEM images of Al_2O_3 particles are shown in Fig. 3.9. Erodent particles were fed from a hopper fitted with a mechanism to control the erodent flow. The air jet impingement angle varied from 30 to 90^{o} in the erosion chamber. The sample working distance was 10 mm. A sample holder fitted on the sample stand hold the sample in place.

Table 3.4 Erosion parameters used for solid particle erosion testing

Erodent particle	**Alumina**
Particle size	53-75 µm
Particle velocity	32±1 m/sec
Air pressure	0.5 kg/cm^2
Particle feed rate	3±0.3 g/min
Impact angle	30^o, 45^o ,60^o and 90^o
Working distance	10 mm
Time of Testing	27 min (3 min cycle)
Nozzle diameter	3 mm

The parameters used in erosion testing are shown in Table 3.4. The polished samples were first ultrasonically cleaned in acetone followed by the drying with dryer. The dried sample was then weighted to an accuracy of 10^{-4} g using an electronic balance. Erosion test was conducted for 3 min and samples were then again cleaned with the acetone. The sample was again weighted to determine the weight loss. The respective volume loss was calculated for 3 min erosion testing. The ratio of volume loss to the weight of eroded particles (i.e. particle feed rate x testing time) causing the loss was then calculated as erosion rate in mm^3/g. The erosion test was repeated with each subsequent test of 3 min duration until a steady state in erosion rate was obtained. The tests were performed at 30^o and 90^o impingement (impact) angles at ambient temperature for all the samples. The plot between the erosion rates (mm^3/g) and cumulative weight of erodent was studied to analyze the erosion rates of the specimens. The eroded surfaces were examined using SEM to study the mechanism of erosion. The cumulative weight losses were also interpreted as functions of microstructure and mechanical properties.

3.8 Surface Roughness measurement

The surface roughness values of the polished and eroded specimens were measured using Surface Roughness Tester (Mitutoyo SJ-400, Japan). An average of 5 readings of the value of surface roughness (R_a) was taken at different positions. The R_a values were obtained by using centre line average method. The surface roughness values are presented in Chapter 4, 5 and 6 of the present study.

Fig. 3.5 A photograph of FEI Quanta 200F scanning electron microscope.

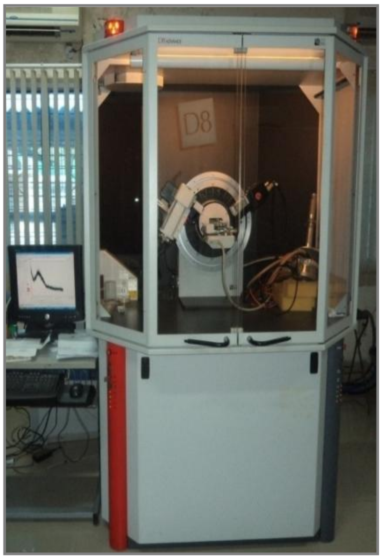

Fig. 3.6 A digital photograph of D8 advanced X-ray diffractometer.

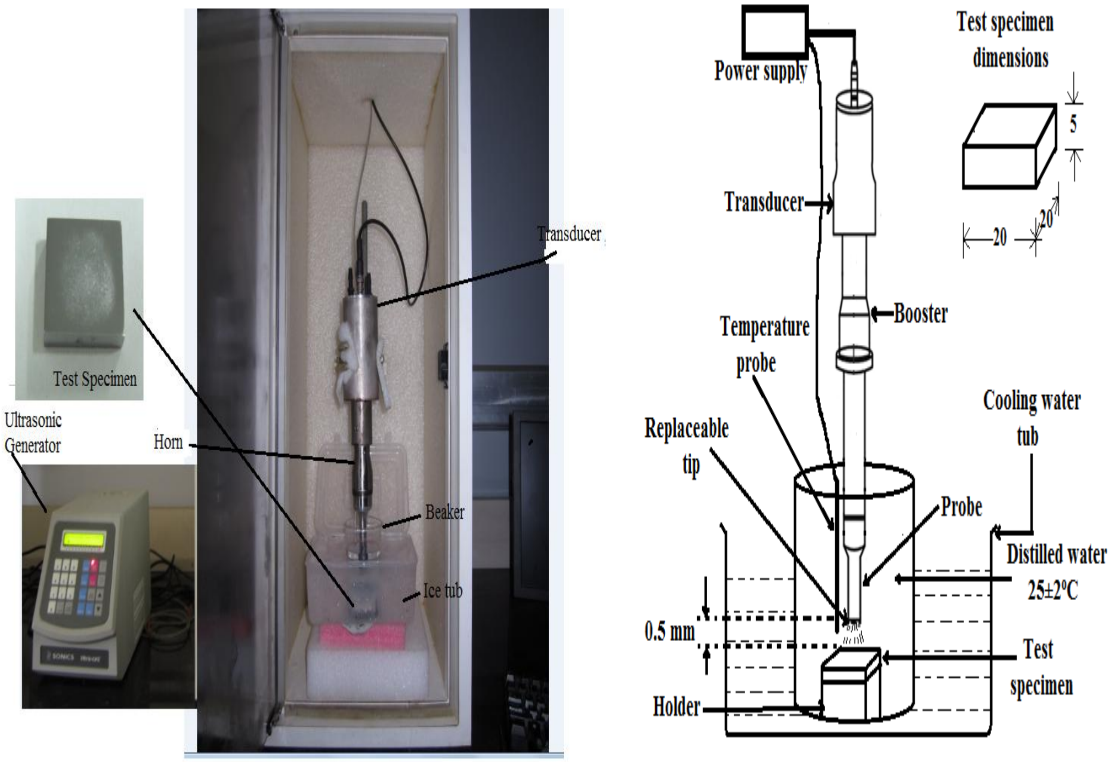

Fig. 3.7 A digital photograph and schematic diagram of the ultrasonic processor used for cavitation test.

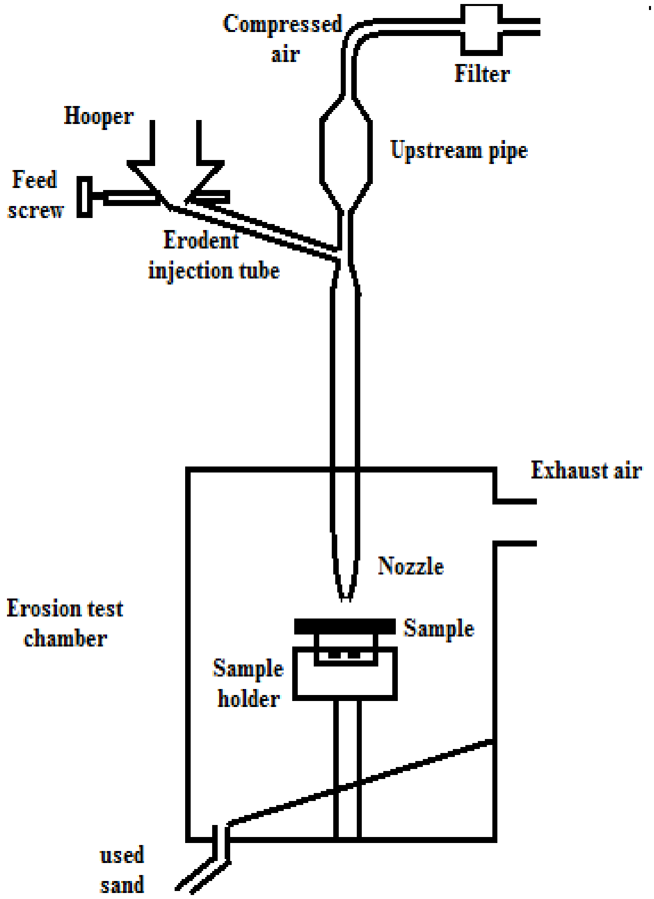

Fig. 3.8 Schematic diagram of air jet erosion tester.

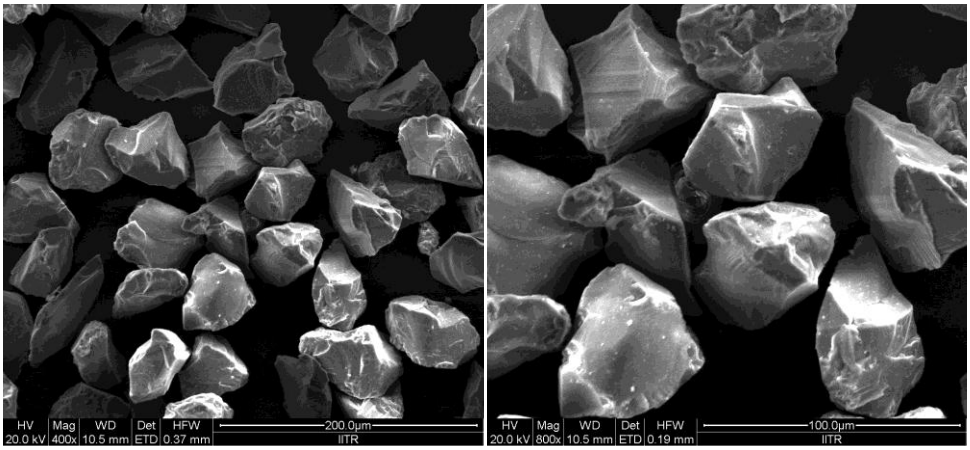

Fig. 3.9 secondary electron SEM micrograph of alumina particles with 400 and 800X magnification.

Chapter 4

Cavitation and Solid particle erosion resistance of 13/4, 21/12N and 23/8N steels

Generally in power plant gray cast iron (GCI) and bronze were used as turbine materials for available impulse and reaction turbines. So, for cavitation erosion the GCI (used in underwater parts as a pivot ring in the Mohmuddpur power plant, Uttarakhand, INDIA) is studied for the comparison purpose. The erosion behaviour of GCI, 13/4, 23/8N and 21/12N steels has been studied as a function of alloying additions, microstructure and mechanical properties.

4.1 Introduction

Erosion occurs by (i) cavitation, (ii) cutting by silt particles, (iii) sub surface damages, (iv) plastic deformation and (v) fatigue [Goel 2008]. Erosion is accountable for failure of machinery in power generation and shipping industries. In cavitation erosion, the material directly comes into contact with flowing water, e.g. hydro-turbines, ship propellers etc. During this process, the bubbles burst which produces very high and transient stress leading to plastic deformation of the material [Karimi 1986]. The hydro-turbine demands specific shape and contour for its efficient operation. Cavitation erosion creates pits or cavities which affect these significant contours generating hindrance to flow of water though the turbine. This seriously affects the operating efficiency of the hydro turbine. Cavitation results in damage up to 10 mm per year to crucial components like impellors, turbine blades and casings [Simoneau 1984]. As a result of this there is a decrease in energy extraction capacity that can lead to losses in terms of productivity, downtime, money and efficiency.

Solid particle erosion results in progressive removal of material that results from repeated impact of solid particles on the surface. Erosion occurred by the impact of hard and abrasive particles is observed in many other industrial applications such as hydroturbine under water parts, pipeline and valves carrying particulate matter etc [ASM Handbook 1992]. Earlier studies [Ness 1996, Mann 1998 and 2000] have identified the factors responsible for severe erosive damages in hydro turbine under water parts due to attack from silt laden water. Impact angle, velocity, abrasive particle size and mechanical properties are operating variables which affect the erosion process [Finnei 1960, Divakar 2005].

Hydro-turbine blades in hydroelectric power plants are subjected to erosion and silt laden water [Goel 2008]. The cast martensitic stainless steel (CA6NM) containing 13%Cr and 4%Ni in wt% (13/4 steel) currently find wide applications in hydroturbines and other industrial equipment subjected to erosion. This steel suffers from several maintenance and welding related problems. The poor weldability of this steel is due to formation of martensite during welding [Santa 2011].

Nitrogen as an alloying element [Kirami 1992] has been reported to raise the strength and wear resistance of austenitic stainless steel. Nitrogen is a strong solid solution hardener having high solubility in austenite. It also improves the corrosion resistance [Ritter 1988]. Addition of nitrogen allows nickel content in stainless steel to be reduced, leading to significant cost saving [Schino 2000]. The present work compares the cavitation erosion behaviour of GCI, 13/4, 21/12N and 23/8N steels. Solid particle erosion behavior of 13/4, 21/12N and 23/8N steels has also been investigated.

4.2 Microstructure

GCI exhibits graphite flakes in a pearlitic matrix and phosphide eutectic (steadite phase) as shown in Fig 4.1a. The microstructure of 13/4 consists of very fine martensitic laths (Fig 4.1b). The structure also exhibits presence of very small amounts of bright phase. This is expected to be δ-ferrite [Santa 2011]. Fig. 4.1b also shows EDS pattern (inset) of as received 13/4 martensitic stainless steel. Figs. 4.1c and 4.1d show the microstructures of as received 23/8N and 21/12N steels, respectively. As received 23/8N steel exhibits austenitic matrix (Fig. 4.1c) with carbide precipitates (upto 8 µm) along the grain boundaries. EDS (Fig. 4.1c inset) confirmed these precipitates to be carbides. 21/12N steel exhibits equiaxed grains. Annealing twins are observed in some grains (Fig. 4.1d). Some fine (<1µm) precipitates are observed along the grain boundaries. EDS confirmed these precipitates to be carbides (Fig.4.1d, inset).

In both nitronic steels (23/8N and 21/12N) M_7C_3 and $M_{23}C_6$ types of carbides are expected [Gadhikar 2014]. In 23/8N steel, the austenitic matrix is strengthened by nitrogen. It also contains higher C and low Ni compared to 21/12N. The microstructure comprises austenitic matrix with the carbides precipitates (Fig. 4.1c). The expected carbides may be M_7C_3, $M_{23}C_6$ and MC, where M can be Ni, Fe, Cr and Mo [Padilha 2002]. The austenitic stainless steels containing of W, Mo and Nb often form M_6C (M = Fe, Mo, Nb, Cr, W and V) carbides [Tillman 1974]. The MC (M = Zr, Ti, Hf, Nb, V and Ta) carbides are most stable and always found to be present in stabilized austenitic stainless steels like Ti stabilized AISI 321 [Kokawa 2002]. On the other hand, M_7C_3 carbide in austenitic stainless steel can be seen only when C: Cr ratio is very high [Tabrett 1996]. In 23/8N steel, as the N content is low and it also has a low C: Cr ratio, the carbide formed may be $M_{23}C_6$ in the steel. The microstrcutrual examination showed the carbides at the grain boundaries (Fig.4.1c). These are expected to be $M_{23}C_6$ as reported by Padilha [2002].

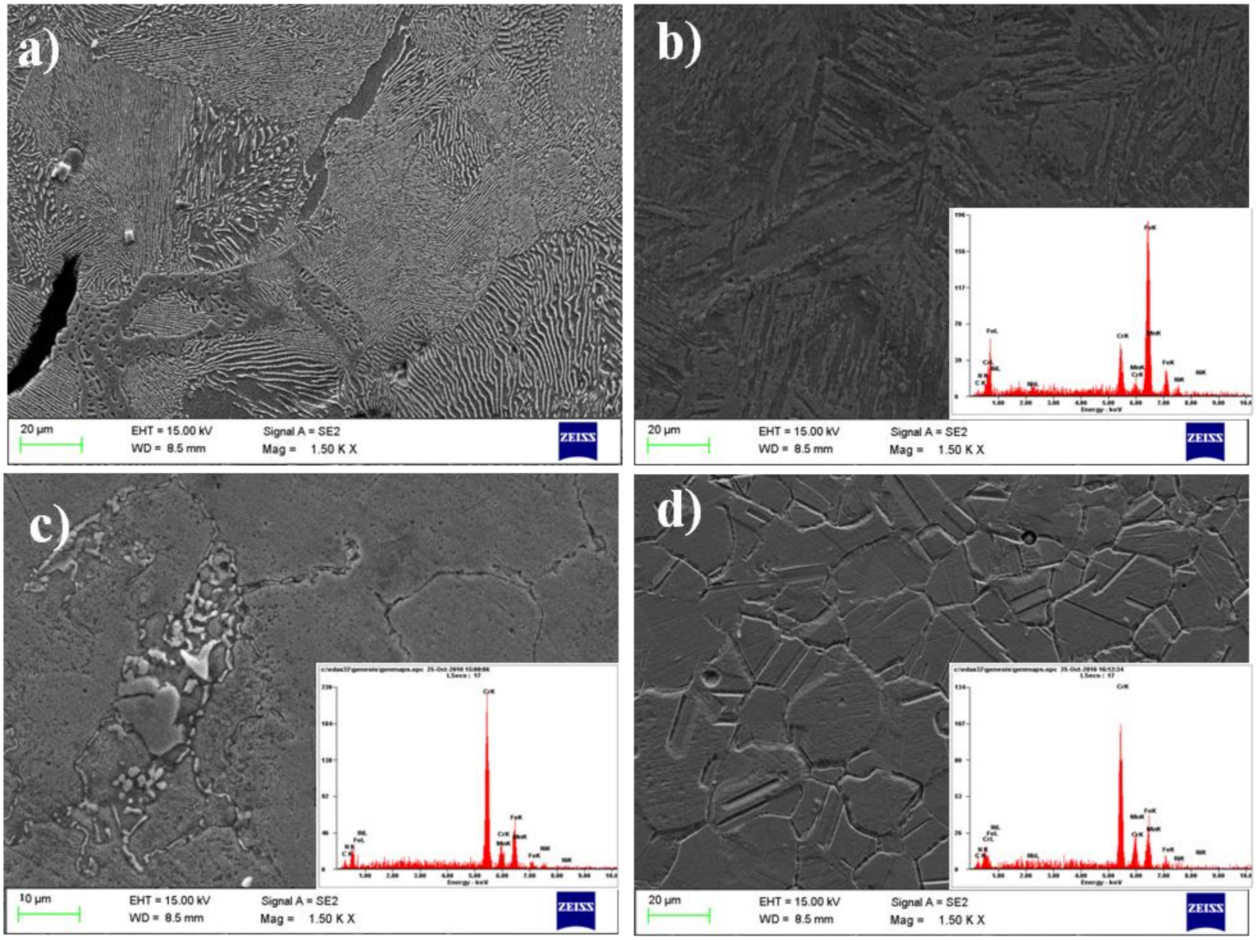

Fig. 4.1 (a) SEM image of GCI with graphite flakes in a pearlitic matrix and phosphide eutectic (steadite phase) (b), SEM image and EDS pattern of 13/4 steel, (c) SEM image of 23/8N steel showing austenite grains with and EDS pattern of chromium carbide (d) SEM image of 21/12N steel showing austenite grains with and EDS pattern of chromium carbide.

In Fig. 4.2, X-ray diffraction results confirm the 13/4 steel to be martensitic. The bright spots observed in Fig. 4.1b are expected to be δ-ferrite [Kishor 2014]. Because of the low amount of carbon presented in 13/4 steel, the diffraction peaks of δ-ferrite and martensite are overlapped. Further the amount of δ-ferrite formed is very small (Fig. 4.1b) and may be difficult to detect by XRD. X-ray diffraction results confirmed 23/8N and 21/12N steels to be austenitic (Fig. 4.2).

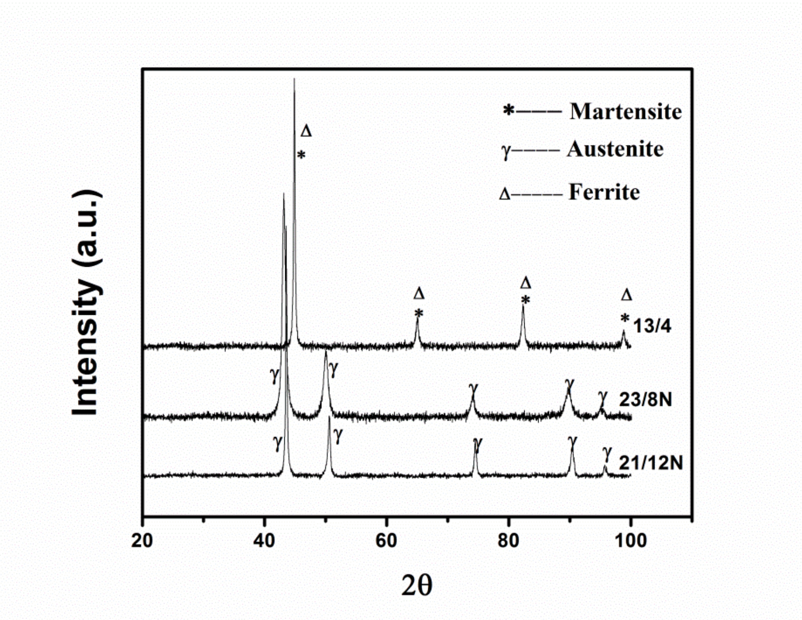

Fig.4.2 XRD trace of 13/4, 23/8N and 21/12N steels.

Identification of the microstructures with the help of Schaeffler diagram

The phases of 13/4, 23/8N and 21/12N steels are also determined with the help of Schaeffler diagram (Fig. 4.3) which is useful to predict the resulting microstructure of stainless steel after solidification [Sugiyama 2008]**.** For the 13/4 steel the chromium equivalent has been empirically calculated using ferrite forming elements:

Cr eq = (Cr) + 2(Si) + 1.5(Mo) + 5(V) + 1.75(Nb) + 0.75(W)

= 13.4 + 2(0.74) + 1.5(0.56) + 1.75 (.003) + 0.75(0.55)

= 16.14

and the nickel equivalent has been calculated by familiar austenite-forming elements:

Ni eq = (Ni) + (Co) + 0.5 (Mn) + 0.3 (Cu) + 25(N) + 30(C)

= 3.9 + 0.035 + 0.5(1.16) + 0.3(.088) +30 (.06)

= 6.34

From Schaeffler diagram (Fig. 4.3), the values of Cr_{eq} and Ni_{eq} for 13/4 steel corresponds to the region of martensite plus δ-ferrite, which is in agreement with the microstructures of 13/4 steel as shown in Fig. 4.1(b). In the second case of 23/8N steel the chromium equivalent has been empirically calculated by most common ferrite forming elements:

$$Cr_{eq} = (Cr) + 2(Si) + 1.5(Mo) + 5(V) + 5.5(Al) + 1.75(Nb) + 1.5(Ti) + 0.75(W)$$

$$= 22.48 + 2(0.765) + 1.5(0.12) + 5(0) + 5.5(0) + 1.75(0) + 1.5(0) + 0.75(0)$$

$$= 24.19$$

and the nickel equivalent has likewise been calculated by familiar austenite forming elements.

$$Ni_{eq} = (Ni) + (Co) + 0.5\,(Mn) + 0.3\,(Cu) + 25(N) + 30(C)$$

$$= 7.67 + (0) + 0.5(2.05) + 0.3(0) + 25(0.285) + 30(0.31)$$

$$= 25.12$$

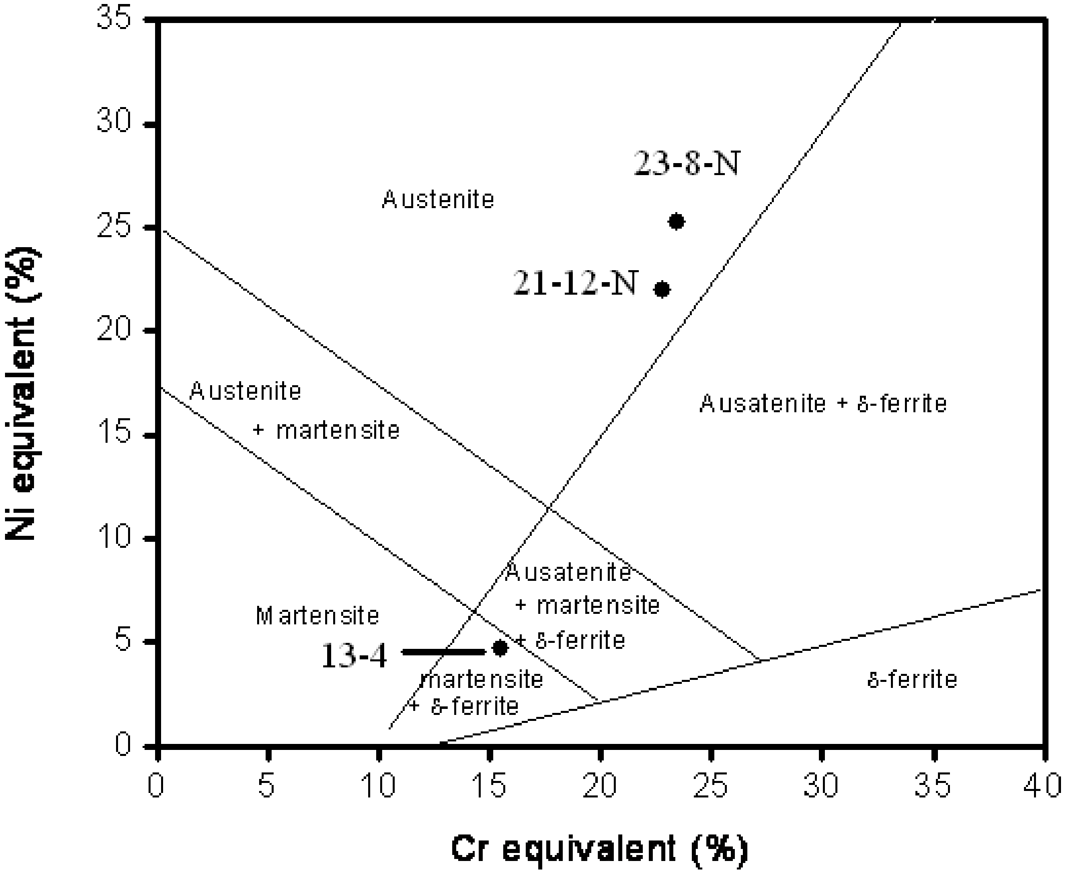

Fig. 4.3 Schaffler diagram [Klueh 1988]

In the third case of 21/12N steel the chromium equivalent has been empirically calculated by the most common ferrite forming elements:

Cr_{eq} = (Cr) + 2(Si) + 1.5(Mo) + 5(V) + 5.5(Al) + 1.75(Nb) + 1.5(Ti) + 0.75(W)

= 20.92 + 2(1.06) + 1.5(0.172) +5(0) +5.5(0) + 1.75(0) + 1.5(0) + 0.75(0)

=23.29

And the nickel equivalent has likewise been calculated.

$$Ni_{eq} = (Ni) + (Co) + 0.5\,(Mn) + 0.3\,(Cu) + 25(N) + 30(C)$$

$$= 10.65 + (0) + 0.5(1.15) + 0.3(0) + 25(0.2) + 30(0.19)$$

$$= 21.92$$

From Schaeffler diagram (Fig 4.3) the values of Cr_{eq} and Ni_{eq} for 23/8N and 21/12N steel correspond to the region of austenite, which is in agreement with microstructure (Fig 4.1c, d).

4.3 Mechanical properties

Table 4.1 shows the mechanical behaviour of 13/4, 21/12N and 23/8 N stainless steels. Fig 4.4 Engineering stress strain curve of the same steels. The 13/4 steel exhibits significantly higher values of yield strength (YS) and ultimate tensile strength (UTS) than corresponding values in 23/8N and 21/12N steels. The ductility, impact energy, tensile toughness (area under the engineering stress-strain curve) and strain hardening exponent of 13/4 steel are lower as compared to 23/8N and 21/12N steels. Average hardness value of GCI is 180 VHN.

The secondary electron SEM fractographs obtained from the fractured tensile and impact specimens of as received specimens of different steels are presented in Fig. 4.5 and Fig. 4.6 respectively. All specimens show predominantly ductile fracture characterized by large number of dimples. Large sizes of voids are observed in 13/4 steel as compare to both Nitronic steels.

Table 4.1 Mechanical properties of the 13/4, 23/8N and 21/12N steels

Properties of steel	13/4	23/8N	21/12N
Hardness (VHN)	301	266	250
Yield Strength (MPa)	763	567	480
Ultimate Tensile Strength (MPa)	833	820	763
Ductility (% Elongation)	22.5	32	45.3
Impact energy (J)	64	85	217
Tensile toughness MJ/m^3	68	240	281
Strain Hardening exponent(n)	0.07	0.55	0.52

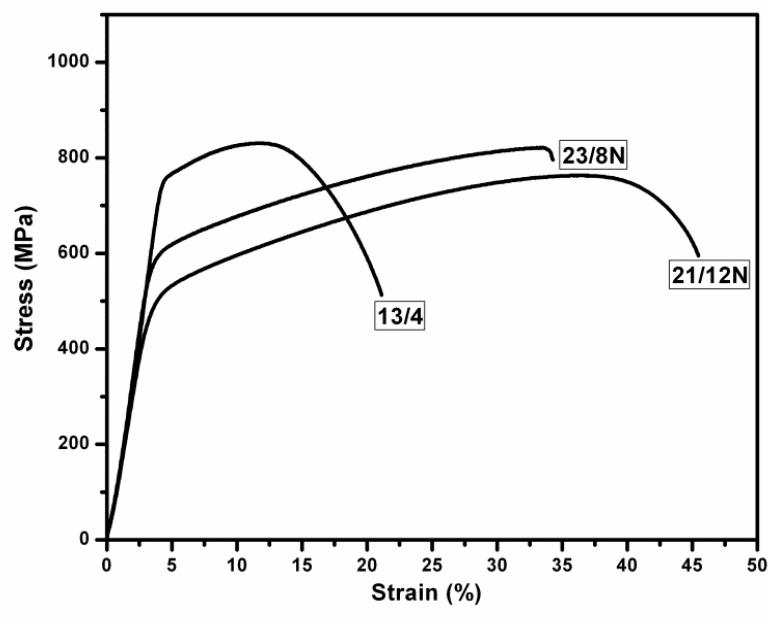

Fig4.4 Engineering stress strain curves for 13/4, 23/8N and 21/12N steels.

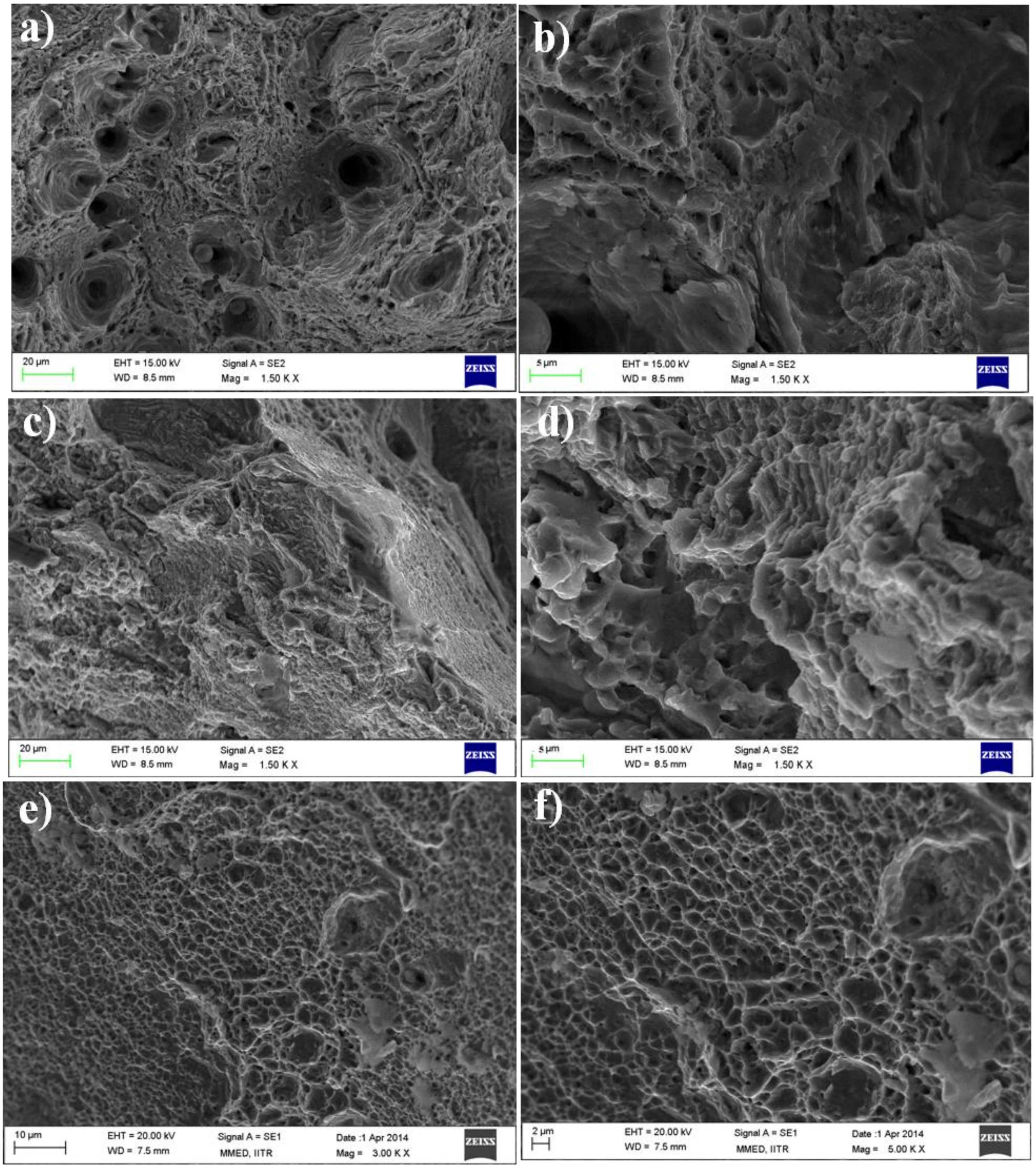

Fig. 4.5 Secondary electron SEM micrographs of tensile test fracture of surface of as received (a, b) 13/4, (c, d) 23/8N and (e, f) 21/12N steels.

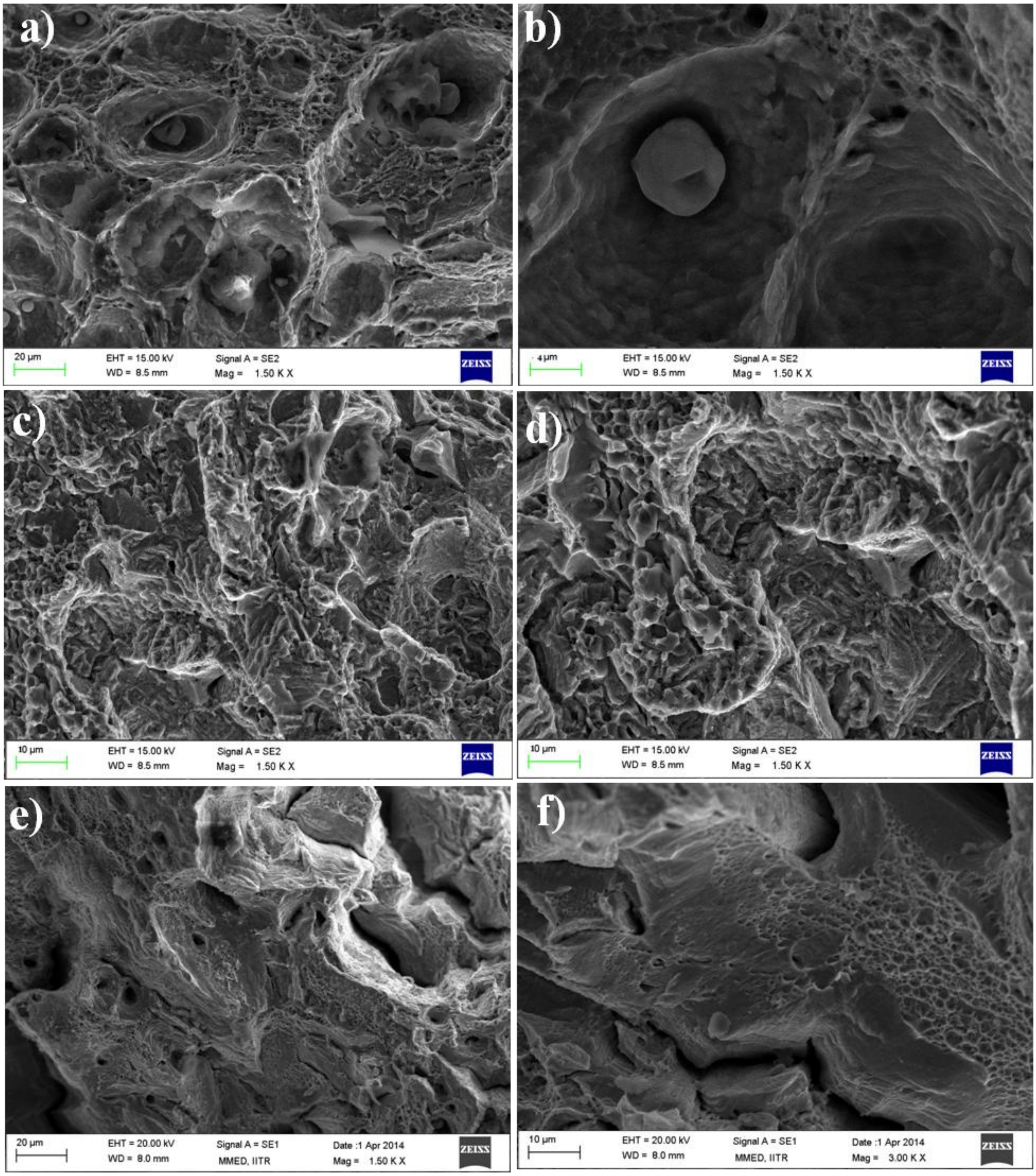

Fig. 4.6 Secondary electron SEM micrographs of impact test fracture surface of as received (a, b) 13/4, (c, d) 23/8N and (e, f) 21/12N steels.

4.4 Cavitation erosion behavior

The data on cumulative mass loss, mean depth of erosion (MDE) and average surface roughness (R_a value) as a result of cavitation erosion for the tested specimens are plotted in Fig. 4.7a, b and c. MDE is determined by using equation 3.1. Cumulative weight loss versus time of erosion (Fig. 4.7a) and MDE as function of time of erosion (Fig. 4.7b) curves are almost identical, because of the minimum difference in the densities of 13/4 (7.795 gcm^{-3}), 21/12N (8.11 gcm^{-3}) and 23/8N (8.137 gcm^{-3}) steels, which is the single variable responsible for MDE.

The erosion rate in GCI, as received 13/4 and 23/8N steels is more than that that in 21/12N steel. The material loss results presented in Fig. 4.7a show a characteristic behavior as a function of time which can be separated into two stages: the first stage is described by an incubation period where there is very little material loss. The second stage shows a steady state erosion condition, where the rate of material removal from the surface is almost constant. The incubation time mainly depends on the microstructure as well as strain hardening ability of the alloys and its values for GCI, 13/4, 23/8N and 21/12N steels are 1hr (I), 4hrs (II), 8hrs (III) and 8hrs (IV) respectively. Very less incubation period is exhibited by GCI which has a pearlitic structure and less incubation period is exhibited by 13/4 which has a martensitic structure. Austenitic 23/8N and 21/12N steels possess high incubation period because of their higher strain hardening ability (strain hardening coefficient vide Table 4.1).

SEM micrographs of eroded surfaces after cavitation erosion and solid particle erosion tests are presented in Figs. 4.8-4.11. Cavitation erosion rate of GCI depends on the size and shape graphite flakes and phase presents in matrix [Okada 1983]. In Fig. 4.8a shows micrograph of before erosion. In Fig. 4.8b, the matrix material surrounding the graphite in GCI is pounded into small fragment then ejected after 6 hrs. After 14 hrs surface of GCI gets severely damaged as shown in Fig. 4.8c. The eroded surfaces of 13/4 steel shown in Fig. 4.9 are very similar to those reported by Liu et al [Liu 2003] for Fe-0.05C-13Cr-5Ni-0.7Mo stainless steel. Fig. 4.9a shows micrograph of before erosion in 13/4 steel. Deformation due to cavitation attack after 6 hrs is mostly confined to martensitic laths (Fig. 4.9b). After 12 hrs laths are not clearly distinguishable (Fig. 4.9c). After 18 hrs martensitic laths are severely damaged (Fig. 4.9d). With higher cavitation erosion period, complete structure gets damaged (Fig. 4.9e).

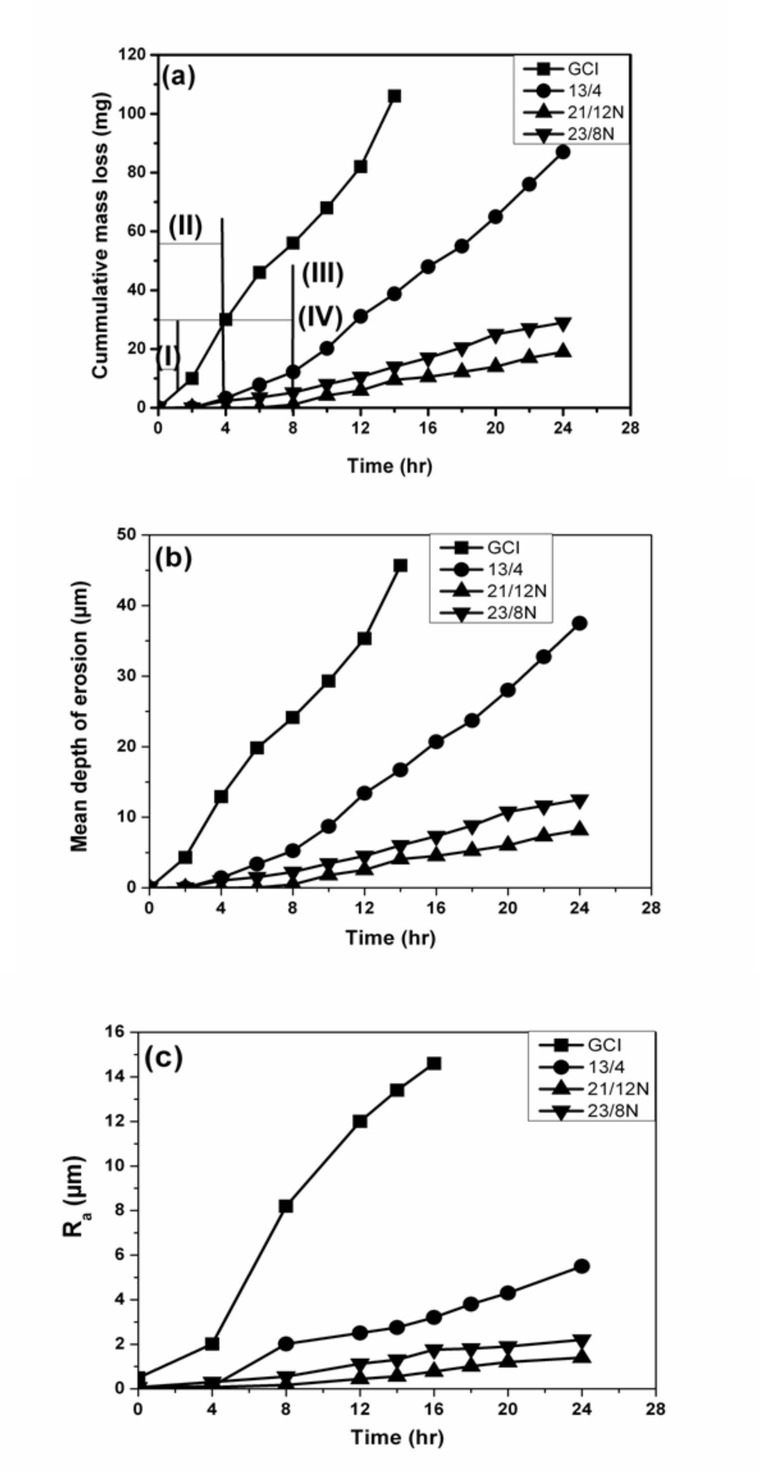

Fig. 4.7 Plot of cavitation erosion of GCI, 13/4, 23/8N and 21/12N steels (a) cumulative weight loss (CWL), (b) mean depth of erosion (MDE) and (c) surface roughness R_a as function of time period.

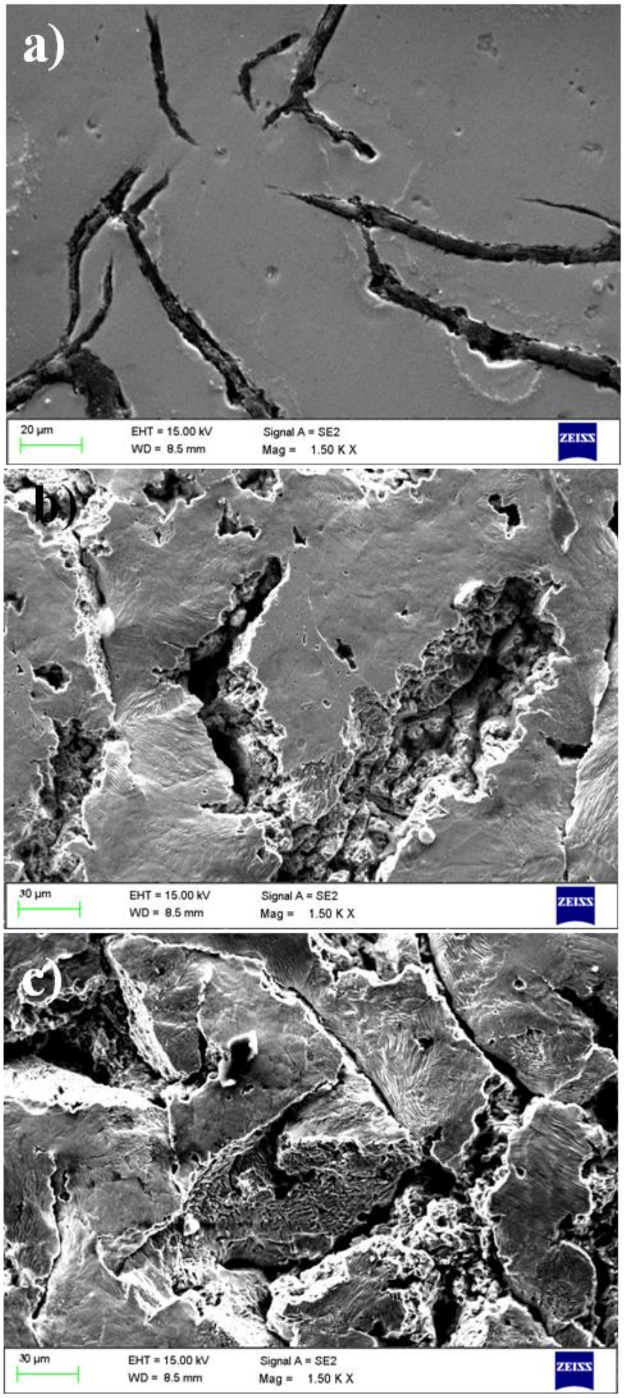

Fig. 4.8 Secondary electron SEM micrographs of eroded surfaces of GCI after (a) 0 hr, (b) 6 hrs and (c) 12 hrs of cavitation erosion.

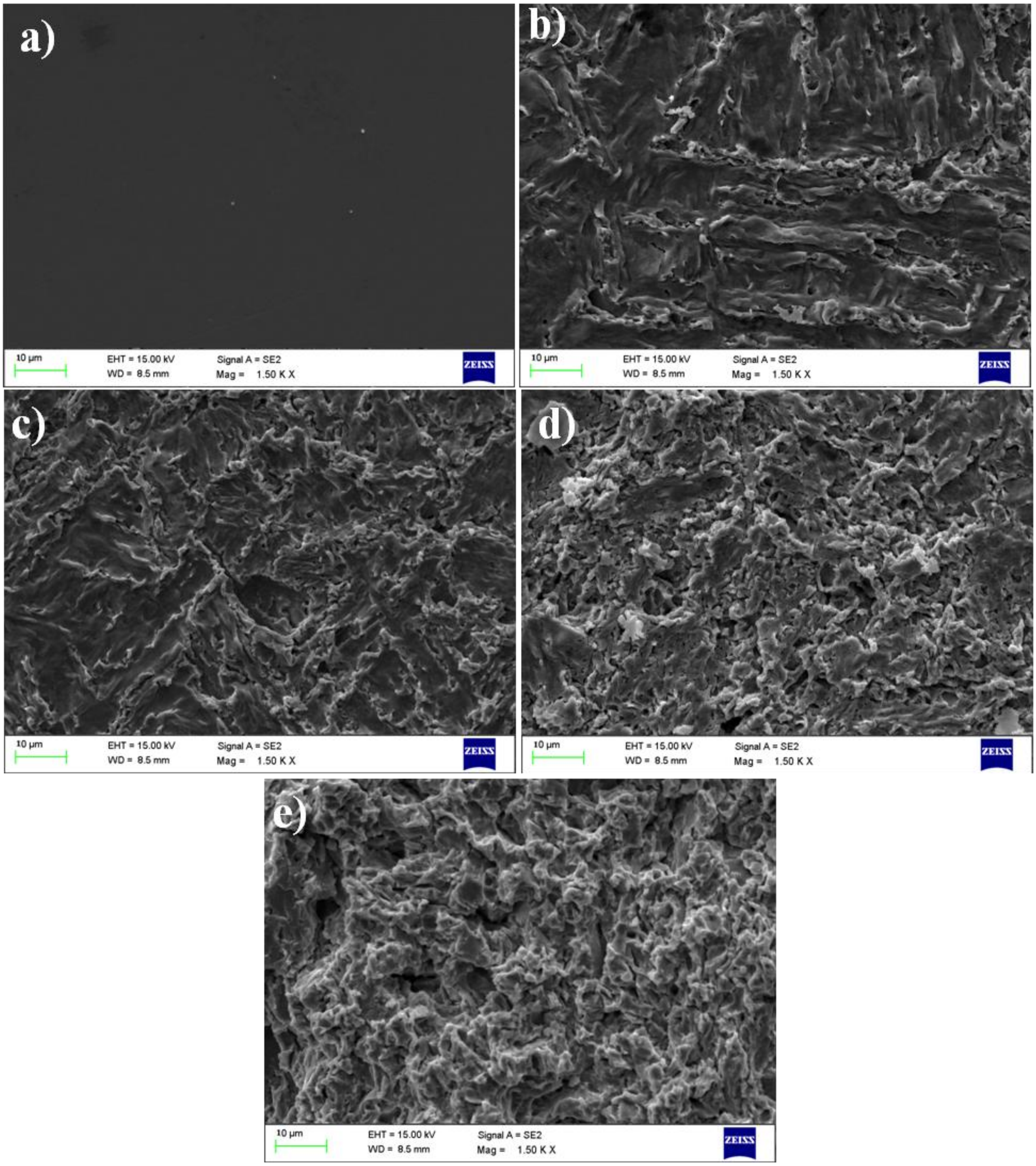

Fig. 4.9 Secondary electron SEM images of eroded surface of 13/4 steel after (a) 0 hr, (b) 6 hrs, (c) 12 hrs and (d) 18 hrs and (e) 24 hrs of cavitation erosion wear marks, craters and some plastic deformations.

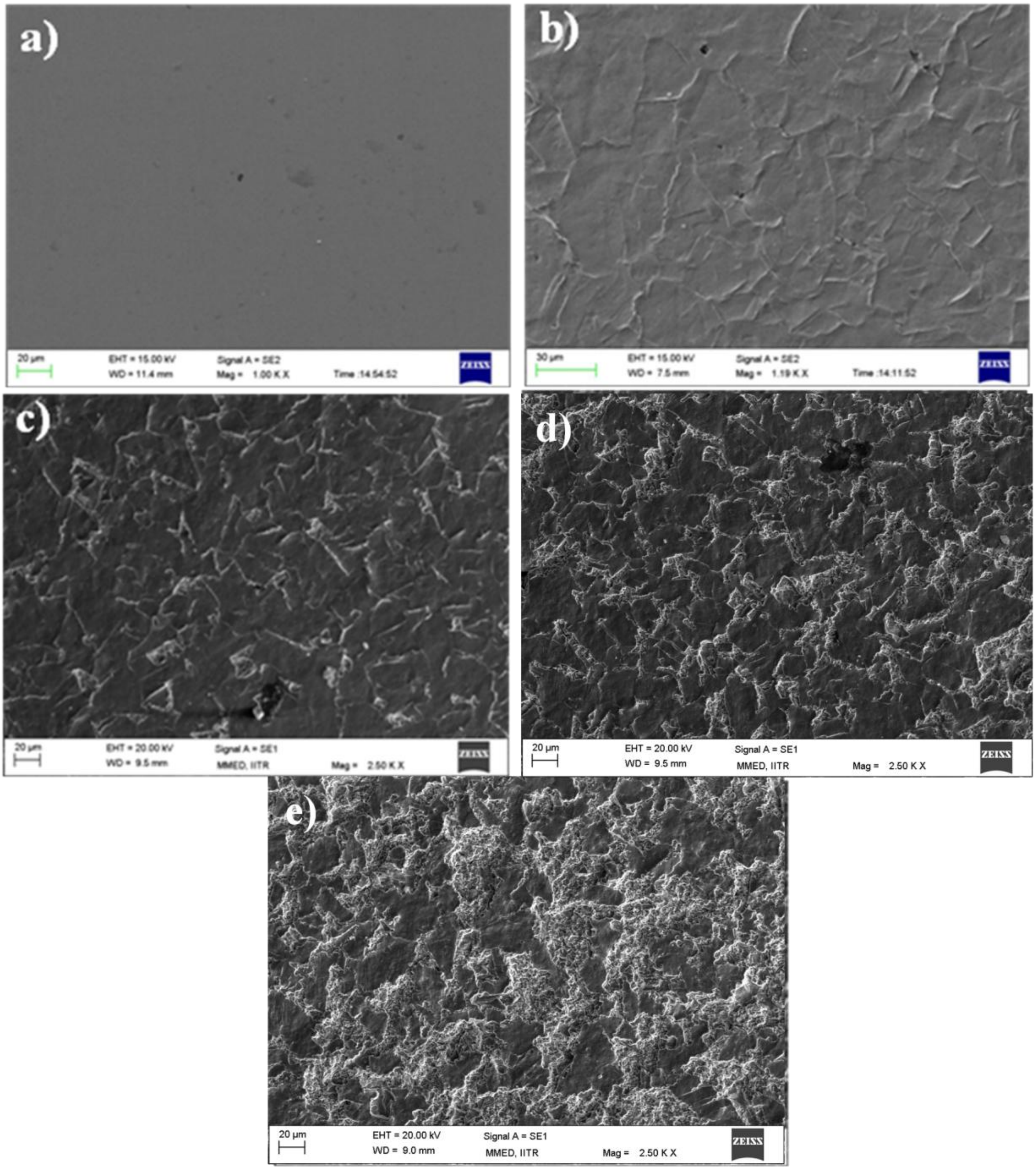

\

Fig. 4.10 SEM micrographs of eroded surface of 23/8N steel after (a) 0 hr, (b) 6 hrs, (c) 12 hrs, (d) 18 hrs and (e) 24 hrs of cavitation erosion.

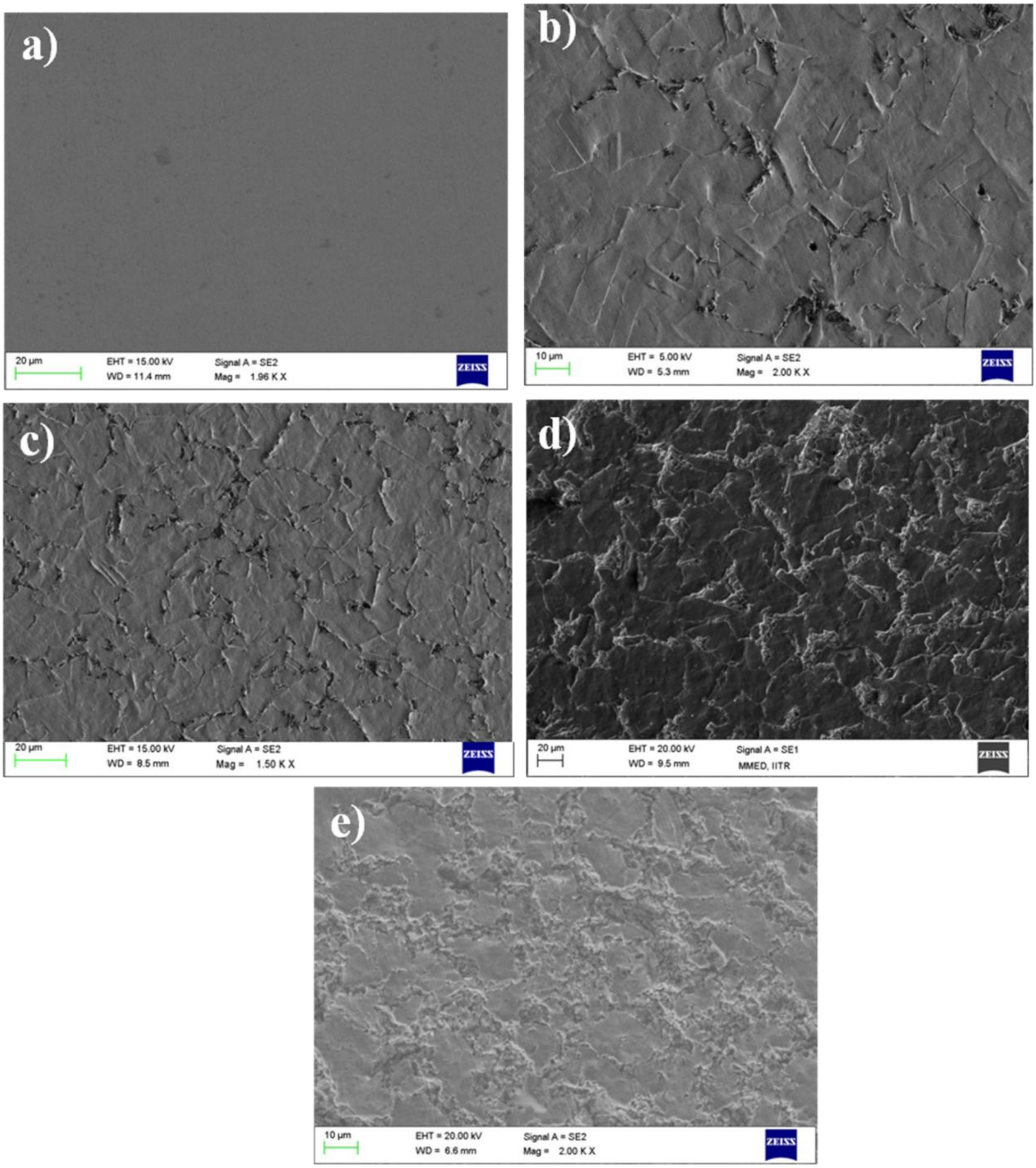

Fig. 4.11 Secondary electron SEM micrographs of eroded surface of 21/12N steel after (a) 0 hr, (b) 6 hrs, (c) 12 hrs, (d) 18 hrs and (e) 24 hrs of cavitation erosion.

No surface damage is observed in the as received 23/8N and 21/12N steels after 6 hrs of cavitation erosion. After 12 hrs (Fig.4.10c and Fig. 4.11c) damage is mainly developed at carbide austenite interface. This is the main characteristic of cavitation i.e. preferential attack on the weakest phase of material [Chavan 2008]. The same observation was identified by Okada et al [Okada 1983] in GCI, in which it has been reported that the graphite provide the required crack initiation centers for rapid wear by brittle fracture. Cavitation holes are found in carbides region (Fig.4.10d and Fig. 4.11d) after erosion for 18 hrs. This may be because of high brittleness related with the carbides. After 24 hrs, matrix damage is also observed in Fig.4.10e and Fig. 4.11e. The SEM micrographs of eroded surface of all the four steels again indicate that higher damage took place in order GCI, 13/4 as compared to 23/8N and 21/12N steels.

The XRD results (Fig.4.12) show that strain induced martensite does not form after cavitation erosion in 23/8N and 21/12N steels. This may be because addition of nitrogen may prevent formation of strain induced martensite in austenitic stainless steels [Bregliozzi 2005].

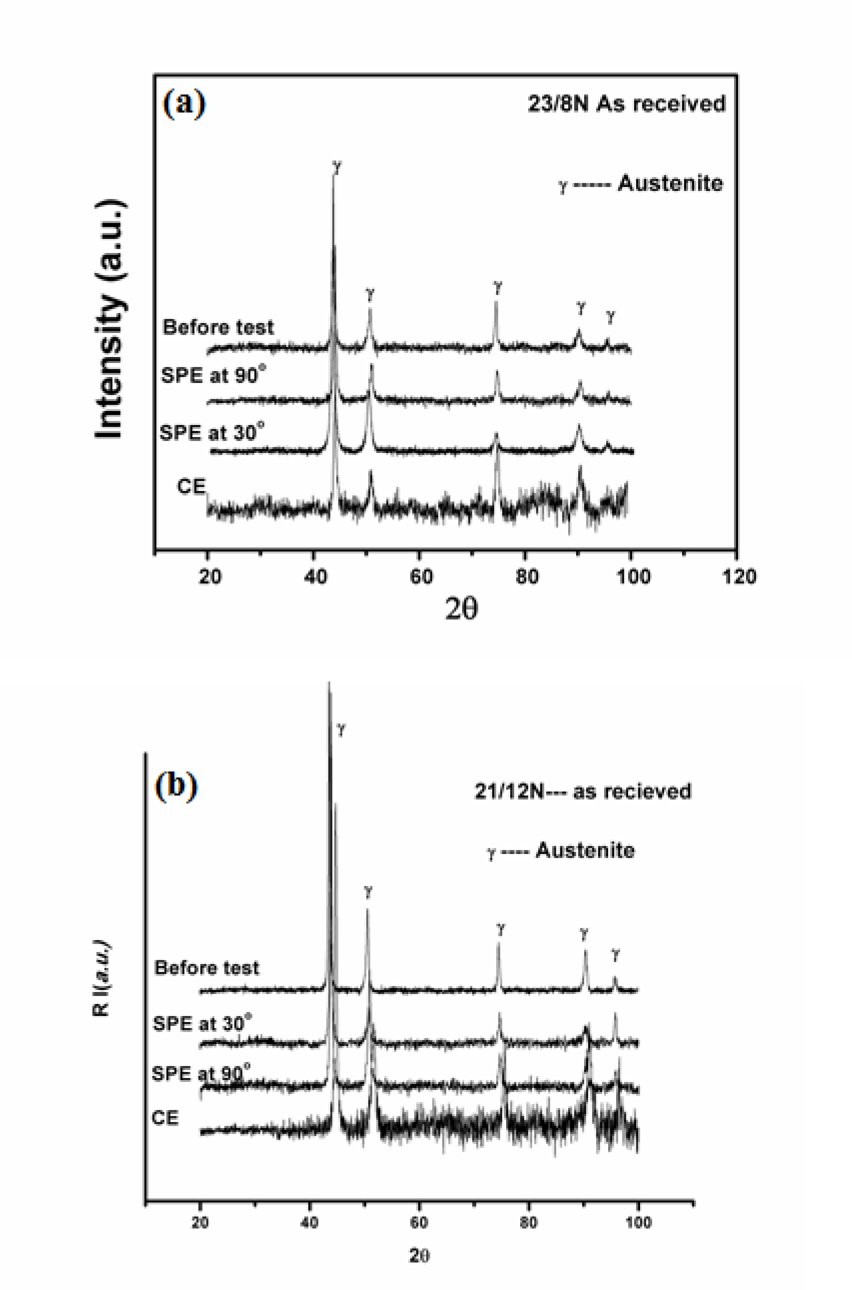

Fig. 4.12 XRD trace of relative intensity vs 2θ showing the absence of strain induced martensite in as received (a) 23/8N and (b) 21/12N steel samples subjected to cavitation erosion and solid particle erosion.

4.5 Solid particle erosion behaviour

Erosion rates calculated in chapter 3 for different intervals of time were plotted against time (min). Fig 4.13 shows plot of erosion rate v/s time for 23/8N steel tested at impingement angle 30° and 90°.

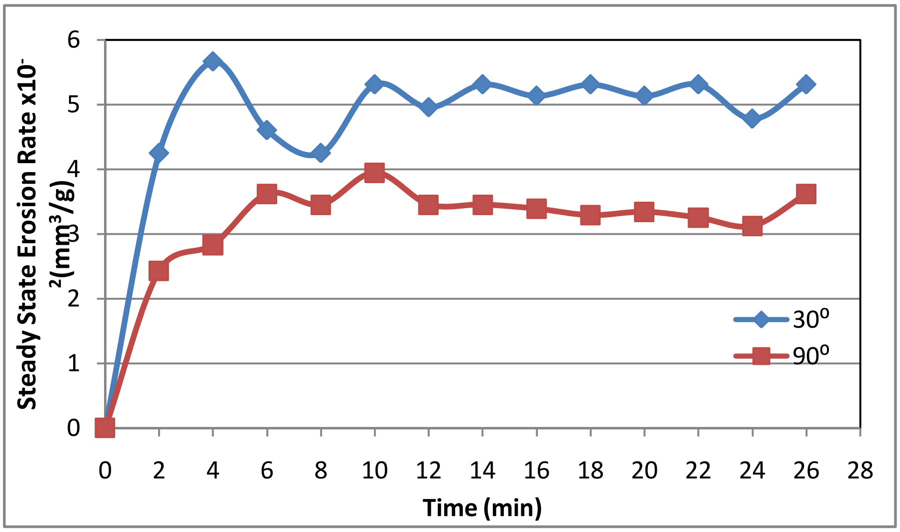

Fig.4.13 Steady state erosion test of 23/8N steel at 30° and 90°.

In the testing it was observed that after 12 min steady state erosion condition occur for 23/8N steel at both the angles on given conditions. Steady state erosion rate can be calculated by taking average of erosion rate values during steady state condition (i.e. after 12 min). Similarly steady state erosion testing was performed for both material at four different angles 30°, 45°, 60° and 90° by adjusting the sample holder. The erosion rate of 23/8N steel is high at 30° than at 90°. Initial fluctuation of erosion curves may be due to change in the erosion rate as a result of differential interaction of erodent particle with polished surface and debris initially, also due to [Chavan 2008] irregular interaction between strain hardening and flake formation at 90°. Steady state erosion rate calculated for both materials at all angles were shown in Table 4.2.

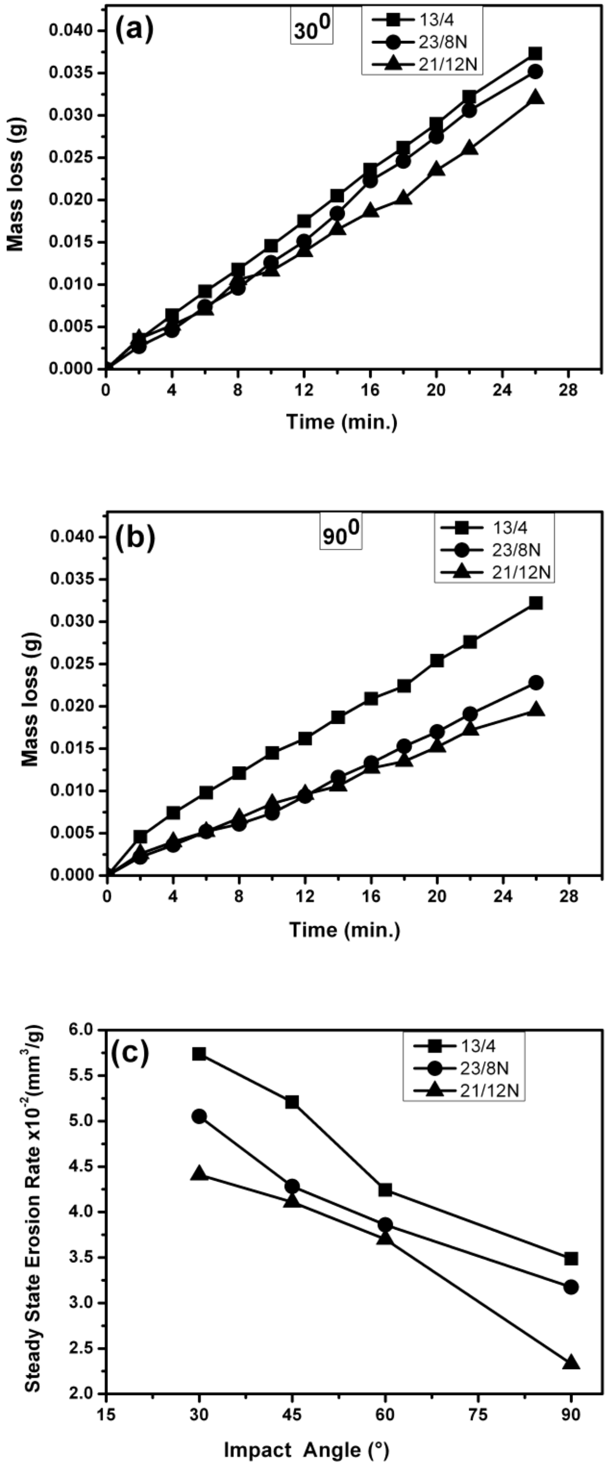

Fig.4.14 Cumulative weight loss (CWL) at (a) 30^{o}, (b) 90^{o}, (c) steady state erosion rate of 13/4, 23/8N and 21/12N steels.

Table 4.2 Steady state erosion rate and Depth of wear scar in µm of 13/4 MSS, 23/8N and 21/12N steels.

	13/4MSS (As-received)		**23-8 N (As-received)**		**21/12 N (As-received)**	
Angle	Steady State Erosion Rate $x10^{-2}(mm^3/g)$	Depth of wear scar (µm)	Steady State Erosion Rate $x10^{-2}(mm^3/g)$	Depth of wear scar (µm)	Steady State Erosion Rate $x10^{-2}(mm^3/g)$	Depth of wear scar (µm)
30°	5.737	223	5.053	140	4.41	72.33
45°	5.209	230.12	4.283	157	4.11	78
60°	4.242	238.19	3.859	176	3.7	86
90°	3.488	251	3.174	202	2.33	109.33

Fig 4.14 a & b shows the cumulative weight loss curves of specimens of different steels at the impact angles of 30^o and 90^o. Cumulative weight loss in 13/4 steel is more than that in the 23/8N and 21/12N steels at both impacting angles. Fig.4.14c gives steady state of erosion rate at various angles (30^o, 45^o, 60^o and 90^o). At all the impact angles, the erosion resistance in increasing order is 13/4 steel, 23/8N and 21/12N steel.

Fig. 4.15 (a)-(f) display the images obtained from all of the tested steels at 30^o and 90^o. 23/8N steel (Fig. 4.15c) at 30^o erosion loss mainly because of shear cutting of surface of the materials. Presence of ploughs with lips formed at the side shows that shear that has occurred. The ploughs in 13/4 steel (Fig. 4.15a) are much wider and deeper than those observed in 23/8N (Fig 4.15c) steel. The 21/12N steel exhibited minimum damage. At 90^o, eroded surfaces are without ploughs and damage is due to flaking and surface cavity formation (Figs.4.15 b, d and f). Intense surface cavities are observed at 90^o compare to 30^o which are created due to removal of material by hard impact alumina particle. The cumulative mass loss at all angles is low for 21/12N steel as compared to 13/4 and marginally higher as compared to 23/8N steel. 13/4 steel comprises martensitic structure and martensitic lathes are associated with high stresses which are not suitable to erosion resistance.

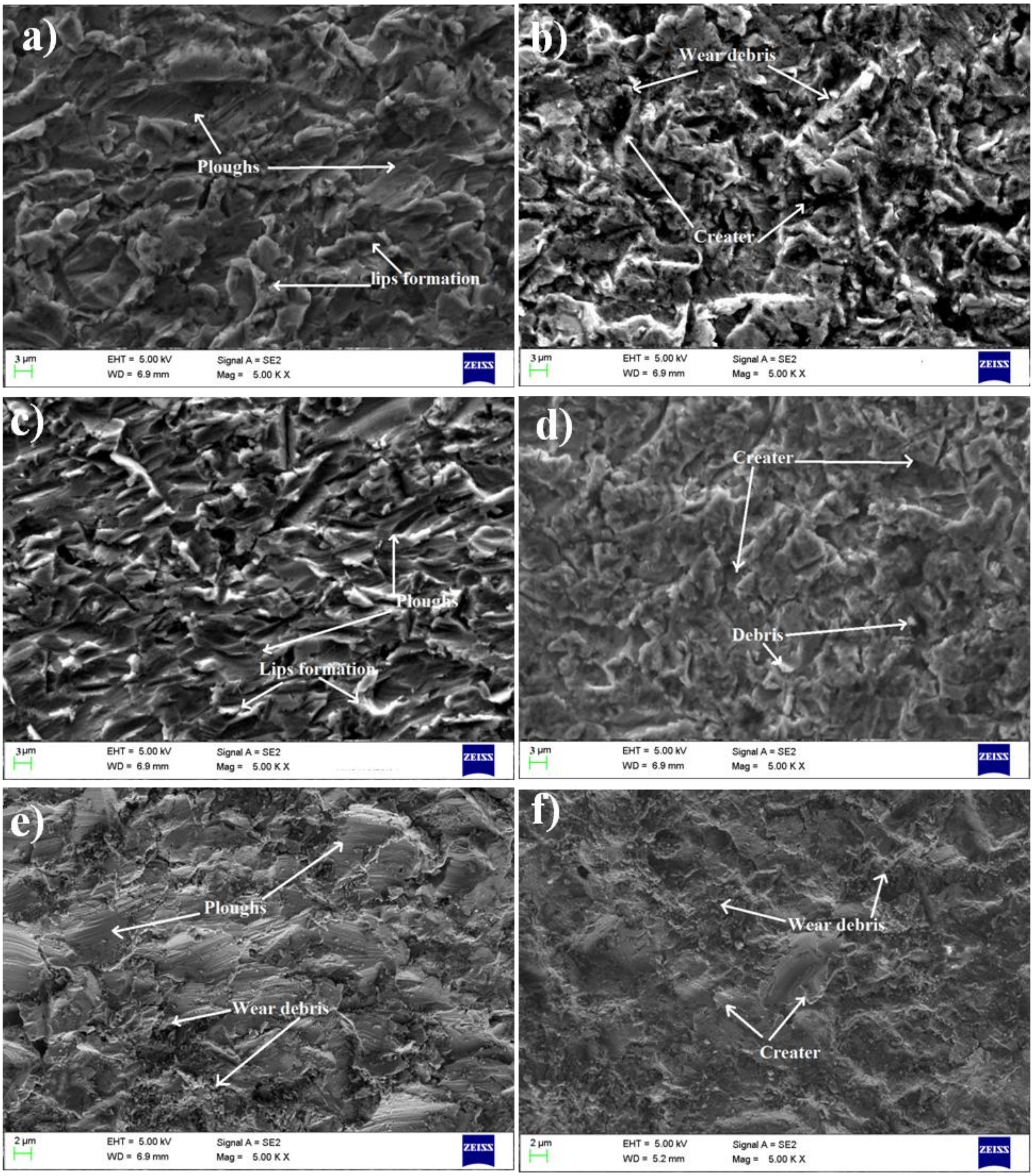

Fig.4.15. Secondary electron SEM micrographs of eroded surfaces after solid particle erosion of as received 13/4, at ((a) 30°, (b) 90°); 23/8N at ((c) 30°, (d) 90°) and 21/12N ((e) 30°, (f) 90°) steels.

Thus, it exhibits higher erosion rate as compare to other steels. Depth of average wear scars (calculated from three measurements in surface profiler) after erosion test reported in table 4.2. It shows that average depths of wear scar for 13/4 steel are higher than that for both nitronic (23/8N and 21/12N) steels.In cavitation erosion, the material was under gone to very high repeated loading by impact wave during cavitation. During the cavitations of GCI the matrix material surrounding the graphite is pounded into small fragment then ejected out leads to material loss. It is observed that in 13/4 steel, martensitic structure is prone to cavitation attack. Higher ductility and tensile toughness of the austenitic matrix of 21/12N steel leads to improved resistance to cavitation erosion. Xi et. al. have reported that the carbide/austenite interface exhibits high stresses in austenitic stainless steels [Xi 1993]. In agreement with Xi et. al. this interface is found to be damaged severely in 23/8N and 21/12N steels in comparison to austenitic matrix. The interface regions are incapable to have strain hardening and thus become brittle and disconnected by cavitation attack. On the other hand, cavitation erosion of austenite in austenitic stainless steel leads to increase in the localized strength with strain hardening. Soussan et al [1991]. have also reported that localized strength of austenite increases with strain hardening. Thus, austenite-carbide interfaces are preferential sites for cavitation erosion than the austenite matrix of 23/8N and 21/12N steels.

Continuous explosion of cavitation impact wave on the surface of target specimen leads to plastic deformation. Both nitronic steels exhibit higher ductility as compared to 13/4 steel. It also undergoes significant work hardening. As a result 23/8N steel becomes tough and able to bear load for longer duration compare to 13/4 steel. Thus the martensitic steel has low ductility (22%) and showed more erosion damage than the steels which exhibit higher ductility (23/8N- 32% and 21/12N- 45%). The material which shows good cavitation erosion resistance should be able to absorb the energy of the cavitation impact wave in order to delay the nucleation of cracks. Tensile toughness measures the capacity of material to absorb energy in the plastic range. Cavitation erosion test produces very high strain rates [Chauhan 2009] leading to rapid work hardening.

A correlation can be established between the tensile toughness and cavitation erosion test result. The tensile toughness of 13/4, 23/8N and 21/12N steels are 68 MJm^{-3}, 240 MJm^{-3} and 281 MJm^{-3}, respectively, as determined from the area under their respective stress-strain curve between yield strength and fracture stress. It can be concluded that higher tensile toughness imparts more cavitation erosion resistance. Higher toughness of steels enables it to absorb high energy to deform plastically during cavitation attack. Austenitic matrix in the steel is more likely to develop in-situ work hardening as compared to steels having martensitic structure. The strain hardening exponents of 13/4, 23/8N and 21/12N steel were observed to be 0.07, 0.55 and 0.52 respectively. The high strain hardening exponent of 23/8N and 21/12N steels lead to higher cavitation erosion resistance as compare to 13/4 steel in cavitation process. The cavitation erosion of 21/12N steel is marginally higher than the 23/8N steel, because of the high ductility coupling with high tensile toughness; maintained tensile strength, hardness and strain hardening exponent. Also because of high carbon content in 23/8N steel chromium carbides volume fraction is more in 23/8N steel as compared to 21/12N. The carbide matrix interfaces are the preferential sites of cavitation attack and thus 23/12N steel exhibits superior cavitation erosion resistance.

Low stacking fault energy leads to high work hardening rate. Schramm et.al. have already reported that Cr rapidly decreases the stacking fault energy in Fe-Cr-Ni based alloys. They have observed that alloying additions such as Cr, Si, Mn and N in Fe-Cr-Ni austenitic alloys tend to reduce stacking fault energy while Ni and C additions tend to enhance the stacking fault energy [Schramm 1975]. In case of 23/8N and 21/12N steels, the low stacking fault energy of their austenitic matrix may lead to higher value of strain hardening exponent.

Mechanical properties are important factor to decide the particle erosion resistance. The target material is deformed plastically due to the repeated attack by hard abrasive particles. High hardness in addition to high ductility leads to more erosion resistance. High hardness plays an important role to override the damaging effect of hard impinging particles. Ductility provides relief from impinging particles with high velocity by the way of partial absorption of their kinetic energy in permitting localized deformation at impact sites, thus minimizing the probabilities of cracking. Tensile strength of steel does not appear to have significant role in affecting the erosion behavior in the present study. Tensile toughness of 21/12N steel is high compared to the 13/4 and 23/8N steels. The tensile toughness is indicative of the ability of a material to absorb kinetic energy of impinging particles which minimizes the chances cracking in the surface of materials. Thus, the target material with higher tensile toughness exhibits higher erosion resistance [Levin 1999]. This shows that during silt impact the stresses developed during tensile test contribute significantly to the mechanism of erosion. Further, the impact energy, as determined by Charpy V-notch test, also plays an important role. 21/12N steel possesses better erosion resistance due to its high impact energy (217 J) than that of 13/4 and 23/8N steels (64 and 85 J).

Nitrogen decrease stacking fault energy. Lower stacking fault energy of steel may lead to higher rate of work hardening which is more likely to develop in austenitic matrix than a martensitic structure [Schramm 1975]. The higher resistance to particle erosion nitronic steels can therefore be attributed to the low stacking fault energy of their austenitic matrix. From stress-strain diagram, it is noticed that severe in situ strain hardening occurs during tensile testing in nitronic steels, whereas less strain hardening takes place during tensile testing of 13/4 steel. During erosion high strain hardening exponent n of nitronic steels leads to higher erosion resistance in comparison to 13/4 steels possessing lower strain hardening exponent.

Voids developed due to localization of strain in the target materials may be an important parameter in determining the erosion resistance. Formation of large concentration of voids in tensile and impact fracture leads to higher erosion rate of 13/4 steel as compared to 23/8N and 21/12N steels. Strain rates developed in the target materials due to erosion may be very high as compared to those generated due to normal mechanical testing [Divakar 2005]. Charpy impact test of 13/4 steel (Figs. 4.5 and 4.6) results in extensive localization of strain. Generally 13/4 steel is found to be more prone to localization of strains due to highly stressed martensitic matrix This causes higher erosion damaged in 13/4 steel as compare to 23/8N and 21/12N steels.

4.6 Conclusions

1. The cavitation erosion resistance of GCI, 13/4 and 23/8N steel is less than 21/12N steel.

2. In GCI erosion starts at graphite flakes and thus the erosion resistance is lowest. The martensitic laths present in 13/4 steel erode more rapidly than austenitic matrix of 23/8N and 21/12N steels. The martensitic laths are already associated with internal stresses and have lower capacity to consume the strain energy due to transient stresses in target material produced by cavitation impact wave.

3. In both nitronic steel (23/8N and 21/12N steel), the damages occur during the cavitation test preferably along carbide/matrix interface. 23/8N steel shows marginally lower cavitation erosion resistance due to large fraction of carbides.

4. 21/12N steel shows higher cavitation erosion resistance because of high hardness coupled with ductility, high tensile toughness and strain hardening exponent as compare to 13/4, 23/8N steels.

5. Solid particle erosion also follow the erosion resistance trend of cavitation erosion, lowest erosion resistance is found in 13/4 steel followed by 23/8N steel; 21/12N steel exhibited the highest particle erosion resistance.

6. The SEM micrographs of worn out surfaces of all tested steels at low impact angle show that the material is removed by ploughing. At normal impact condition, no ploughing is observed. The material is removed by flaking of the material.

Chapter 5

Effect of heat treatment on cavitation and solid particle erosion behaviour of 21/12N and 23/8N steels

This chapter deals with the results of heat treatment of 21/12N and 23/8N steels. The effect of heat treatment on microstructure and mechanical properties has been studied. Due to heat treatment, the grain size of the nitrogen containing austenitic steel increases. Its effect on the solid particle erosion and cavitation erosion behavior is also studied.

5.1 Introduction

Nitrogen-added austenitic stainless steels possess attractive properties such as good corrosion resistance, high strength, good weldability and reduced tendency to grain boundary sensitization. [Kirami 1992, Hanninen 2001] Cavitation erosion (CE) of valves, turbine blades, ship propellers and pump impellers can lead to failure and/or to high maintenance costs [Hajian 2014, Selokar 2013]. Currently 13/4 martensitic stainless steels are used in these parts because of their high resistance to erosion. Cr–Mn–N austenitic stainless steels have potential to substitute these Cr–Ni–Mo stainless steels because of their lower cost and higher CE resistance [Liu 2003].

Change in grain size has a significant effect on cavitation erosion of austenitic stainless steel [Bregliozzi 2005, Hajian 2014]. Finer grain size leads to higher hardness and an improved resistance to cavitation erosion. Austenitic stainless steels also exhibit resistance to solid particle erosion [Foley 1983]. Levy [1981] emphasized that within limits, the erosion rate is minimum for continuous ductile matrix. However, when the matrix becomes more ductile, the strength of the steel is markedly reduced and becomes the dominant factor in erosion. Mechanical properties of the target material exert a strong effect on erosive wear. The erosive rates may increase when a material is intentionally hardened. This can be illustrated by comparing the relative erosion resistance of target metals as a function of impact angle. When the impingement angle is high, hardened steel shows higher erosion than softer one; the reverse is true in case of shallow impingement angles. The increase in the hardness of steel as a result of heat treatment reduces erosive wear at low impinging angles but increases erosive wear at high angles. Ball [1999] has tried to determine regimes of erosion of hard metals, falling in the range “plasticity-dominated” to “fracture-dominated” behaviour. For brittle materials such as glass and alumina, the erosion rate is decided by particle size, kinetic energy and relative hardness and toughness of erodent particles. However, the shape and kinetic energy of erodent particles are the most important factors deciding the erosion rate of ductile materials. He also reported that there is no significant effect of toughness and hardness of erodent particles on erosion.

Foley and Levy [1983] noticed that the ductility has a significant effect on erosion resistance of steels. Erosion resistance increases with increasing ductility while strength, hardness, impact strength and fracture toughness have only a slight effect on erosion behavior. Ninham [1988] has reported that the work hardening or aging treatments carried out on high temperature alloys had no essential change in the erosion rates. He also reported that the carbide particles which are responsible for abrasion resistance to alloys are found to obstruct plastic flow around the indentation, resulting in void formation and fracture and concluded that the carbides are unfavorable to erosion of steel. The grain size and chemical composition of nitrogen alloyed steels is reported to influence mechanical properties, corrosion resistance and wear resistance [Bregliozzi 2005].

5.2 Effect of heat treatment on cavitation and solid particle erosion behaviour of 21/12N steel.

In this section 5.2, the cavitation and solid particle erosion behaviour of heat treated 21/12N steel have been studied.

5.2.1 Microstructure

The as received 21/12N (AR) steel was solutionized by heat treating at 1000 °C (HT-1), 1100 °C and 1150 °C (HT-2) for 3 hrs followed by water quenching. X-ray diffraction results confirmed the steel to be austenitic. Fig. 5.1a, b and c show the microstructures of AR, HT-1 and HT-2 heat treated steels, respectively. AR steel exhibits equiaxed grains. Some fine (<1µm) precipitates are observed along the grain boundaries. EDS confirmed these precipitates to be carbides (Fig. 5.1d). These are expected to be M_7C_3 and $M_{23}C_6$ types of carbides [Gadhikar 2014]. Annealing twins are observed in some grains. The solutionising treatment also resulted in grain coarsening. The average grain size measured after different conditions is 15 µm (fine grain AR), 25 µm (medium grain HT-1) and 65 µm (coarse grain HT-2), respectively.

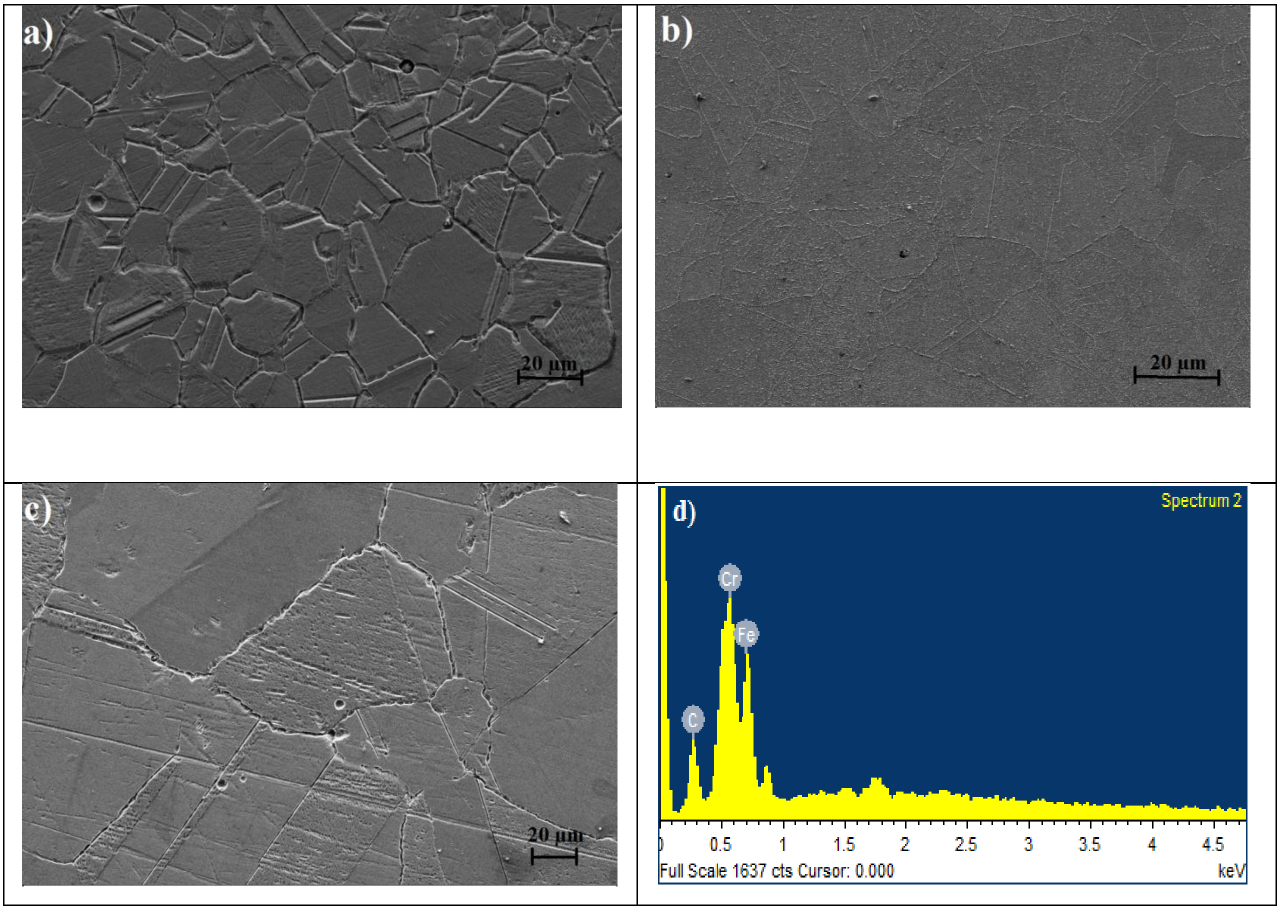

Fig. 5.1 Secondary electron SEM micrographs (a to c) showing Microstructure of 21/12N (a) AR, (b) HT-1, (c) HT-2 steels. EDS spectrum (d) of grain boundary precipitates of chromium carbide in AR steel.

5.2.2 Mechanical properties

The mechanical properties of AR, HT-1 and HT-2 21/12N steels are listed in Table 5.1. The heat treatment results in reduction in hardness, yield strength (YS), ultimate tensile strength (UTS) and strain hardening exponent. This is mainly due to increase in the grain size. After the heat treatment, the impact strength, tensile toughness and ductility show marginal improvement. Fig 5.2a Engineering stress strain curve of the same steels. Fig5.2b shows volume fractions of equilibrium phases as a function of temperature as estimated from Thermo-Calc® software of 21/12N (C 0.19 wt. %) steel. It shows that $M_{23}C_6$ type of carbide is present upto the 1000 ^{o}C after that it completely dissolved.

Table 5.1 Mechanical properties of the AR, HT-1 and HT-2 21/12N steel.

Properties of steel	**AR**	**HT-1**	**HT-2**
Hardness (VHN)	250	235	218
Yield Strength (MPa)	480	445	382
Ultimate Tensile Strength (MPa)	763	732	716
Ductility (% Elongation)	45.3	46.5	50.5
Impact strength (J)	217	266	299
Tensile toughness MJ/mm3	281	288	291
Strain Hardening exponent(n)	0.52	0.47	0.46

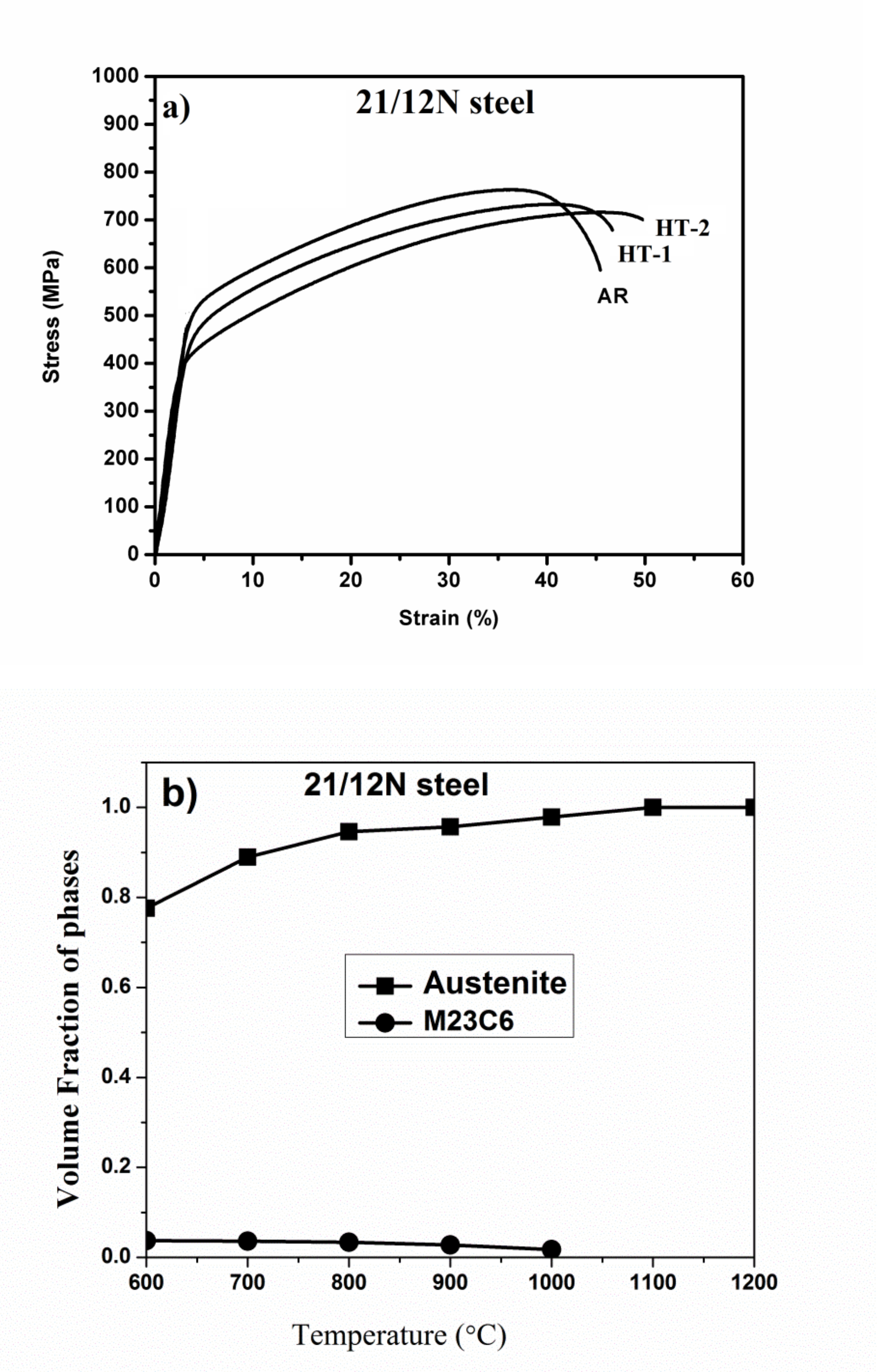

Fig. 5.2 (a) Engineering stress strain curves for AR, HT-1 and HT-2 steel (b) Volume fractions of equilibrium phases as a function of temperature as estimated from Thermo-Calc® software of 21/12N (C 0.19 wt. %) steel.

5.2.3 Cavitation and solid particle erosion of 21/12N steel (AR, HT-1 and HT-2 steel)

The cumulative weight loss (CWL) after cavitation erosion test is measured and plotted against different interval of time shown in Fig. 5.3a, while Fig. 5.3b shows mean depth of erosion (MDE) against time of erosion. The erosion rate consistently increases with time for the steel solution treated at 1100 °C. The erosion rate increases gradually up to 6 hrs and then increases sharply for the HT-1 and HT-2 steels. The AR steel which had the finest grain size exhibited the best erosion resistance. Thus the erosion rate seems to increase with increase in grain size. Bregliozzi et al have reported that fine grains give rise to large surface to volume ratio of grain boundary, which provides supporting action during cavitation process [Bregliozzi 2005]. This was attributed to constraint in dislocation motion at the grain boundaries, which act as slip barriers. While, coarse grains provide less grain boundary area for obstructing the movement of dislocation. Thus, coarse grain size after the heat treatment may cause an increase in the erosion rate. The surface roughness R_a values after cavitation erosion are shown in Fig. 5.3c. R_a value of HT-1 and HT-2 steel increased sharply after 6 hrs.

Fig. 5.4(a-e) shows SEM images of eroded surfaces after cavitation testing. Fig. 5.4a shows that damage mainly occurred at the austenite grain boundaries. The carbides are located at the grain boundaries and the interface regions between carbide and austenite serve as high stress regions [Xi 1993]. These regions served as the preferential sites for erosion. These weakest phases of the material served as preferential sites for cavitation erosion [Chauhan 2008, Zhao 1993]. A few holes are seen in the carbides region after erosion for 12 hrs (Fig. 5.4b). This is probably due to removal of carbides due to erosion. Thus, carbide-austenite interfaces are largely attacked as compare to austenite grains. After 24 hrs of cavitation erosion, wide and deep cavities are produced due to removal of carbides and matrix (Fig. 5.4c and 5.4f).

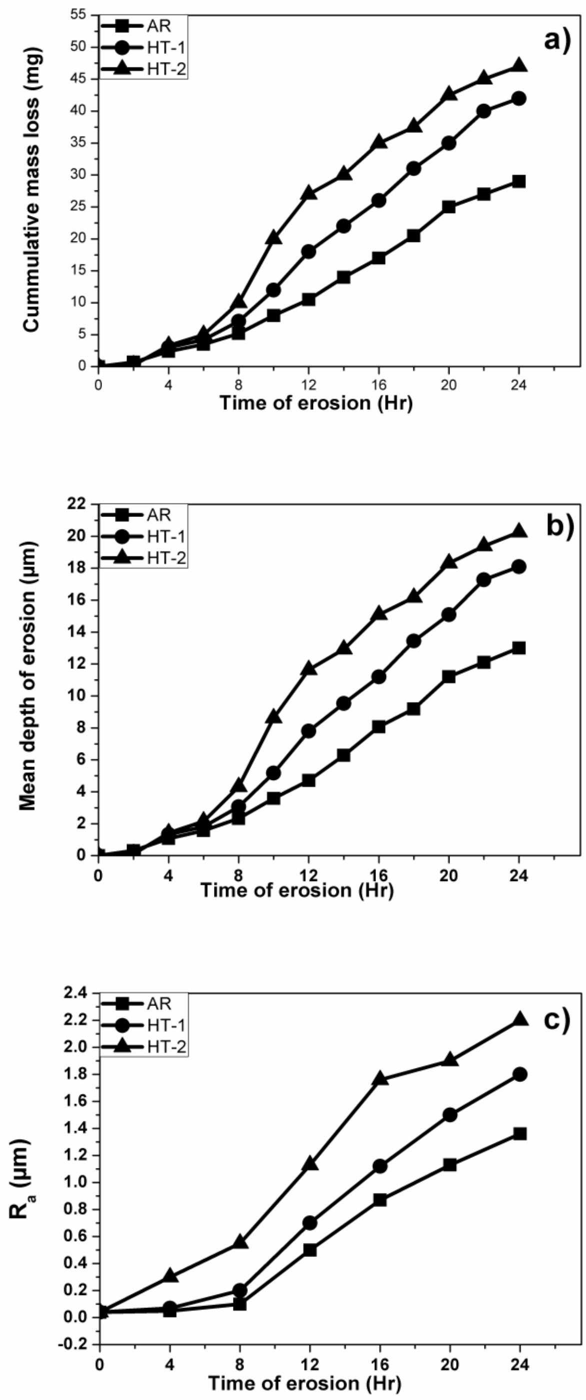

Fig. 5.3 Plot of cavitation erosion of as received, HT-1 and HT-2 steels (a) cumulative weight loss (CWL), (b) mean depth of erosion (MDE) and (c) surface roughness R_a as function of time.

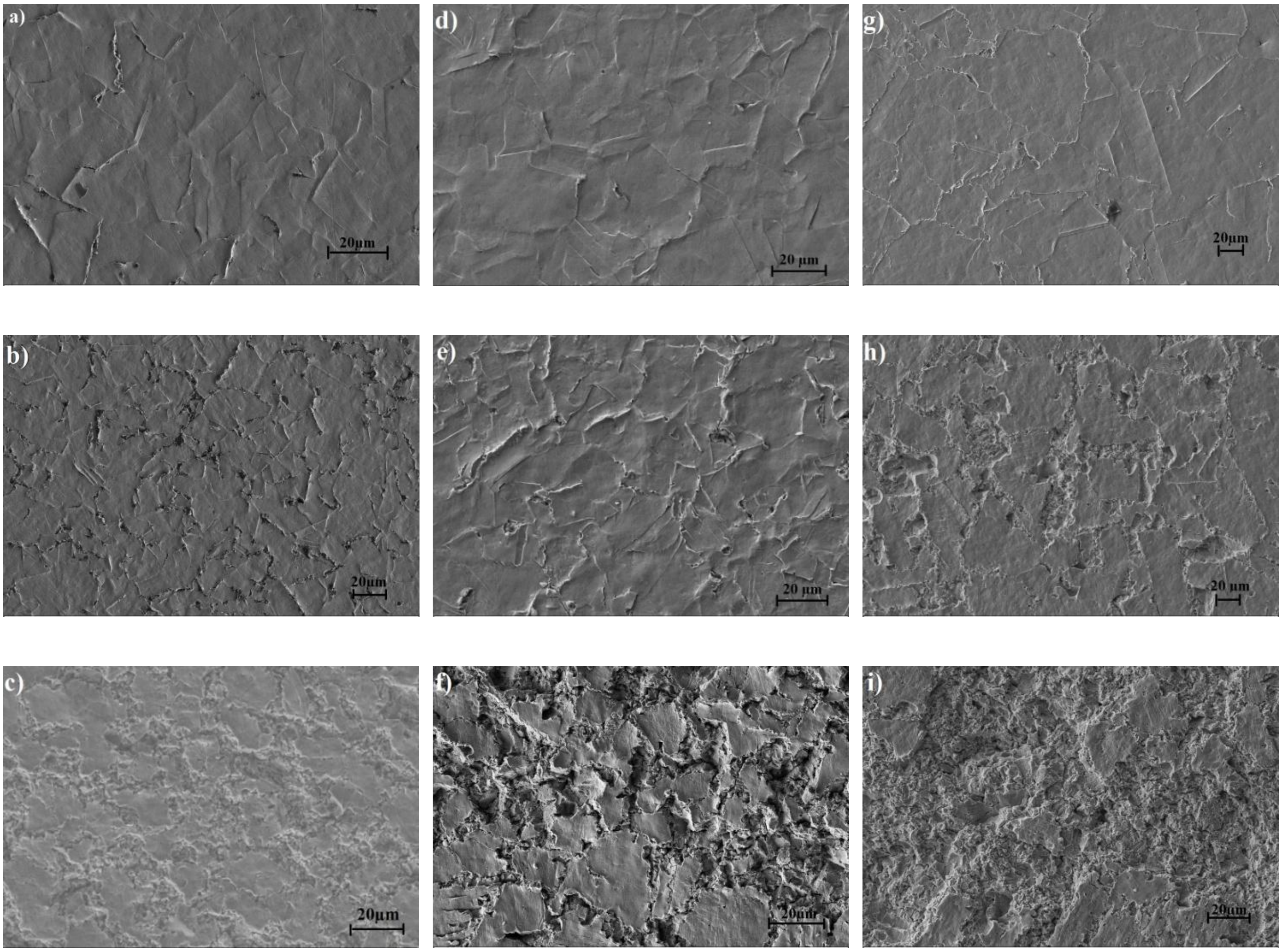

Fig. 5.4 Secondary electron SEM micrographs of AR steel (a) 6 hrs, (b) 12 hrs, (c) 24 hrs, HT-1 steel (d) 6 hrs, (e) 12 hrs, (f) 24 hrs and HT-2 steel (g) 6 hrs, (h) 12 hrs, (i) 24 hrs after cavitation erosion.

Fig. 5.5 shows the morphology of coarse grain heat treated steel after 12 hrs of cavitation erosion. Cavitation testing promotes the formation of slip lines inside the individual grains of austenite that end at the boundaries. The formation of waviness on surface corresponding to the presence of grain boundaries and slip bands can be observed (Fig. 5.5a). The number of slip lines increases for longer exposure to cavitation. The slip lines as well as grain boundaries act as preferential sites of stress concentration. The continual impact of micro-jets produces these defects and later, material removal starts from these sites. Similar mechanism of material removal has been reported for other austenitic steels [Bregliozzi 2005]. Fig. 5.5b shows material removal from annealing twins in the same sample.

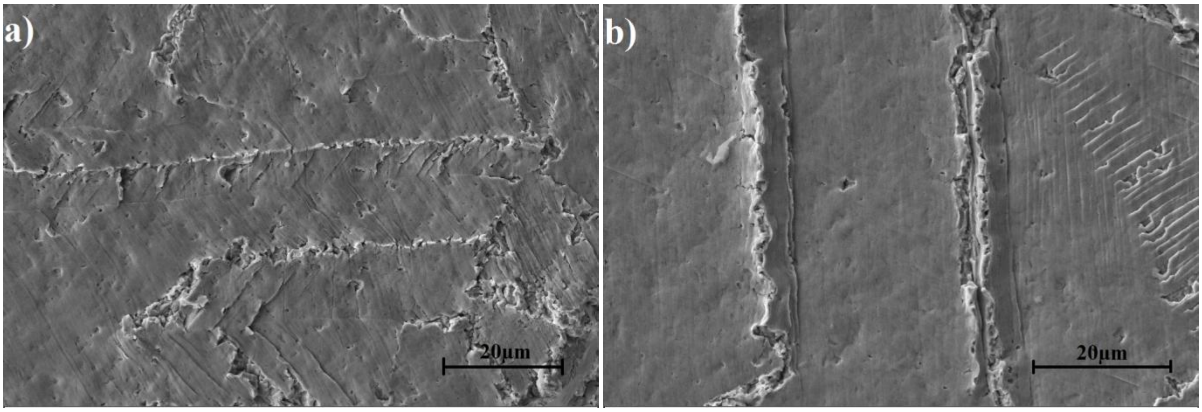

Fig. 5.5 (a) and (b) Secondary electron SEM micrographs of heat treated (HT-2) steel after cavitation erosion for 12 hrs.

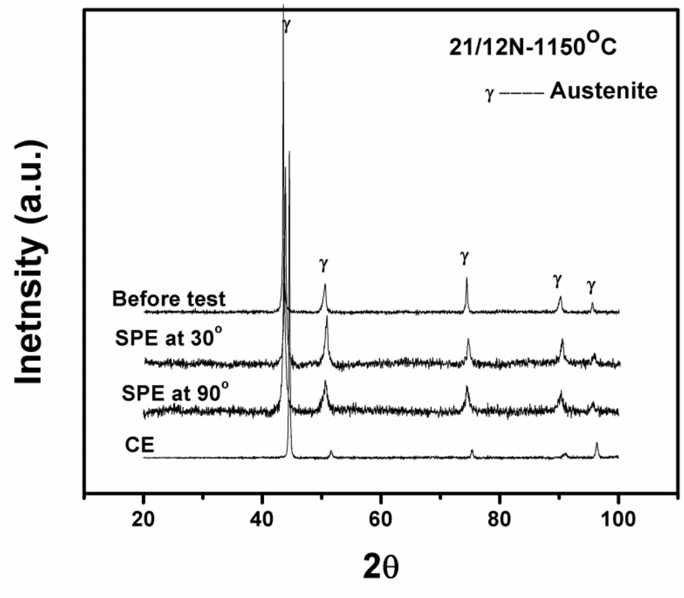

Fig. 5.6 X-ray diffraction trace of relative intensity vs 2θ showing the absence of strain induced martensite in solution annealed at 1150°C nitrogen steel samples subjected to cavitation erosion and solid particle erosion.

The X-ray diffraction results show that strain induced martensite does not form after cavitation erosion. This may be because addition of nitrogen may prevent formation of strain induced martensite [Bregliozzi 2005]. Fig. 5.7a and b show the cumulative weight loss (CWL) curves in AR and heat treated 21/12N steels at the impact angles of 30^o and 90^o. At both the angles, CWL in heat treated steels is almost same as that in the AR steel. Fig.5.7c gives the steady state of erosion rate at various angles (30^o, 60^o and 90^o). At all impact angles, erosion rate in heat treated steel is slightly more than that of AR steel. Erosion behaviour is affected by the impinging angle of erodent with erosion rate being higher at 90^o.

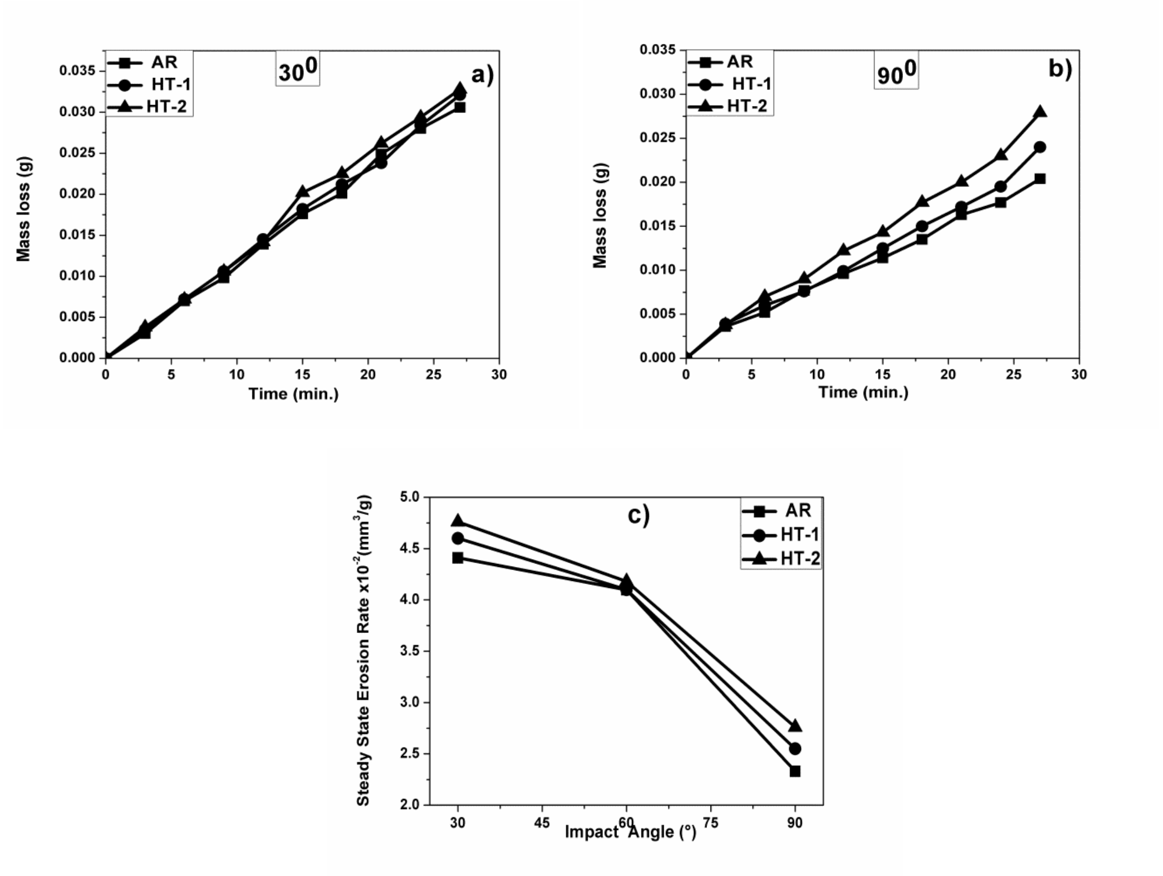

Fig. 5.7 Cumulative weight loss (CWL) at (a) 30^o, (b) 90^o, and (c) steady state erosion rate of AR, HT-1 and HT-2 steels.

In general, the erosion rate is highest at a low angle (30°) for a ductile material while reverse is true for brittle material [ASM Handbook 1992]. The higher erosion rate observed at

30^o in AR as well as heat treated steels in the present study indicates ductile nature [Hutchings 1992].

Table 5.2 Depth of wear scar (µm) after particle erosion.

No. of test	AR depth (µm)		HT-1 depth (µm)		HT-2 depth (µm	
	30^0	90^0	30^0	90^0	30^0	90^0
1	70	105	79	117	80	135
2	72	115	76	119	81	127
3	75	108	71	111	75	125
Avg. value	72.33	109.33	75.33	115.67	78.67	129

The depth of the wear scars after erosion test at 30^o and 90^o is shown in Table 5.2. The depth of erosion is more for samples tested at 90^o. This is because the area of impact reduces with increase in impact angle from 30^o to 90^o. Thus variation in depth of wear is reverse of that for data for material removal (Fig. 5.7). Weight loss during particle erosion is a better measure of the erosion rate.

Fig. 5.8 (a-f) display the images of worn surfaces obtained from AR and heat treated steels at 30^o and 90^o. The erosion at 30^o in AR and heat treated steels mainly occurred due to ploughing. Shear phenomenon was found indicated by the presence of ploughs with lip formation at sides. At impact angle of 30^o, the erosion loss occurred because of shear cutting of surface material. However, wider and deeper ploughs are observed in heat treated steel (Fig. 5.8c and e) than that in AR steel (Fig. 5.8a). The erosion occurred at 90^o shows rougher surface in comparison to 30^o. The removal of the material occurred by pitting as well as formation of deep surface cavities. Some wear debris were moved into the cavities produced by abrasive particles. The same phenomenon was observed in the brittle fracture in ceramics and other hard materials [Wheeler 2001, Telling 1999, Marshall 1982]. The ploughing is significantly less in the surfaces eroded at 90^o in AR and heat treated steels. Deeper cavities are observed in heat treated steel (Fig. 5.8(d) and (f)) as compared to AR steel (Fig. 5.8(b)). The rate of erosion is slightly higher for heat treated steels as compared to AR steel for any impact angles

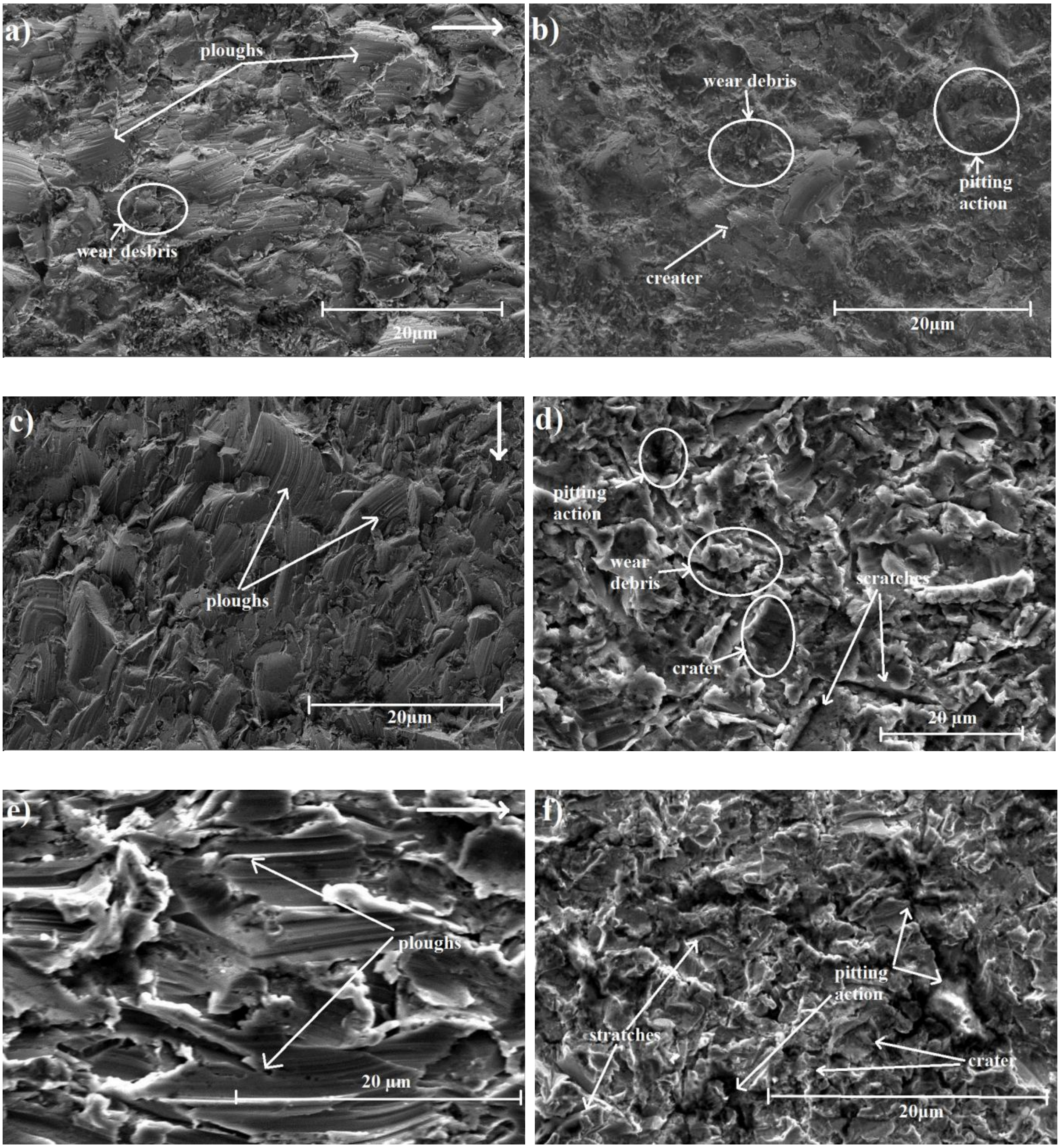

Fig. 5.8 Secondary electron SEM micrographs of eroded surfaces after solid particle erosion of as received steel (AR) at ((a) 30^o, (b) 90^o); HT-1 at ((c) 30^o, (d) 90^o) and HT-2 ((e) 30^o, (f) 90^o).

The austenitic phase has advantage in solid particle erosion due to its plasticity and toughness. The localized strength of austenitic phase increases with work hardening of matrix resulting in improvement in the erosion resistance [Divakar 2005]. The target material deforms plastically due to the repeated attack by hard abrasive alumina particles. The tensile toughness also plays important role in erosion resistance as the tough material absorbs kinetic energy of impinging particles [Chauhan, 2009]. The erosion rate decreases with increasing toughness and ductility [ASM Handbook 1992]. In the present work there is no significant variation in ductility and tensile toughness of the nitrogen steel with heat treatment. During erosion, the high strain hardening exponent (n) of AR steel leads to significant strain hardening and higher erosion resistance in comparison to heat treated steel. The grain size does not seem to significantly affect the particle erosion behavior in the nitrogen steel tested. This is in agreement with the observation that grain boundaries did not act as preferential sites for solid particle erosion.

The higher tensile toughness of nitrogen steel tested may also explain the improved resistance to cavitation erosion observed. The higher hardness and strength of AR steel is responsible for its higher resistance to cavitation erosion (Fig. 5.3) as all the three nitrogen steel samples have similar tensile toughness (Table 5.1).

5.2.4 Conclusions

The nitrogen alloyed austenitic stainless was subjected to solutionizing heat treatment. The grain size was also found to be increased from 15 to 65 μm as a result of this treatment. The influence of grain size on cavitation erosion and particle erosion behaviour was studied. The following are the major conclusions:

1) The 21/12N nitrogen alloyed austenitic stainless steel with fine grain size exhibits superior resistance to cavitation erosion.
2) The cavitation erosion damage started near grain boundary carbides at carbide matrix interface
3) No significant effect of grain size was observed on particle erosion behaviour.
4) No formation of strain induced martensite in the nitrogen alloyed austenitic stainless steel during erosion studies.

5.3 Effect of heat treatment on cavitation and solid particle erosion behaviour of 23/8N steel.

The present section deals with the heat treatment effect on cavitation and solid particle erosion behaviour of 23/8N steel. The heat treatment results in change in the microstructure and mechanical properties of 23/8N steel. The solution annealing heat treatment causes dissolution of the carbides. The presence of hard phase carbide increases the erosion resistance of material by reducing the sharpness of impinging particle on it, which lead to a measurable reduction in mass loss from target material. On the other side, the brittleness of carbide may increase the mass loss due to erosion by completely removal of cracked carbide due to impact of erodent particle.

5.3.1 Microstructure

The heat treatment of 23/8N steel was carried out at various temperatures (1000^{o}C, 1050^{o}C, 1100^{o}C and 1150^{o}C) for 3 hrs followed by water quenching. 23/8N steel samples quenched from 1100^{o}C were aged at 700^{o}C for 20 hrs. The microstructures of 23/8N steel solution annealed at 1000^{o}C and 1150^{o}C for 3 hrs followed by water quenching are shown in Fig. 5.9. The microstructures of solution annealed at 1000^{o}C temperature for 3 hrs followed by water quenching consists of carbides in the matrix of austenite (Fig. 5.9a). This resembles with the microstructure of as received 23/8N steel (Fig. 4.1c). At 1100^{o}C, very less amount of carbide precipitates along the grain boundary (Fig. 5.9b), since during water quenching very few amount of carbides are precipitated. In Fig. 5.9c, the microstructure of 23/8N after 1150^{o}C exhibits coarse grain size with no carbides along the grain boundary. Thus, 23/8N steel specimen solution annealed at 1150^{o}C has less hardness (Table 5.3). The uniform distribution of carbides was achieved by the reprecipitation (aging) heat treatment. The microstructure after solution annealing at 1100^{o}C followed by water quenching and aging at 700^{o}C for 20 hrs exhibits carbides along the grain boundaries as well as inside the grain (Fig. 5.9d). The carbides are again precipitate and distributed uniformly after this heat treatment.

Annealing twins are observed in after various heat treatments. The solution annealed treatments also result in grain coarsening. The resulting grain size is 10±2 µm (fine grain as-recieved), 16 ± 2 µm at 1000 ^{o}C, 22 ± 3 µm at 1000 ^{o}C and 45 ± 4 µm at 1150 ^{o}C.

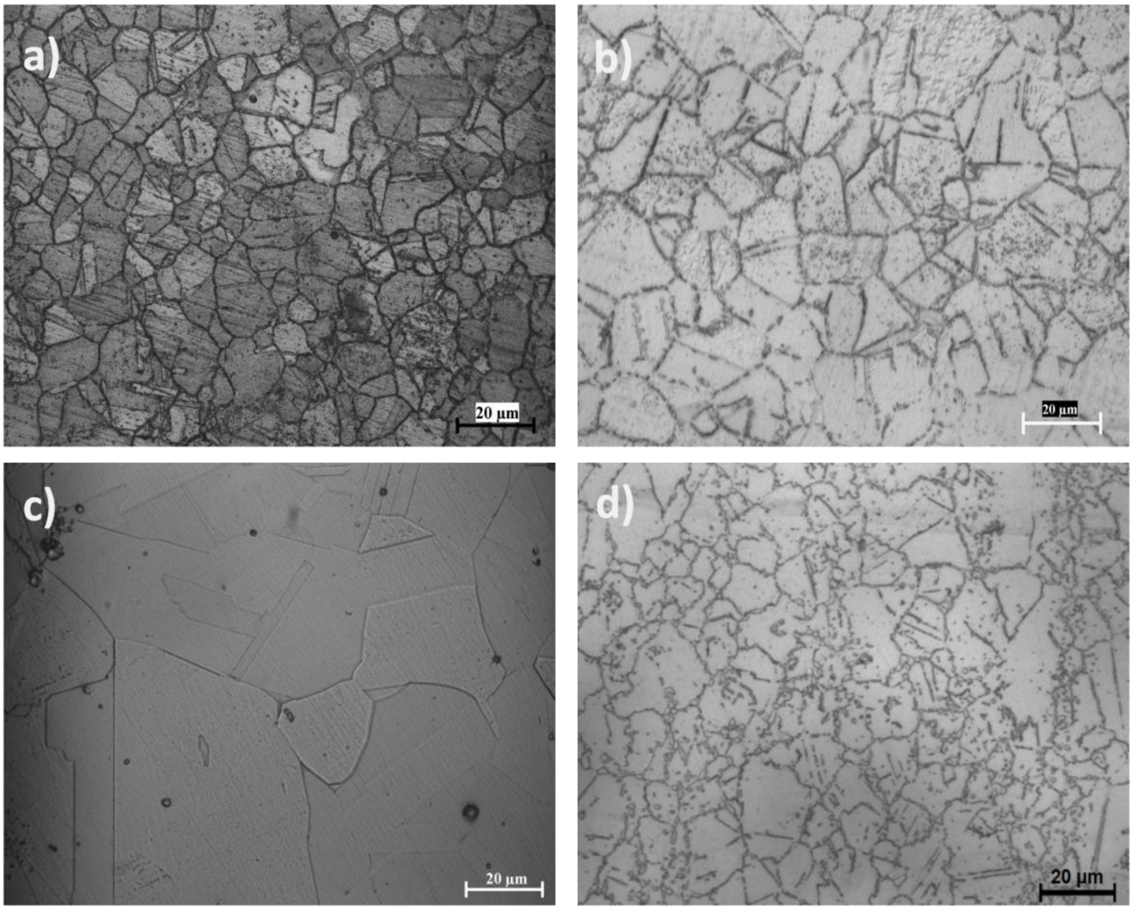

Fig. 5.9 Optical Microstructures of 23/8N steel after solution annealed at (a) 1000°C, (b) 1100°C, (c) 1150°C and (d) at 1100°C followed by aging at 700°C.

Fig. 5.9c shows that all carbides are dissolved at 1150 °C. Also, X-ray diffraction results confirm the steel to be austenitic (Fig. 5.16) after these heat treatments. Fig. 5.10 shows volume fractions of equilibrium phases as a function of temperature as estimated from Thermo-Calc® software of 23/8N (C 0.31wt. %) steel. It also plays supportive role to microstructure that very less volume fraction of carbide are present in austenitic matrix present at 1000°C. Carbides are complete dissolved around at 1100°C (Fig. 5.10). Thus, it is observed that the dissolution of carbides increases with increase in the temperature of solution treatment.

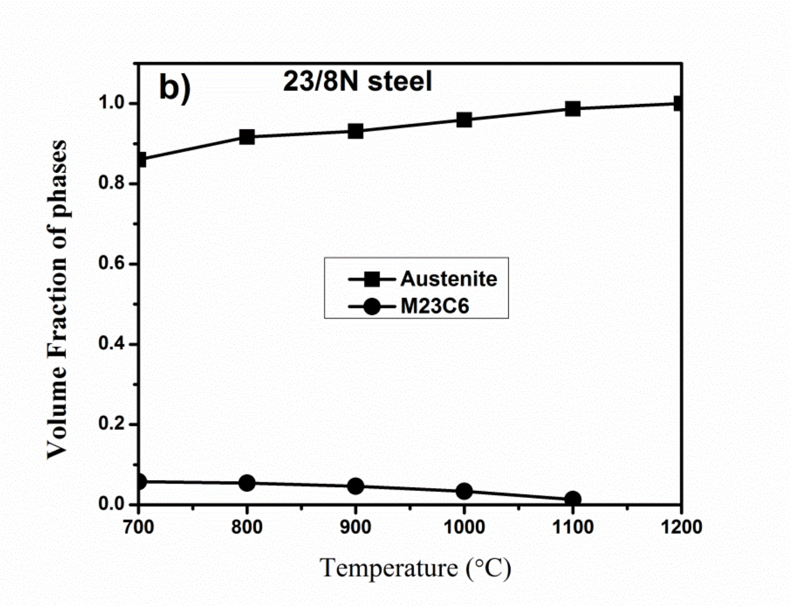

Fig. 5.10 Volume fractions of equilibrium phases as a function of temperature as estimated from Thermo-Calc® software of 23/8N (C 0.31 wt. %) steel.

5.3.2 Mechanical properties

Table 5.3 shows the mechanical properties of 23/8N steels various heat treated steels. The heat treatment results in marginally reduction in hardness, improvement in yield strength (YS), ultimate tensile strength (UTS) and strain hardening exponent. This is mainly due to dissolution of carbon and chromium from the carbides in to austenitic matrix. Dissolution of carbides improves the stability of austenitic matrix. The mechanical properties such as impact strength, tensile toughness and ductility show improvement after solutionizing heat treatements.

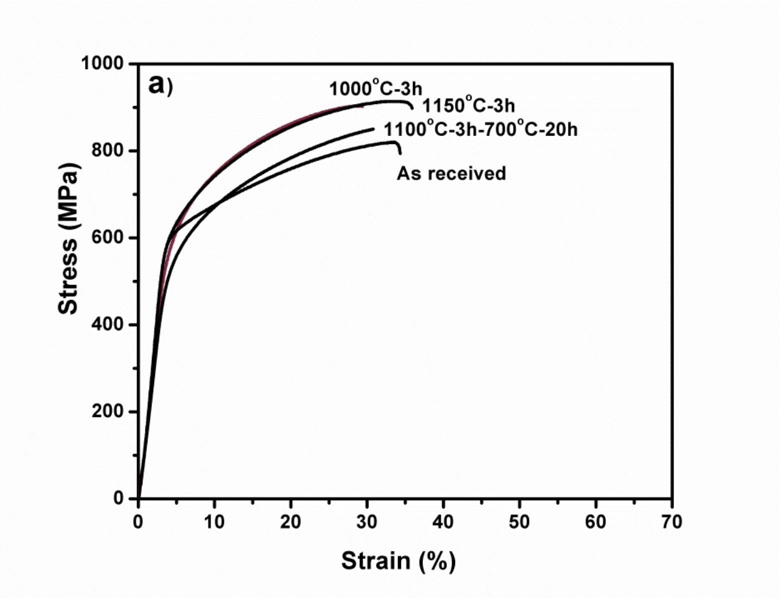

Fig. 5.11 Engineering stress strain curves for as received and various solution annealed heat treatments i.e. 1000 °C, 1150^{o}C, and at 1100°C followed by aging at 700^{o}C.

Table 5.3 Mechanical properties of the heat treated 23/8N steel.

Properties of steel	23/8N steel				
	Solution annealed (3 hrs) at				Sol. Annealed at 1100^{o}C (3 hrs) followed by aging at 700^{o}C (20 hrs)
	1000^{o}C	1050^{o}C	1100^{o}C	1150^{o}C	
Hardness (VHN)	260	255	255	245	270
Yield Strength (MPa)	598	590	595	600	519
Ultimate Tensile Strength (MPa)	902	900	910	914	824
Ductility (% Elongation)	29.6	32.3	34	36	30
Impact strength (J)	68	72	74	105	66
Tensile toughnessMJ/mm^{3}	242	251	261	270	245
Strain Hardening exponent(n)	0.56	0.55	0.56	0.56	0.54

5.3.3 Cavitation and solid particle erosion of heat treated 23/8N steel

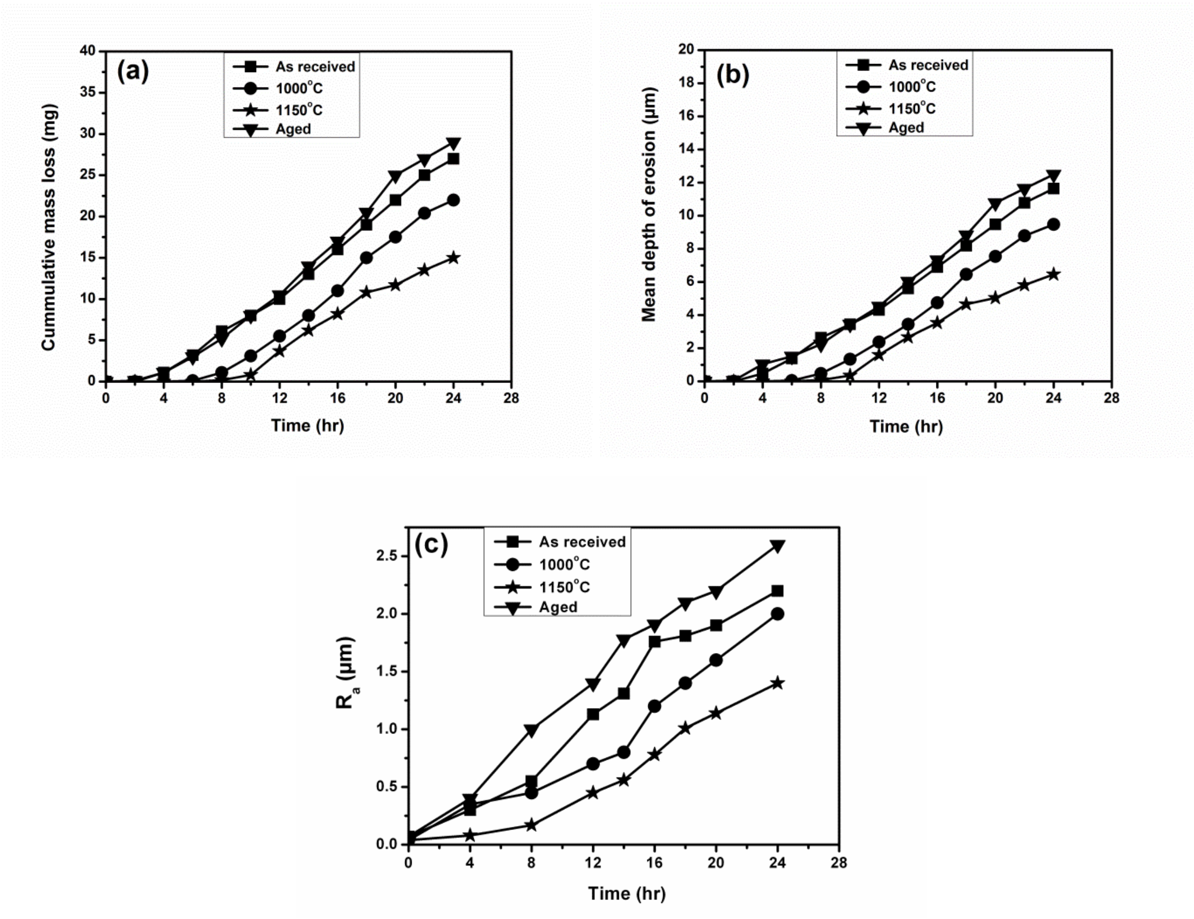

Fig. 5.12 Plot of cavitation erosion of as received, and heat treated specimen of 23/8N steel (a) cumulative weight loss (CWL), (b) mean depth of erosion (MDE) and (c) surface roughness R_a as function of time.

The cumulative weight loss (CWL) after cavitation erosion test is plotted versus time in Fig. 5.12(a), while Fig. 5.12(b) shows mean depth of erosion (MDE) versus time of erosion. The erosion rate consistently increases with time for the steel. The mass loss observed for aged steel is after 4 hrs, which indicates depletion of erosion resistance as compare to as received condition. Mass loss is observed for the steel solutionized at 1150°C approximately after 10 hrs of cavitation testing. It then increased at constant rate (Fig 5.12a).

As earlier discussed erosion started from matrix carbide interface followed by removal of carbides. Therefore, the mass loss increased suddenly at the fall of these carbides in as received and aged condition. This is the reason the aged steel shows lots of fluctuations in the slope of the erosion curves. Eventually, the cumulative weight loss in aged condition is much higher due to reprecipitation of carbides. Fig. 5.12 b shows the erosion rate of solutionized steel is low compared to steel in as received and aged condition.

Erosion rate of aged steel is higher than the as received condition. The surface roughness R_a values after cavitation erosion are shown in Fig. 5.12(c). R_a value follows the trend of erosion rate which is higher for aged condition then as received and low R_a for the solutionized steel at 1150°C.

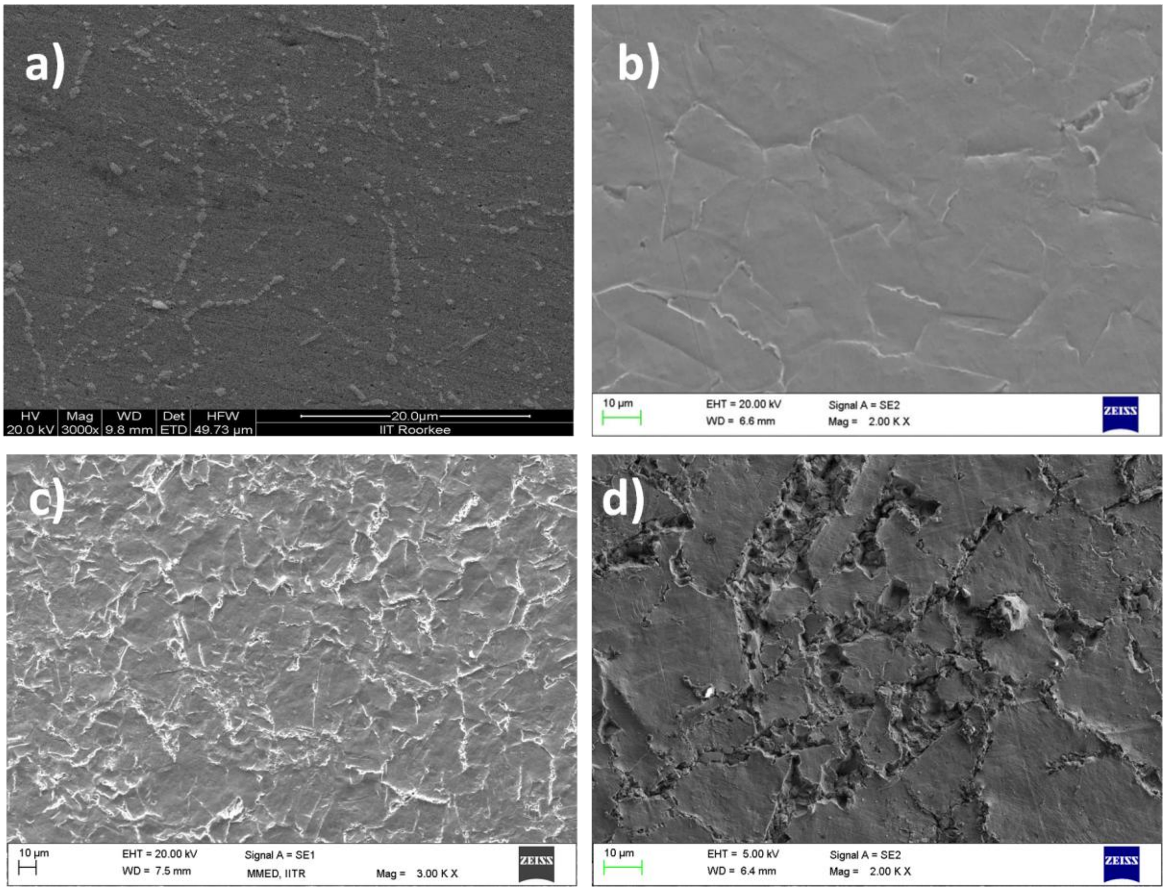

Fig. 5.13 Secondary electron SEM micrographs of eroded surface of 23/8N steel solutionized at 1000 °C (a) 0 hr, (b) 6 hrs, (c) 12 hrs and (d) 24 hrs after cavitation erosion.

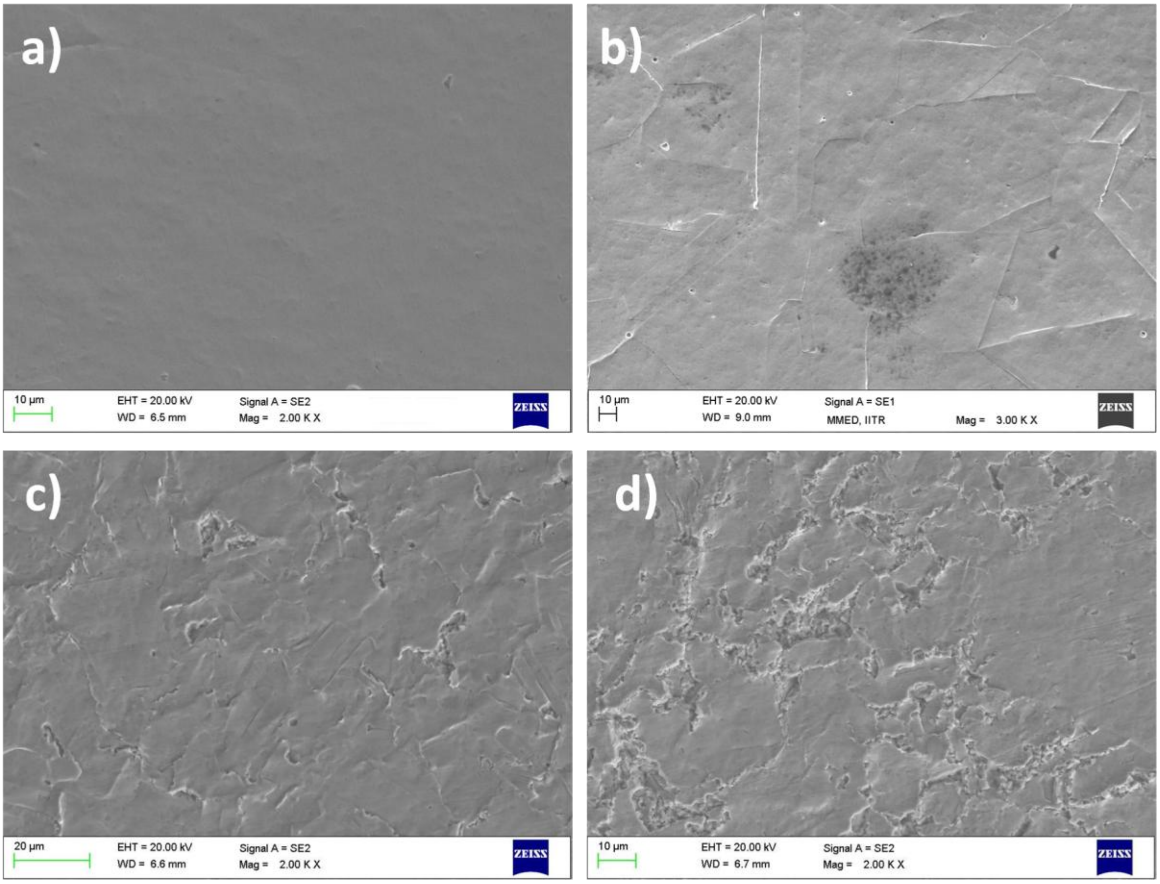

Fig. 5.14 Secondary electron SEM micrographs of eroded surface of 23/8N steel s solutionized at 1150 ^{o}C (3 hrs) (a) 0 hr, (b) 6 hrs, (c) 12 hrs and (d) 24 hrs after cavitation erosion.

Fig. 5.13-5.15 (a-d) shows SEM images of eroded surfaces of heat treated 23/8N steel after cavitation testing. As discussed earlier in Chapter 4, Fig. 5.13 (a) shows that damage primarily occurred at the austenite grain boundaries. The carbides are located at the grain boundaries and the interface regions between carbide and austenite serve as high stress regions [Xi 1993]. These regions are the preferential sites for erosion. In steel solutionized at 1000^{o}C and aged at 700^{o}C, a few holes are seen in the carbides region after erosion for 6 hrs (Fig. 5.13b and 5.15b). This is probably due to brittleness associated with the carbides. Thus, the carbide-austenite interfaces are largely attacked in comparison to austenite grains.

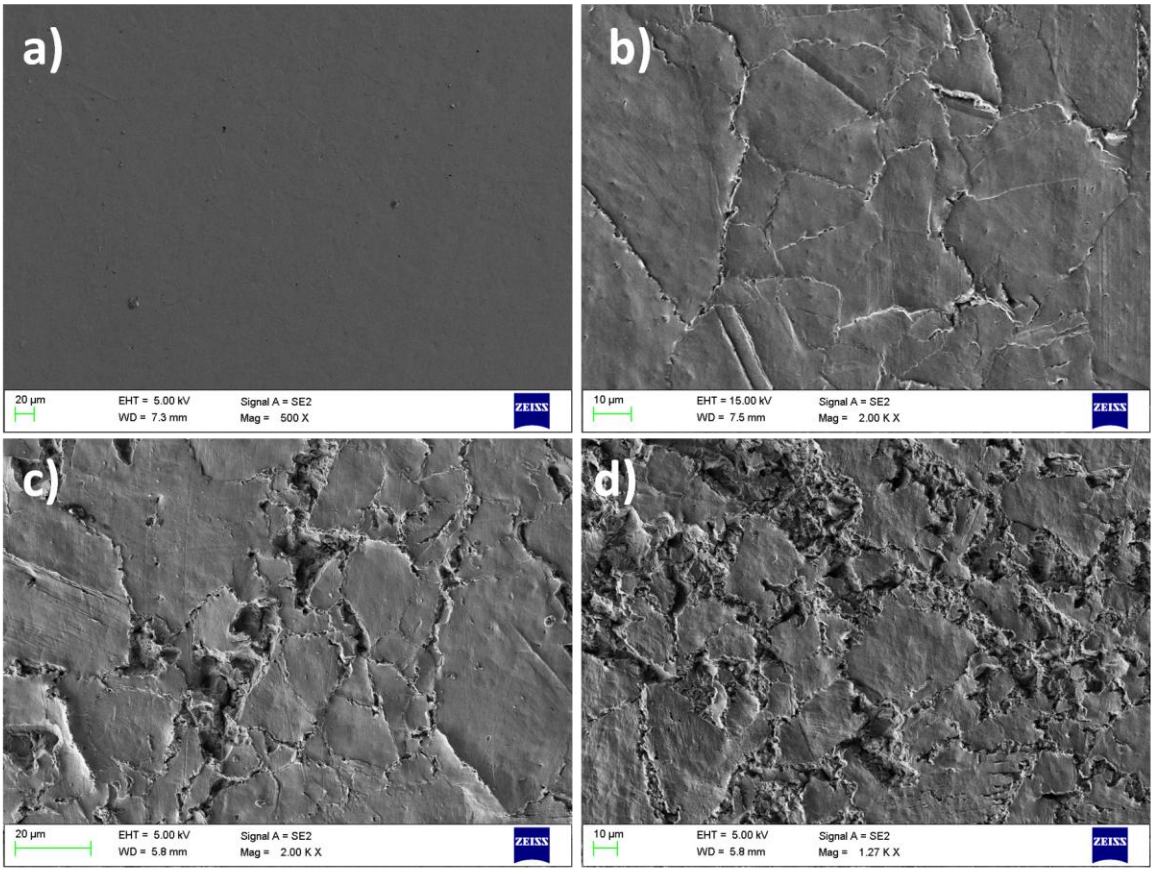

Fig. 5.15 Secondary electron SEM micrographs of eroded surface of 23/8N steel solutionized at 1100 ^{o}C (3 hrs) followed by aging at 700^{o}C (20 hrs) (a) 0 hr, (b) 6 hrs, (c) 12 hrs and (d) 24 hrs after cavitation erosion.

The depth and width of these holes and also the numbers of holes are increased (Fig. 5.13c and 5.15c) with time. After 24 hrs of cavitation erosion, wide and deep cavities are formed due to removal of carbides and matrix (Fig. 5.13c and 5.15c). Steel solutionized at 1150^{o}C shows remarkably less the overall cavitation damages and this condition shows the highest erosion resistance to cavitation attack (Fig. 5.14). In alloy system, the highest erosion resistance has been obtained either in the solution treated condition or in the over aged condition, where carbides either dissolve or coalesce [Sundararajan 1995]. Ninham and Levy 1988 have found a decrease in erosion resistance of spheroidized plain carbon steels with increase in carbide volume fraction. This was attributed to decrease in ductility resulted fracture and void formation at carbides. Increase in grain size was shown to increase the erosion resistance in section 5.1. Here reverse is observed. This may be because improved strength as well as ductility with constant strain hardenability. Further, dissolution of carbides at the grain boundaries decreases the preferential sites for cavitation attack. The overall effects due to the synergies of these mechanisms are responsible factors for the highest erosion resistance for the steel solution annealed at 1150°C.

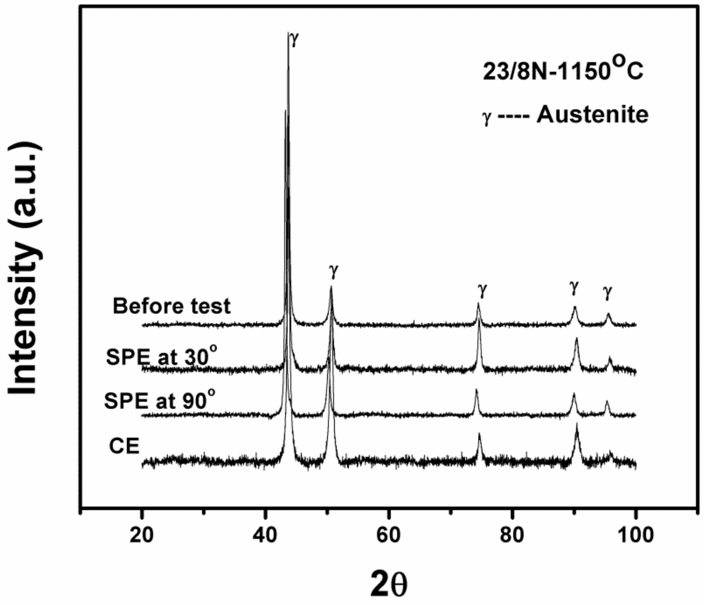

Fig. 5.16 X-ray diffraction trace of relative intensity vs 2θ showing the absence of strain induced martensite in solution annealed at 1150°C nitrogen steel samples subjected to cavitation erosion and solid particle erosion.

The same X-ray diffraction results obtained like as received 23/8N steel. It showed that strain induced martensite does not form in solution annealed at 1150°C nitrogen steel samples subjected to cavitation erosion and solid particle erosion (Fig. 5.16).

Solid particle erosion

For 23/8N steel, both solution annealed heat treatments i.e. 1000°C and 1150°C have better particle erosion resistance (at both 30° and 90° impact angles) as compared to as received and aged heat treatment i.e 1100^{o}C followed by 700^{o}C as shown in Fig. 5.17. It is also observed that there is deterioration in particle erosion resistance of 23/8N steel after aging heat treatment (Fig. 5.17). However, the deterioration is found to be less at 30^{o} impingement angle as compared to that at 90^{o} impingement angle. Among these, higher cumulative weight and steady state of erosion rate are observed for steels solutionized at 1000^{o}C compare to those solutionized at 1150^{o}C due to presence of some carbides shown in Fig 5.17. From the steady state erosion rate curves of as received as well as heat treated 23/8N steel (Fig. 5.17c), it has been noticed that erosion rate at 30^{o} impact angles is high and decreases at 90^{o}C impact angle. 23/8N steel eroded at 30^{o} impact angle attains the steady state erosion rate after 12 min test period. At 30^{o} impact angle the erosion is mainly due to shearing and cutting of the surface of target material, whereas at 90^{o} impact angle damage during erosion is due to strain hardening, plastic deformation and flaking of the target material.

Fig. 5.18(a. c and e) shows the SEM micrographs of eroded surfaces of 23/8N steel in solution annealed and aged conditions eroded at 30^{o} impingement angle. It is observed that in both the samples, the erosion occurs by shearing and ploughing mechanisms. The deeper ploughs observed in the SEM micrograph of aged 23/8N steel as compared to annealed 23/8N steel. This indicates more erosion damage is occurred in aged 23/8N steel. The cracks are seen in the SEM images of worn out surface of aged 23/8N steel (Fig. 5.18b), while the eroded surface of solution annealed 23/8N steel is free from such cracks (Fig. 5.18a). Fig. 5.18 (b, d and f) shows the SEM micrographs of eroded surfaces of 23/8N steel in solution annealed and aged conditions eroded at 90^{o} impingement angle. It is observed that at 90^{o} impact angle, the erosion occurs because of the formation of flakes and/or cracks and fragmentation of them. The deeper flakes are observed in the SEM micrograph of aged 23/8N steel (Fig. 5.18f) and is in agreement with more erosion damage in aged 23/8N steel as compared to that in solution annealed 23/8N steel (Fig. 5.18b and d). It is observed that the formation of flakes and their fragmentation is more severe in 23/8N steel in both as received and aged conditions in comparison to solution annealed 23/8N steel causing less erosion damage in solution annealed 23/8N steel.

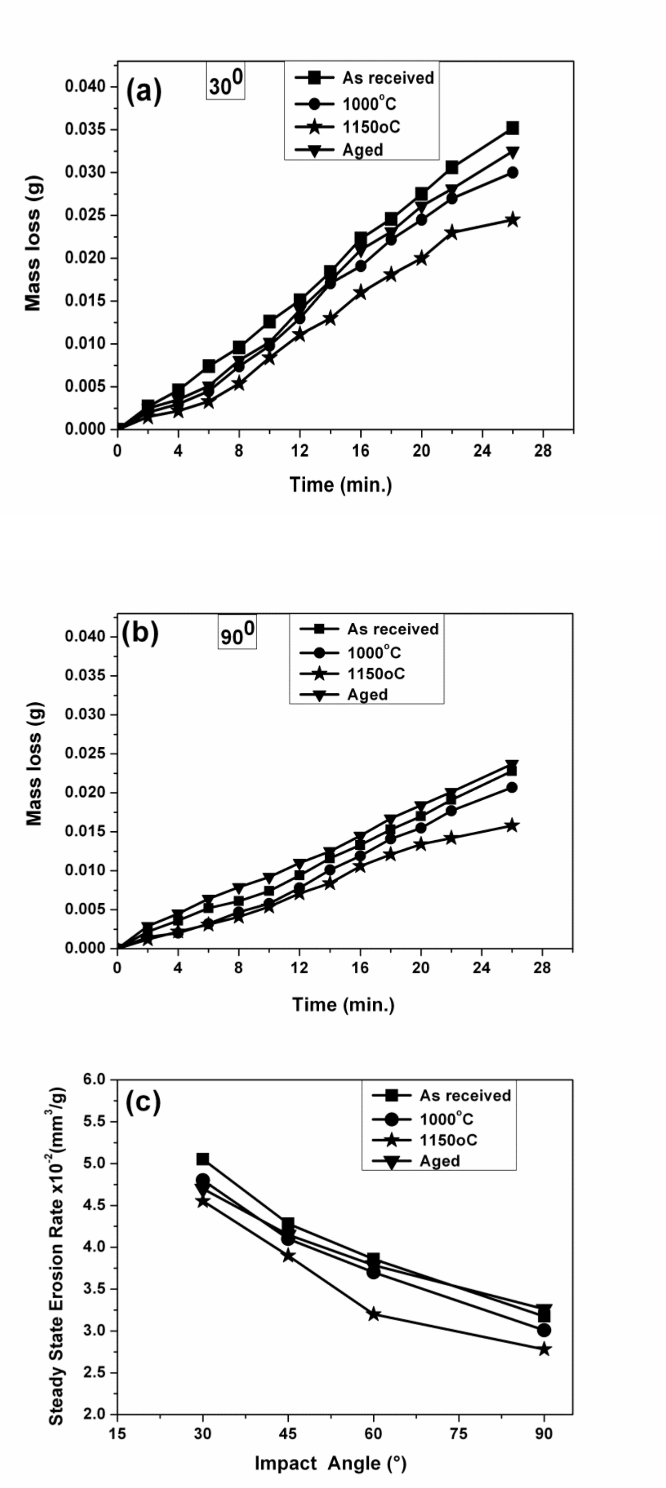

Fig. 5.17 Plot of solid particle erosion of Cumulative weight loss (CWL) at (a) 30^{o}, (b) 90^{o}, and (c) steady state erosion rate of as received, heat treated 1000^{o}C, 1150^{o}C and aged 23/8N steels.

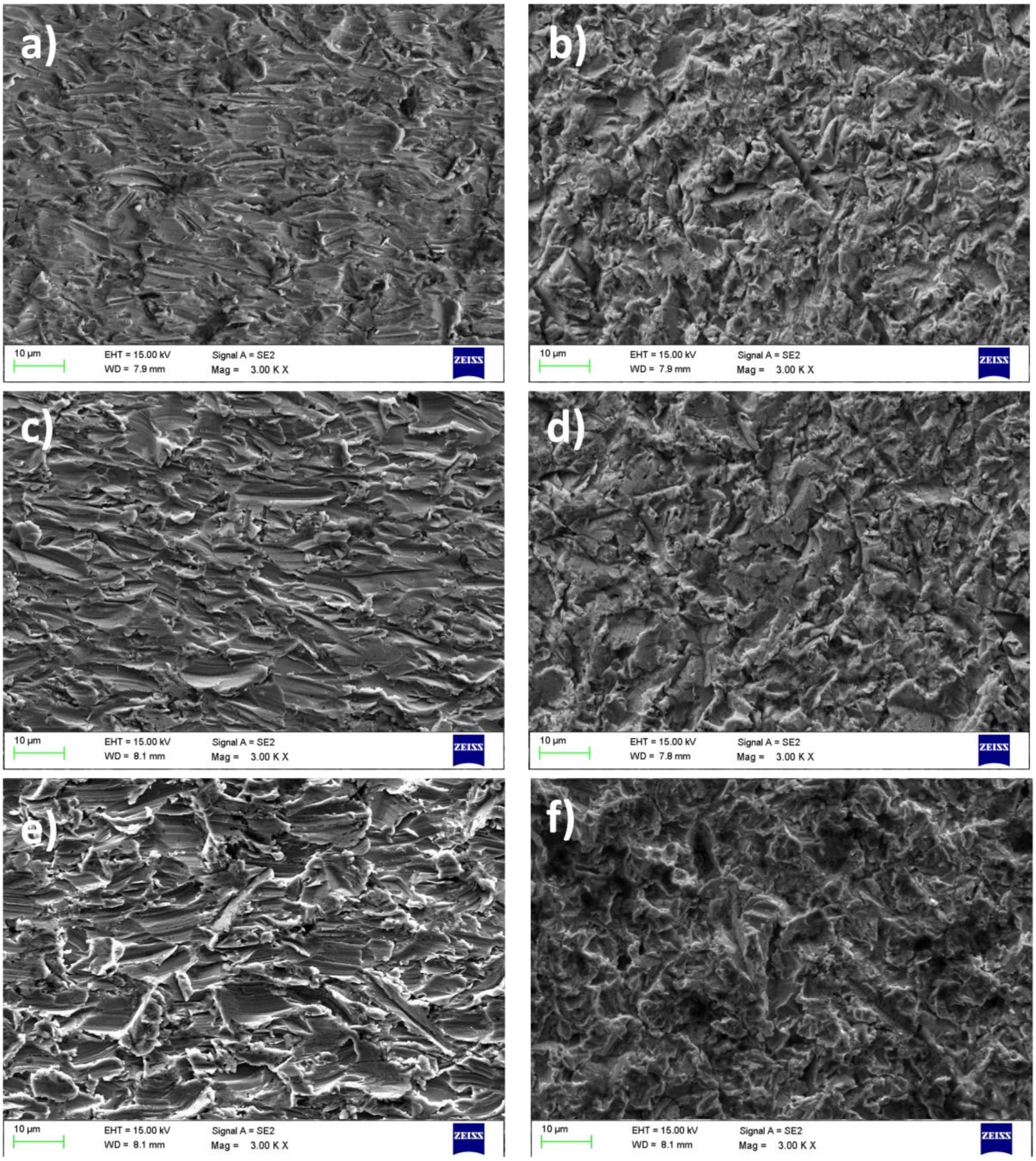

Fig. 5.18 Secondary electron SEM images of worn out surfaces after solid particle erosion of a heat treated 1000 °C at ((a) 30°, (b) 90°); at 1150 °C ((c) 30°, (d) 90°) and aged ((e) 30°, (f) 90°).

Table 5.4 Depth of wear scar (μm) after particle erosion after heat treatment (23/8N steel).

No. of test	1000^{o}C depth (μm)		1150^{o}C depth (μm)		aged depth (μm	
	30^0	90^0	30^0	90^0	30^0	90^0
1	115	156	85	131	134	221
2	114	155	89	131	131	220
3	115	151	84	130	140	223
Avg. value	115	154	86	131	135	221

Heat treatments effect on the erosion of the steels under investigations is analyzed in terms of microstructure and mechanical properties. These were changed during heat treatment processes. In Chapter 4, it has been reported earlier that 23/8N steel has stabilized austenitic structure which result good erosion resistance. Stabilized austenitic structure exhibits toughness and plasticity which causes improvement in localized strength and strain hardening. Because of its austenitic structure, it is considered to be a worthwhile parameter in solid particle erosion. At 30^o impingement angle, the erosion damage in 23/8N steel after solutionizing annealing heat treatment is less as compare to as received 23/8N steel.

Ninham and Levy (1988) has reported decrease in erosion resistance of spheroidized plain carbon steels with increase in carbide volume fraction. This was attributed to decrease in ductility resulted fracture and void formation at carbides. The presence of M_7C_3 and $M_{23}C_6$ complex carbides in the microstructure of quenched carbon and low alloy steels leads to increase in erosion resistance [Suchánek 2009]. In solutionize annealed at 1150^{o}C 23/8N steel, carbides are completely soluble (Fig. 5.10b) in the matrix causing stabilization of the austenitic matrix as compare to solutionize annealed at 1000^{o}C (Fig. 5.10b). This causes better resistance to erosion. Levy [1981] interpreted the similar observation, that the erosion rate is directly dependent on distribution of soft, ductile phases, hard and brittle in the material. He observed that in some limits, the ductile matrix shows lower the erosion rate. The erosion resistance is found to lower in aged 23/8N steel as compared to that in solution annealed 23/8N steel. It is due to precipitation of carbides during aging at 700^{o}C, which are deleterious to erosion resistance. In aged 23/8N steel, the continuous ductile matrix of austenite causes more erosion damages. At 90^o impingement angle, the interfaces between the carbides and austenite as well as the carbides are more prone to erosion damages, because they have less tendency to absorb the kinetic energy of the erodent particles as compared to the austenitic matrix. At 90^o impingement angle, the least erosion damage is observed in solution annealed 23/8N steel due to very few carbides precipitation. As received as well as aged 23/8N steel having higher amount of carbides show higher erosion damage at 90^o impingement angle.

It can be seen from the results obtained for 23/8N steel in different conditions that, 23/8N steel in as received condition (Fig. 5.14) shows higher erosion at both the impingement angles; while least erosion is observed in solution annealed 23/8N steel (Figs. 5.14). In 23/8N steel, the ductility in addition to hardness play vital role in determining the erosion resistance. Divakar et al [2005] have shown that the erosion resistance increases with increasing hardness provided the ductility remains constant. The ductility of the target material is necessary to absorb the stresses imposed by high velocity erodent particles. Figs. 5.14 (a and b) show the cumulative weight loss of 23/8N steel at 30^o and 90^o impingement angles respectively as function of various mechanical properties. From Figs. 5.14a, at 30^o impingement angle the lower erosion damage in solution annealed at 1150^oC of 23/8N steel as compared to as received and aged 23/8N steel is due to higher ductility and tensile toughness in the solution annealed condition. The decrease in hardness and strain hardening ability in solution annealed 23/8N steel causes increase in erosion damage through ploughing and scratching action, but cumulative effect of all the mechanical properties of solution annealed 23/8N steel causes less erosion. The ploughs formed due to impingement of erodent particles at 30^o impingement angle are elongated more in annealed 23/8N steel, which indicates delay in the flaking and dislodging of the ploughs and results in lower erosion in solution annealed at 1150^oC 23/8N steel. The erosion damage increases in aged 23/8N steel in which the ductility and tensile toughness decreases substantially whereas hardness and strain hardening exponent increases. The ploughs formed in this specimen are strain hardened and dislodged earlier due to lower ductility and tensile toughness.

Fig. 5.14b reveals that at 90^o impingement angle again, solution annealed 23/8N steel exhibits least erosion damage. Due to higher tensile toughness in solution annealed 23/8N steel, enables to absorb more kinetic energy of the erodent particles and formation of strain hardened sub surface layer at the impact site is delayed.

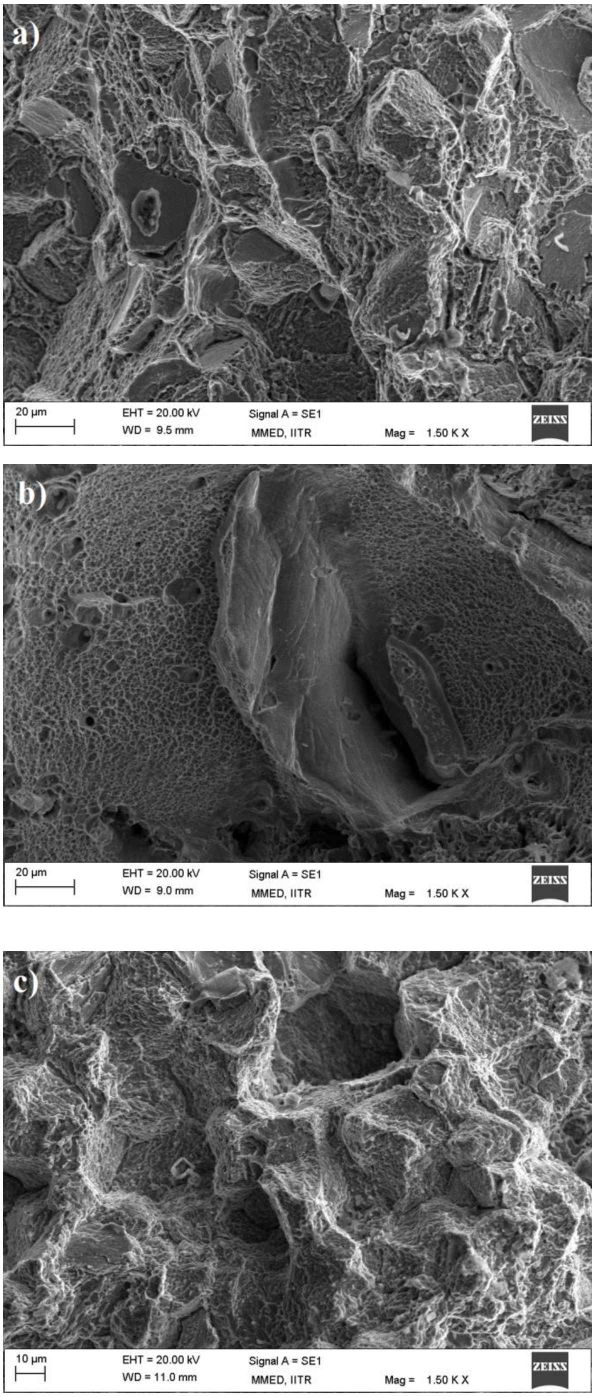

Fig. 5.19 Secondary electron SEM micrographs of tensile test fracture of surface of solutionized at (a) 1000 ^{o}C, (b) 1150 ^{o}C and (c) aged of 23/8N steels.

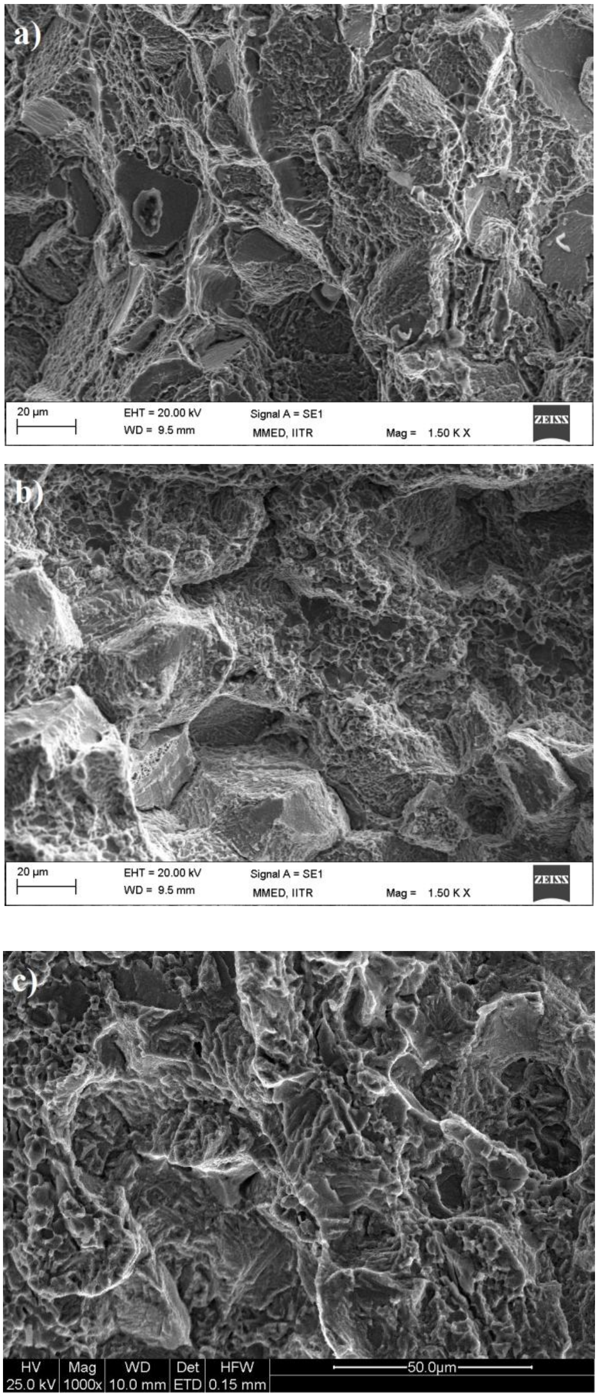

Fig. 5.20 SEM micrographs of impact test fracture surface of (a) solution annealed at 1000 ^{o}C, (b) at 1150 ^{o}C and (c) aged of 23/8N steels.

The higher ductility of solution annealed 23/8N steel allows local plastic deformation of the subsurface region, which also causes delay in dislodging of the material due to erodent particles impacted. Solution annealed 23/8N steel resists normal stresses imposed by the erodent particles by absorbing the kinetic energy due to higher tensile toughness. Solution annealed 23/8N steel also sustains higher tensile stress and higher elastic-plastic deformation as compared to as received and aged 23/8N steel (Fig. 5.11). As described in Chapter 4, the formation of voids due to localization of strain plays significant role in deciding the erosion resistance of the target material. Higher erosion damage of as received 13/4 and 23/8N steel at 90^o impingement angle corresponds to large concentration of voids as compared to that in solution annealed 23/8N steel in each condition.

At 90^o impingement angle, the impacted erodent particles cause development of more cracks in as received 13/4 steel because of severe localization of strain, which results in more void formation. Fig. 5.16 shows the fracture appearance and SEM micrographs of fracture surfaces of solution annealed and aged 23/8N steel after tensile tests. Fig. 5.17 shows SEM micrographs of fracture surfaces of solution annealed 23/8N steel and aged 23/8N steel after Charpy V-notch impact test. It is observed that the fracture mode of solution annealed 23/8N steel is more ductile (Fig. 5.23) as compared to that in as received (Fig. 4.13) and aged 23/8N steel (Fig. 5.24) in tensile testing.

Solution annealing heat treatment 23/8N steel improves cavitation as well as solid particle erosion resistance. The reverse effect has been obtained in case of 21/12N steel. This is mainly because 23/8N steel possesses high volume fraction of carbides compared to 21/12N steel. Carbides dissolution improves the toughness and ductility without the sacrifice of strength and hardness, though the grain growth takes place in 23/8N.

5.3.4 Conclusions

1. Notable enhancement in the erosion resistance of 23/8N steel at both the impingement angles of 30° and 90° is observed as a result of solutionize annealing at 1150°C. However, aging treatment of solution annealed 23/8N steel causes deterioration in erosion resistance at both impingement angles.

2. The improved erosion resistance of 23/8N steel as a result of solutionizing annealing at 1150°C is due to substantial dissolution of carbides in the austenitic matrix. Again reprecipitations of carbides in the aged 23/8N steel are accountable for decreased erosion resistance.

3. The erosion resistance of 23/8N steel was largely affected by the mechanical properties. Tensile toughness and ductility increased after solution annealing heat treatment which enhanced the erosion resistance. Although, hardness and ability of strain hardening decreased which may be responsible for diminution in erosion resistance; but overall combine effect of all mechanical properties results in increased erosion resistance.

4. SEM study shows that erosion at 30° impingement angle occurs by formation of ploughs, whereas at 90° impingement angle the erosion damage is caused by formation of cavities and cracks.

Chapter 6

Weldability and erosion behaviour of 23/8N steel

6.1 Introduction

Welding is the most commonly used fabrication method employed for joining of materials. 13/4 martensitic stainless steel is used in almost all hydroelectric power plants. Severe damage of underwater parts due to erosion leads to frequent shut down of the power project which causes reduction in power production. A number of researchers have reported the repair welding of the 13/4 martensitic stainless steel [Eschobar 1990, Goel 1996] but the performances of these repaired parts is still not satisfactory. The welding practice is yet to be standardized. Worn out underwater parts are repaired by different kind of welding procedures in various hydroelectric power plants.

In chapter 5 the comparative erosion behaviour of 13/4 and 23/8N steels was reported. It was concluded that the erosion resistance of 23/8N nitrogen alloyed austenitic stainless steel is higher due to its austenitic structure and good mechanical properties. In the present chapter, investigations have been carried out on the weldability of the 23/8N grade steel with 309L steel as a filler metal. Cavitation and particle erosion test performed on the weld overlays (309L steel) surface under laboratory environment and these observations are compared with the 23/8N steel which is used as a base metal.

6.2 Microstructure

No defects were observed in weld surface by Dye penetration test after fine grinding. The microstructure of the base metal comprised austenitic matrix with chromium carbides at the grain boundaries (Fig. 6.1a) as already discussed in chapter 4.

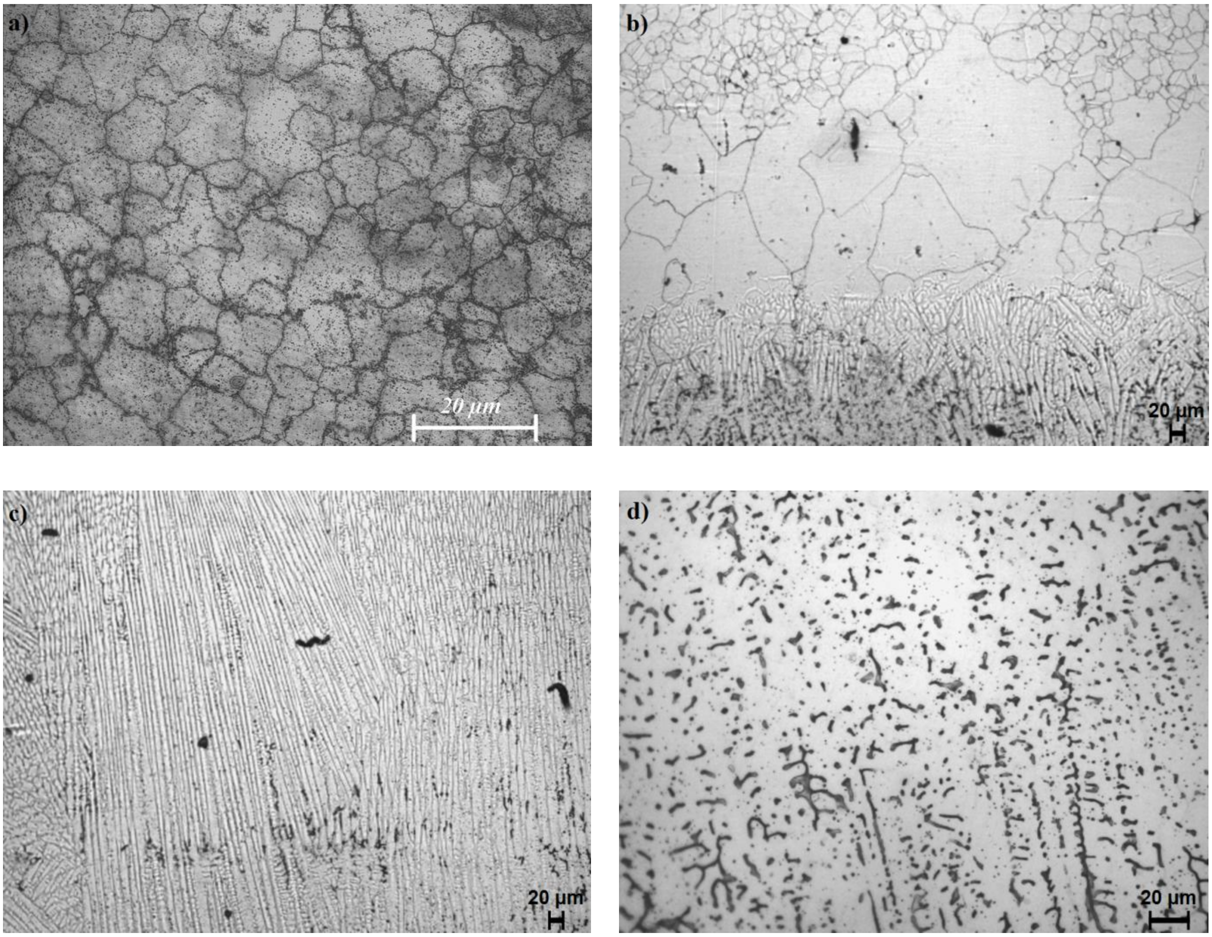

Fig. 6.1 Optical microstructure of 309L steel weld overlay over on 23/8N steel shows (a) base metal 23/8N steel, (b) typical microstructure of heat affected zone near to fusion line, (c) weld deposited adjacent to fusion line and (d) all weld deposit.

Interface of base and weld metal with HAZ region is shown in Fig. 6.1b. Here it has been observed that grain coarsening takes place at HAZ region adjacent to fusion line. Dendrite morphology is observed in interface towards weld metal in Fig. 6.1c. The weld overlay microstructure of 309L steel is composed of austenitic matrix with δ-ferrite solidified as skeleton form at the austenite grain boundaries (Fig. 6.1d) [Hajiannia 2014]. The volume fraction of δ-ferrite is 8-10% determined using optical microscopy. The amount of delta ferrite is 7.8% calculated from ferrite scope.

Identification of the microstructures with the help of Schaeffler diagram

The structure of weld overlay of 309L steels is also determined with the help of Schaeffler diagram (Fig. 6.2) which is useful to predict the resulting microstructure of stainless steel after solidification [Klueh 1998]**.** For the 309L steel the chromium equivalent has been calculated using ferrite forming elements,

$$\begin{aligned} Cr_{eq} &= (Cr) + 2(Si) + 1.5(Mo) + 5(V) + 1.75(Nb) + 0.75(W) \\ &= 22.03 + 2(0.053) + 1.5(0.045) + 1.75\,(-) + 0.75(-) \\ &= 22.15 \end{aligned}$$

and the nickel equivalent has been has been calculated using austenite forming elements,

$$\begin{aligned} Ni_{eq} &= (Ni) + (Co) + 0.5\,(Mn) + 0.3\,(Cu) + 25(N) + 30(C) \\ &= 11.81 + 0.0 + 0.5(1.25) + 0.3(0.19) + 25(0.0) + 30\,(0.045) \\ &= 13.79 \end{aligned}$$

Table 6.1 The calculated values of Cr_{eq}/Ni_{eq} of weld metal 309L and base metal 23/8N steels.

Specimen	$\mathbf{Cr_{eq}}$	$\mathbf{Ni_{eq}}$	$\mathbf{Cr_{eq}/Ni_{eq}}$
Weld metal 309L	22.15	13.79	1.6
23/8N steel	24.19	25.12	0.96

From Schaeffler diagram (Fig. 6.2)**,** the values of Cr_{eq} and Ni_{eq} for filler metal 309L steel corresponds to the region of austenite and δ-ferrite with5-10% in volume fraction, which is in agreement with the microstructures of 309L steel as shown in Fig. 6.1. The structure consists of austenitic matrix and δ-ferrite.

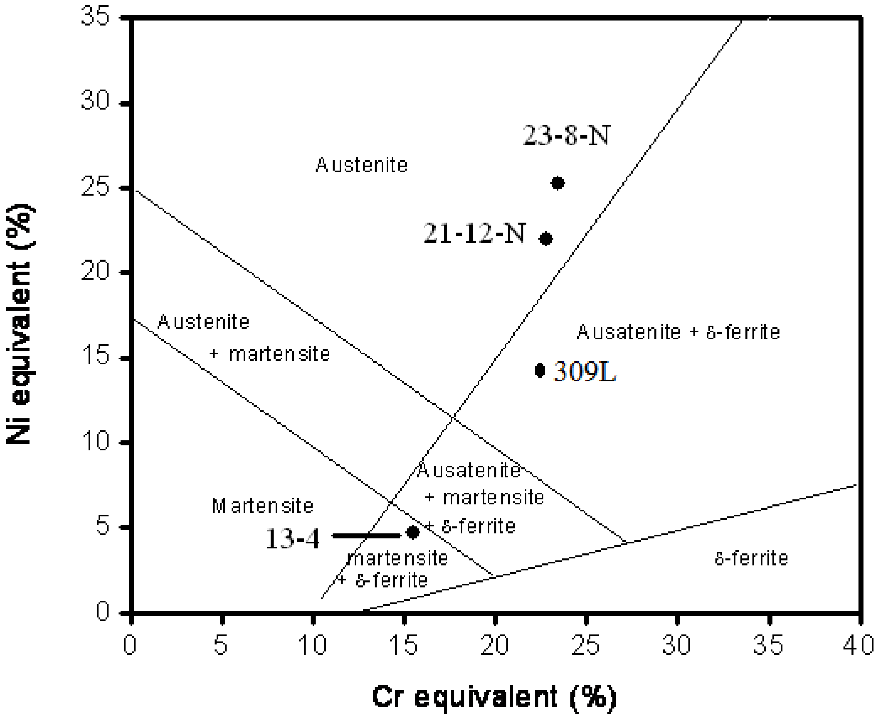

Fig. 6.2 Schaffler diagram [Klueh 1998].

Ferrite formation in the HAZ grain boundaries restricted the grain growth and also minimizes susceptibility to HAZ liquation cracking [Hajiannia 2013]. Similar results were reported by Lippold. According to him when cooling rate of weldment is moderate skeletal ferrite morphology may be observed in the ferrite-austenitic range [Lippold 1995].

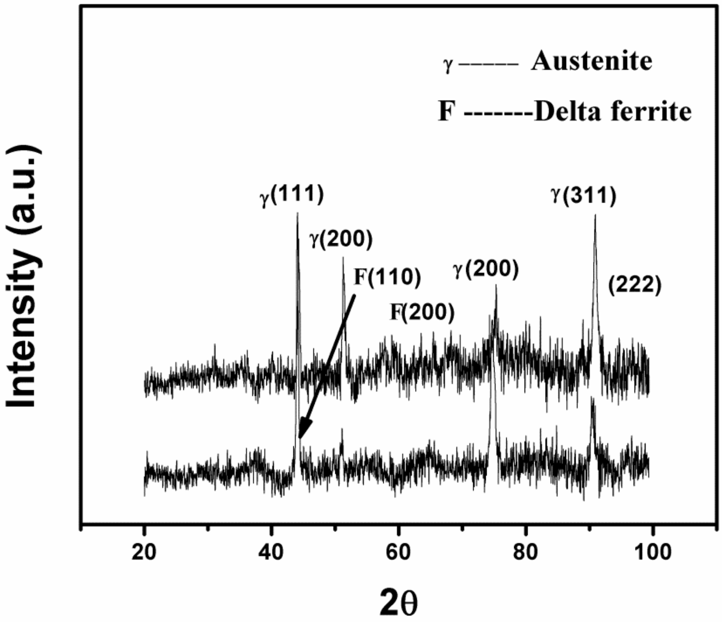

Fig. 6.3 X-ray diffraction trace of relative intensity vs 2θ showing the absence of strain induced martensite in 309L weld overlay steel samples subjected to cavitation erosion and solid particle erosion.

X-ray diffraction patterns of 23/8N steel (Fig 4.2 in chapter 4) and 309L (Fig. 6.3) steel specimens were obtained before and after the cavitation tests. X-ray diffraction results after erosion test did not reveal the formation of martensite. The X-ray diffraction patterns for 309L steel show a texture arrangement of austenite as indicated by the relative intensities of (1 1 1) and (2 0 0) peaks. The higher stability of austenite in 23/8N steel could be attributed to the combined effects of the alloying elements since in this material the (Cr_{eq}/Ni_{eq}) ratio is low which stabilizes austenite. High Cr_{eq}/Ni_{eq} ratio (1.6) is responsible for ferrite formation in 309L steel.

6.3 Mechanical properties

6.3.1 Microhardness

The average value of micro hardness of fusion zone is 192VHN. Fig.6.4 shows a decrease of micro hardness from the base material to fusion zone. Grain growth of the base metal in HAZ leads to lower hardness.

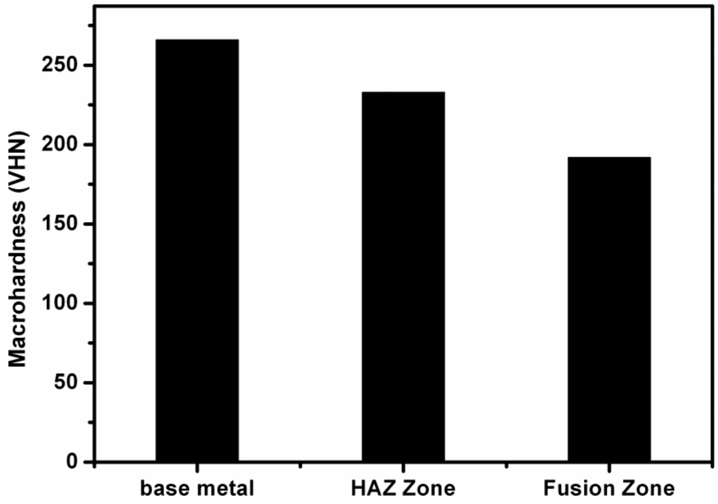

Fig 6.4 The micro hardness of welding of 23/8N with 309L steels.

6.3.2. Tensile and impact properties

Table 6.2 Mechanical properties of the 23/8N and 309L steels.

Properties of steel	**23/8N**	**309L**	
		All weld (Longitudinal)	Axial weld (Transverse)
Hardness (VHN)	266	192	-
Yield Strength (MPa)	567	472	477
Ultimate Tensile Strength (MPa)	820	596	631
Ductility (% Elongation)	32	42	25
Impact energy (J)	85	55	65
Tensile toughness MJ/m^3	240	150	133

The tensile and impact properties of base, axial weld and all weld metal are shown in table 6.2. Tensile specimen breaks at the weld metal. Typical fractographs of axial tensile and Charpy impact specimens have been shown in Fig.6.5 and Fig.6.6. Table 6.2 shows that the base metal has higher yield strength than all weld and axial tensile specimens. Fine dimples are observed on fracture surface (Fig.6.5d). Also the globular oxides are observed at the dimples of both tensile and impact fracture surfaces (Fig 6.5d and 6.6d). Impact fracture shows (Fig.6.6) fine dimples like tensile fracture it reveals ductile nature of the fracture.

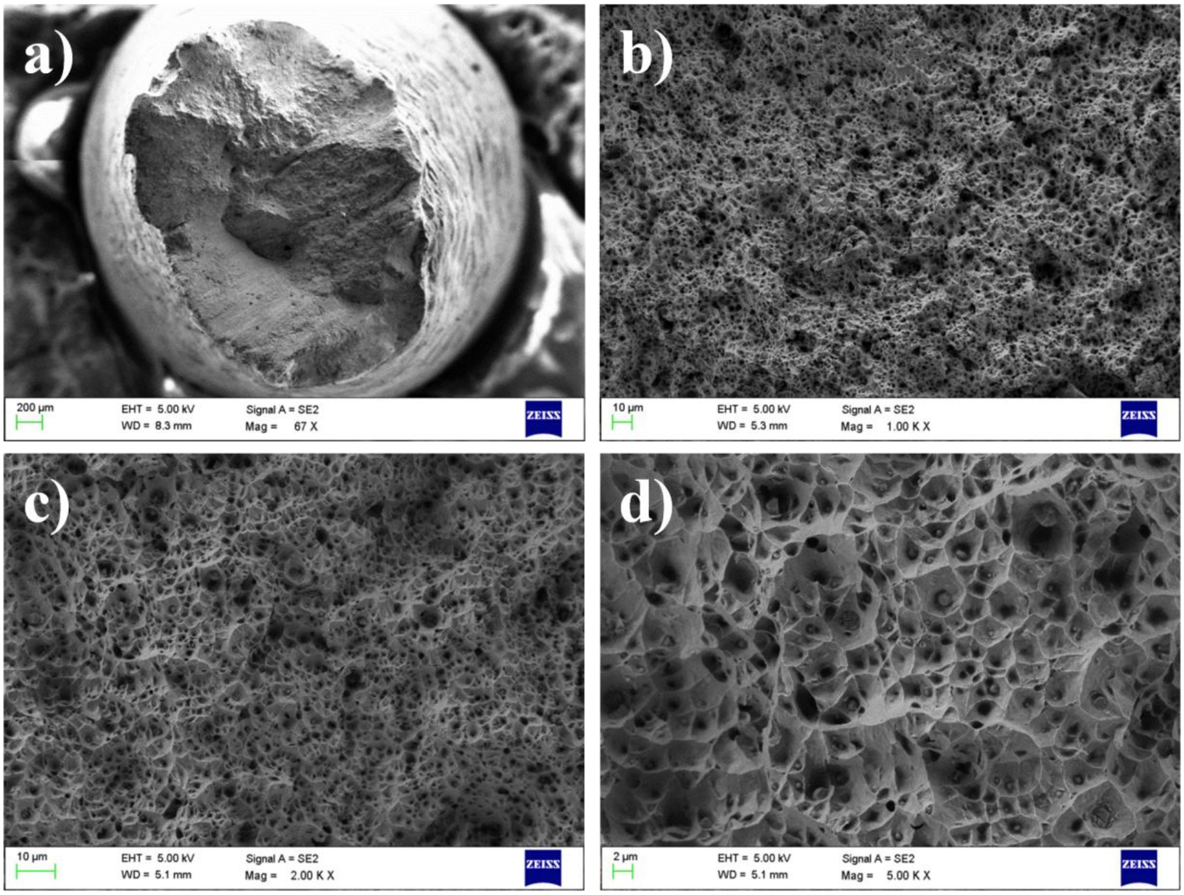

Fig. 6.5 SEM images of fractured surface of tensile specimen of 309L austenitic stainless steel with various magnifications.

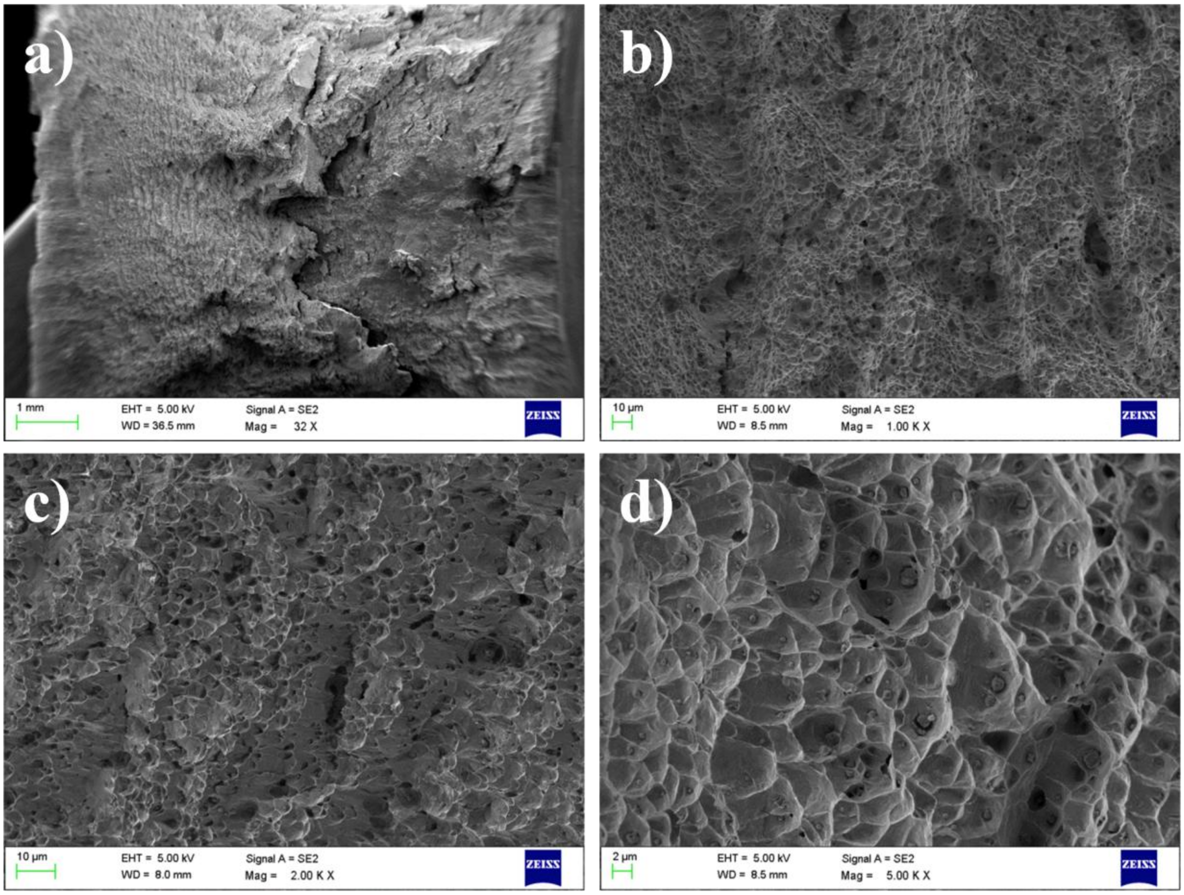

Fig. 6.6 SEM images of fractured surface of Charpy impact specimen of 309L austenitic stainless steel with various magnifications.

6.4 Cavitation erosion behaviour

The cumulative weight loss (CWL) and mean depth of erosion (MDE) versus exposure duration of erosion graphs are plotted in Fig. 6.7a and Fig. 6.7b respectively. For weld metal 309L, the mass loss is not observed upto 2 hrs. The erosion rate sharply increases with time after 2 hrs. The mass loss is not observed upto 8 hrs for base metal. After that the erosion rate increases gradually. The incubation period for 309L weld metal is 2 hrs (Phase I) and for base metal is 8 hrs (Phase II) shown in Fig. 6.7a. Continuous explosion of cavitation impact wave on the surface of target material leads to plastic deformation. Both materials undergo significant work hardening. 23/8N steel possesses higher ductility than the 309L steel. As result 23/8N steel is able to sustain load for longer period.

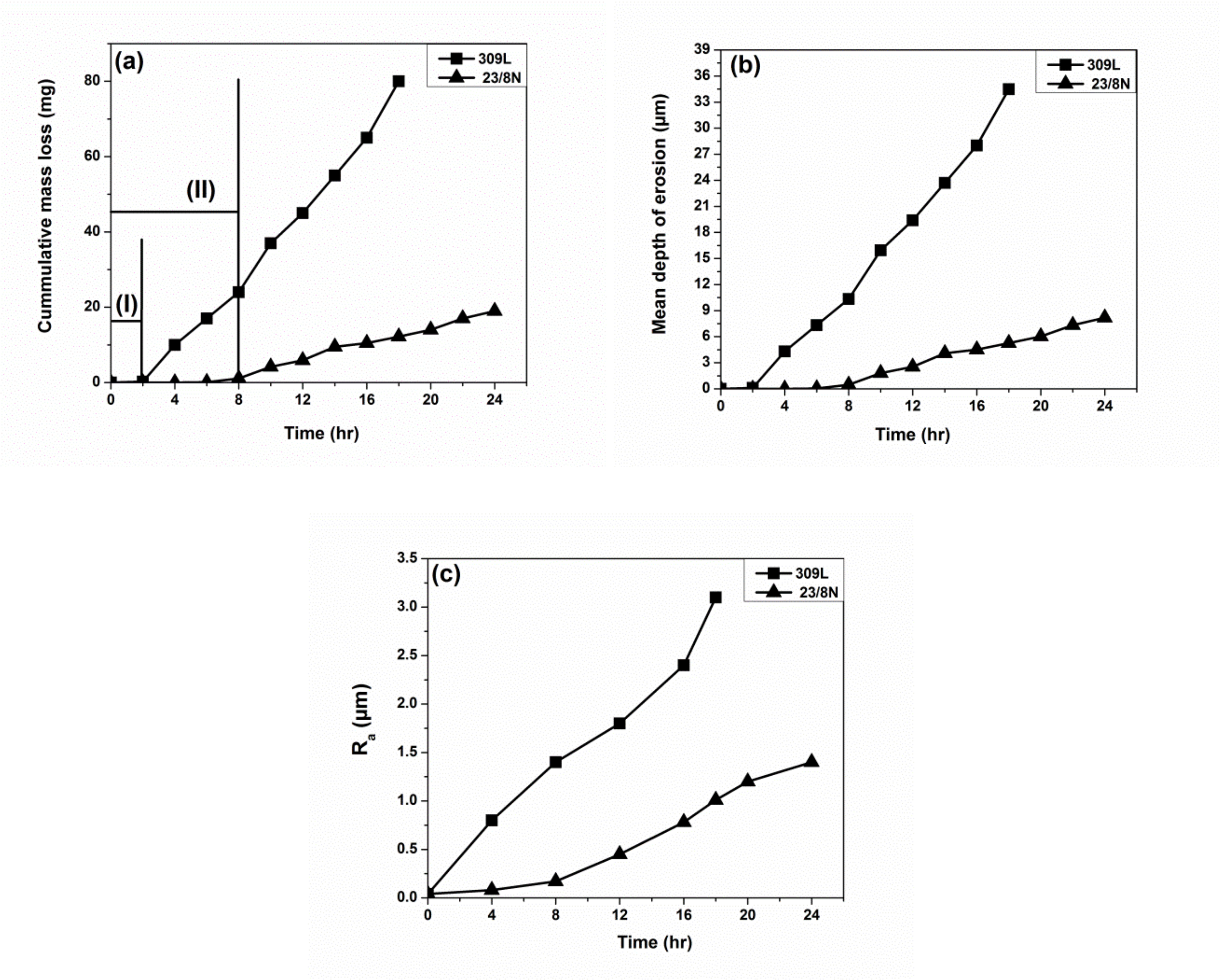

Fig. 6.7 Plot of cavitation erosion of base metal (23/8N) and weld overlay 309L steels (a) cumulative weight loss, (b) mean depth of erosion and (c) surface roughness R_a as function of time.

This is attributed to a restriction in the movement of the dislocation at the grain boundaries, which act as slip barriers in 23/8N steel. The δ-ferrite phase shows higher erosion rate than the 23/8N steel. The surface roughness R_a values after cavitation erosion of 23/8N and weld overlay 309L steels are shown in Fig. 6.7c. R_a value of 309L steel increased sharply after 2 hrs. R_a value of base metal increased at a lower rate. The cavitation erosion behavior for the 23/8N steel is better than that observed for 309L steel (Fig. 6.7b).

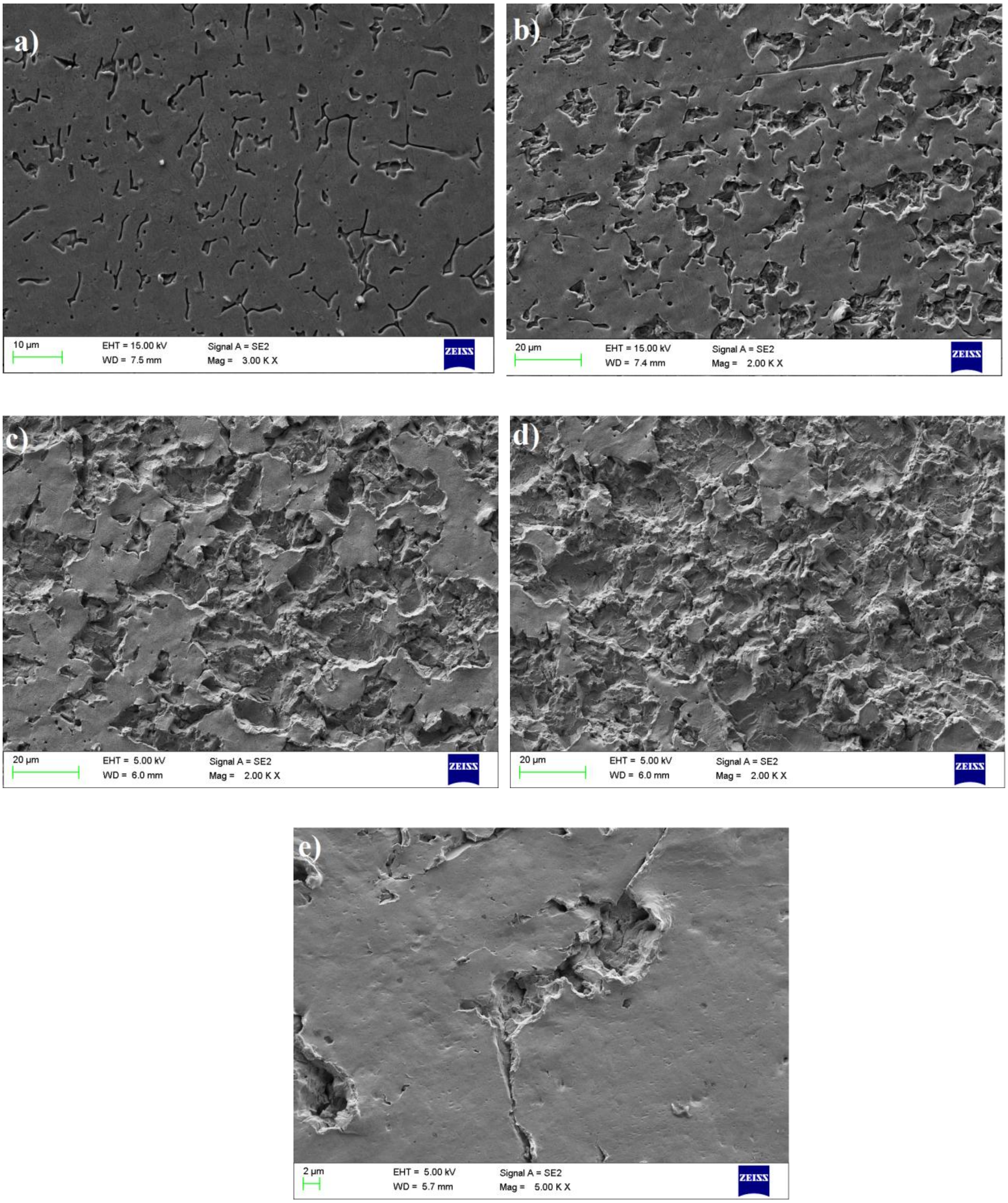

Fig. 6.8 Secondary electron SEM micrographs of eroded surface of weld overlay coating of 309L after (a) 0 hr, (b,e) 6 hrs, (c) 12 hrs and (d) 18 hrs of cavitation erosion.

Since cavitation erosion is highly dependent on materials respond on impact of shock wave generated due to implode of micro-jet bubbles. Continuous impact of shock wave primarily lead to work hardening then after went for microcrack growth, propagation of crack and finally mass loss due to localized fracture [Santa 2006]. The X-ray diffraction results before and after cavitation erosion test are shown in Fig.6.3 which reveal that lowering the peak of δ-ferrite phase. This is because ferrite phase is more sensitive to the cavitation erosion, thereby is selectively fractured.

Fig. 6.8(a-e) shows SEM images of eroded surfaces after cavitation testing. The high mass losses in the weld overlay 309L steel can be related to the features of phases present in the microstructure. Fig. 6.8b shows that damage mainly occurred at the interface of δ-ferrite and austenitic matrix. The δ-ferrite are located at the grain boundaries and the interface regions between δ-ferrite and austenite serve as high stress regions [Kwok 1998]. These regions served as the preferential sites for erosion. Stachowiak studied that, preferential attack on the weakest phase of material is a characteristic of cavitation erosion [Stachowiak 2006]. A few holes are seen in the δ-ferrite region after erosion for 6 hrs (Fig 6.8b). Thus, the δ-ferrite-austenite interfaces are largely attacked in comparison to austenite grains. In study of duplex stainless steel, erosion resistance will be depend on mechanical resistance of material and different way that these two phases and their interfaces deformed plastically during the cavitation process. First ferrite phase attain its highest work hardening [Karimi 1987]. The microcracks are observed in 309L steel as shown in Fig 6.8e. After 12 hrs of cavitation erosion, wide and deep cavities are formed due to removal of δ-ferrite and austenitic matrix (Fig. 6.8c). Surface is completely vanished after the 18 hrs. Moreover, the higher hardness and tensile properties of 23/8N steel is also responsible for increase in higher resistance to cavitation erosion.

In order to restore the phase balance, filler materials are usually over alloyed with 2–4% more Ni than in the base material. The filler metal used in this investigation is over alloyed with 4% more Ni than the base metal. This higher Ni content is not sufficient to retain 100% austenitic structure in the welded sample when the shielding gas used is pure argon probably due to loss of nitrogen from the base metal during welding. In order to retain austenite the shielding gas should be composed of Ar–N_2 [Laxminarayanan 2009].

6.5 Solid particle erosion

Fig 6.9 (a) & (b) gives the cumulative weight loss curves of the test materials at the impact angles of 30° and 90°. At both the angles, cumulative weight loss in weld coating 309L steel is more than that in the 23/8N steel. Fig 6.9 (c) gives steady state of erosion rate at various angles (30°, 45°, 60° and 90°). At all impact angles, erosion rate of weld coating 309L is more than the base metal 23/8N steel. It shows that more erosion resistance observed in base metal 23/8N than the weld coating of 309L.

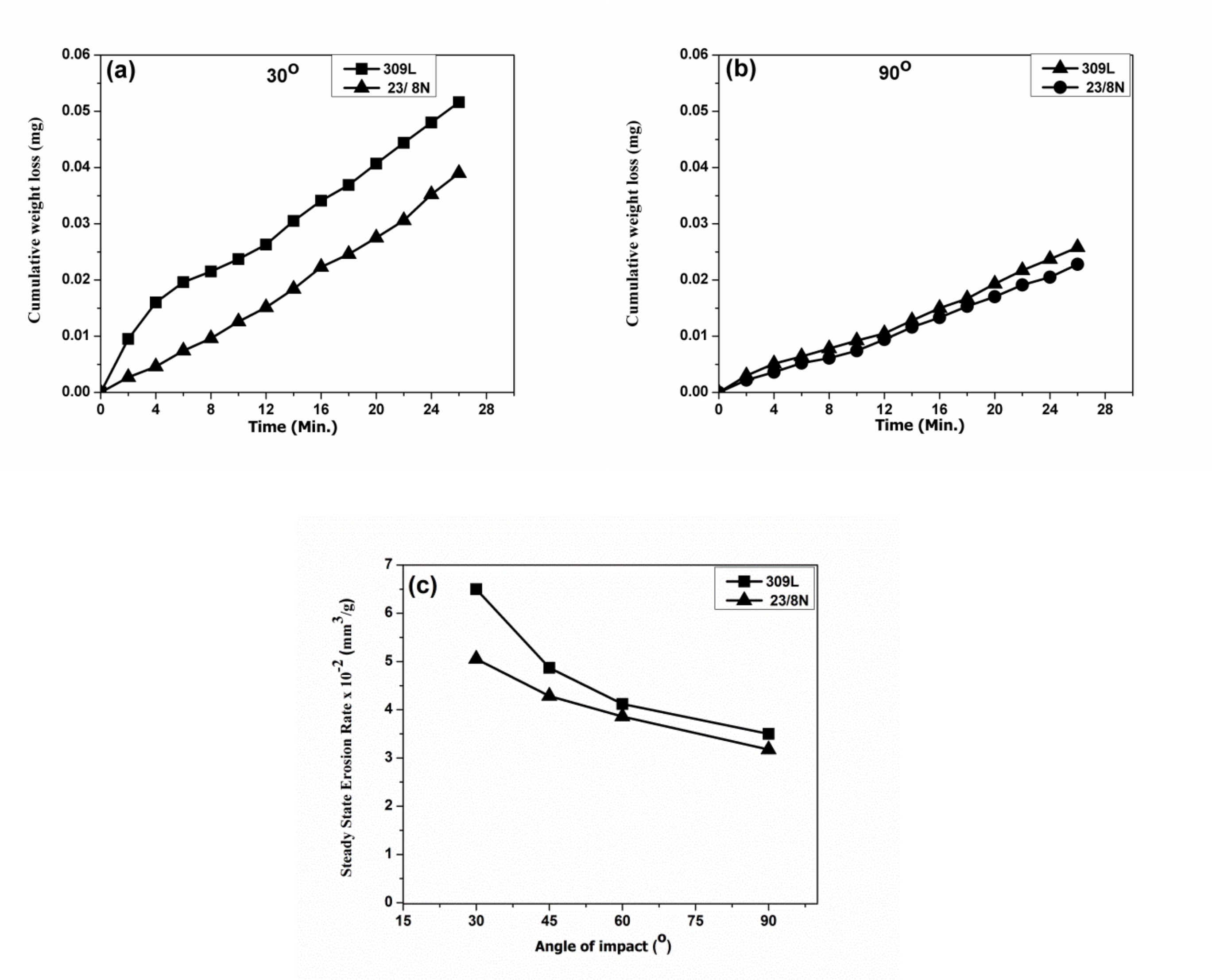

Fig. 6.9 Cumulative weight loss (CWL) at (a) 30°, (b) 90°, (c) steady state erosion rate of weld overlay 309L and 23/8N steel.

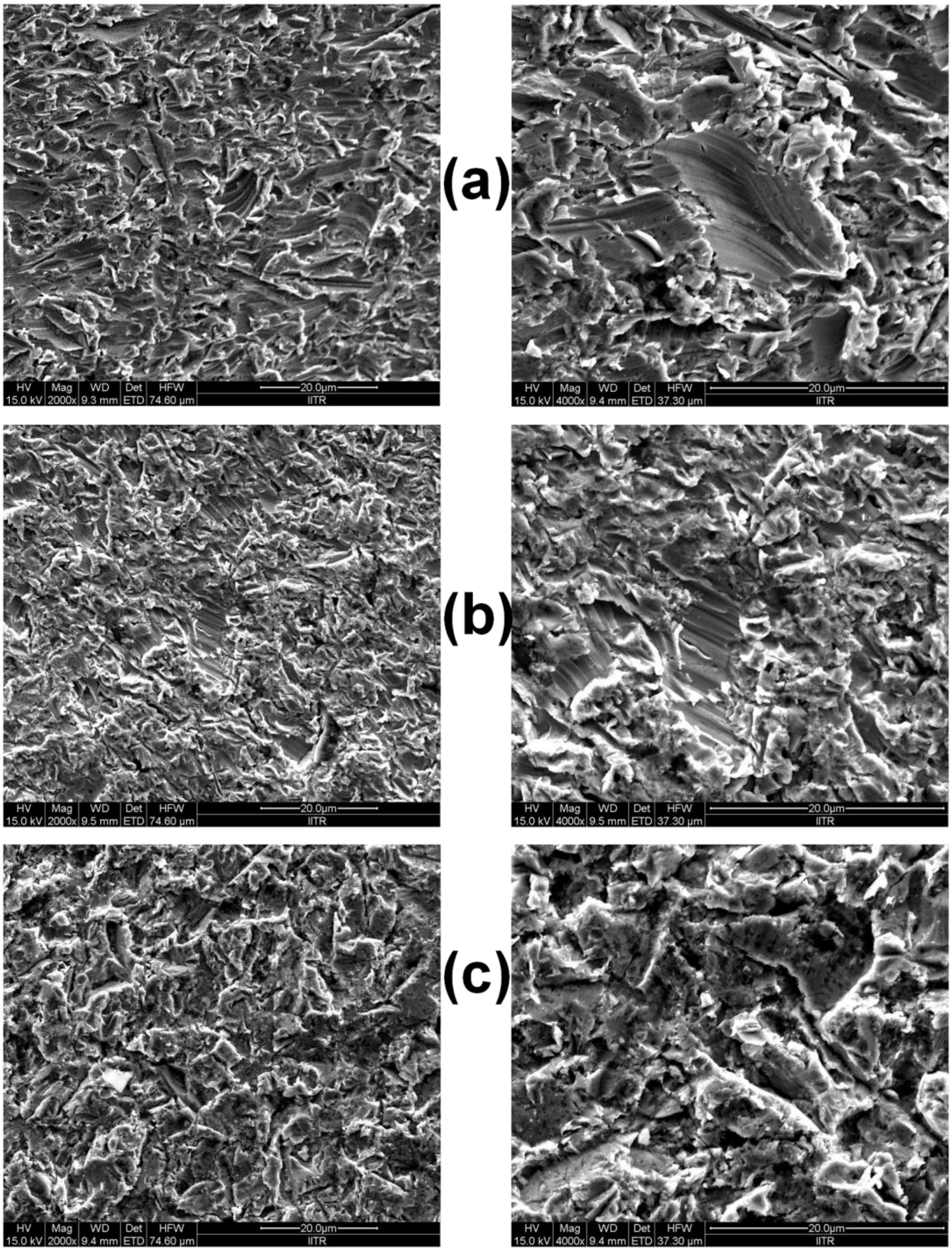

Fig. 6.10 Secondary electron SEM micrographs of eroded surfaces after solid particle erosion of weld overlay of 309L steel with different magnification at (a) 30°, (b) 60° and (c) 90°.

Morphology of eroded surfaces

Fig. 6.10 (a-c) shows worn out surfaces after the particle erosion test of weld overlay 309L steels at 30^{o}, 60^{o} and 90^{o}. 23/8N steel (Fig. 4.15c) at 30^{o} erosion loss mainly because of shear cutting of surface of the materials. Presence of ploughs with lips formed at the side shows that shear that has occurred. The ploughs in weld metal (Fig. 6.10a) are much wider and deeper than those observed in 23/8N (Fig 4.15c) steel. At 90^{o}, eroded surfaces are without ploughs and damage is due to flaking and surface cavity formation (Figs.6.10c). Intense surface cavities are observed at 90^{o} compare to 30^{o} which are created due to removal of material by hard impact alumina particle. The cumulative mass loss at all angles is low for base metal 23/8N steel as compared to weld metal. Weld overlay of 309L steel comprises austenitic and ferritic structure are associated with stresses which are not suitable to erosion resistance. Thus, it exhibits higher erosion rate as compare to base metal 23/8N steel. Depth of average wear scars (calculated from three measurements in surface profiler) after erosion test reported in table 4.2. It shows that average depths of wear scar for weld overlay are higher than that for base metal23/8N steel.

Table 6.3 Depth of wear scar in µm of base metal 23/8N and weld overlay 309L steels.

No. of test	23/8N depth (µm)		309L depth (µm)	
	30^{0}	90^{0}	30^{0}	90^{0}
1	143	203	186	174
2	139	199	187	168
3	138	204	179	271
Avg. value	140	202	184	271

Tensile toughness of weld overlay steel is low compared to the base metal 23/8N steels. The tensile toughness is indicative of the ability of a material to absorb kinetic energy of impinging particles which minimizes the chances cracking in the surface of materials. Thus, the target material with higher tensile toughness exhibits higher erosion resistance [Levin 1999]. Weld overlay possesses less erosion resistance due to its lower impact energy (65 J) than that of 23/8N steels (85 J).

6.6 Conclusions

1. In weld overlay of 309L steel erosion starts at the interface regions between δ-ferrite and austenite serve as high stress regions, afterwards microcracks, wide and deep cavities are formed due to removal of δ-ferrite.
2. 309L austenitic coating applied by welding shows lower cavitation as well as particle erosion resistance compared to base metal of 23/8N steel.
3. The eroded surfaces of weld overlay at low impact angle show that the material is removed by ploughing. At normal impact condition, no ploughing is observed. The material is removed by flaking of the material.

Chapter 7

Suggestions for future work

1. The present study has shown that in 23/8N steel there is a strong tendency of carbide formation. These carbides are undesirable from the view point of erosion resistance. Aging at 700°C after solution annealing again deteriorates the resistance to erosion due to carbide precipitation. Hence investigations need to be undertaken to develop the austenitic matrix free of carbides. An approach in this direction is to reduce the C content in nitronic steels. The steel investigated in this study possesses 0.31% C. Studies on erosion behaviour with lower C concentration may provide useful results.
2. In this investigation erosion tests have involved use of abrasive particles plus air jet as the erosive medium. Separate tests on cavitation erosion have also been conducted using water only without any erodent particles. To simulate actual field conditions in hydroelectric projects, investigations need to be taken up to study the erosion behaviour of nitronic steel in silt-water slurry with varying parameters.
3. Best performance against erosion has been observed in 23/8N steel after solution annealed condition at 1150°C. But this treatment increased the grain size of nitronic steel. The treatment which will provide a fine grain austenitic matrix free of carbides or hot rolling of this steel. It is possible to fabricate various underwater components by hot rolling / forging at such a high temperature. To obtain a fine grain matrix free of carbides, investigations may be undertaken on low C nitronic steels micro-alloyed with grain refining elements like B, Al, V and Ti.
4. This investigation has revealed that all mechanical properties play vital role in influencing the erosion behaviour of nitronic steel. It is well known that some of the mechanical properties, like impact energy, tensile toughness and ductility are strongly temperature dependent. In this study, all the mechanical properties have been determined at room temperature, whereas in certain critical applications, like underwater parts in hydroelectric projects, erosion occurs at sub zero temperatures. Hence studies need to be undertaken to correlate the erosion behaviour with mechanical properties determined at low temperatures.

5. *In situ* strain hardening occurring during erosion applications has been identified as an important parameter contributing resistance to erosion in nitronic steel. In this study the tendency of strain hardening has been correlated with strain hardening coefficient n determined from the slope of log true stress – log true strain diagram. Investigations on the nature and depth of *in situ* hardening may provide useful information on its actual role in erosion behaviour. This may require study of nature of sub surfaces undergoing erosion damages by optical metallography, transmission electron microscopy and X-ray analysis.

6. An important aspect in the development of a steel for a specific application is availability of complete know how of its manufacturing and fabrication technology. Although the foundry practices of nitronic steels (23/8N and 21/12N) are well established, studies conducted on its weldability, which is of vital importance for the maintenance of partially damaged components. Welding parameters need to be standardized and studies on development of suitable welding electrodes need to be undertaken. Similarly the practice of hot working by rolling / forging is also to be well established.

1. Ambelli G., Levy A.V., “Particulate erosion of NiO scales”, Wear, 68, 305-331, (1981).
2. Amirhaghi S., Reehal H.S. , Plappert E., Bajic Z., Wood R.J.K., Wheeler D.W., “Growth and erosive wear performance of diamond coatings on WC substrates”, Diamond and Related Materials, 8, 845-849, (1999).
3. Arnold J.C., Hutchings I.M., “The mechanisms of erosion of unfilled elastomers by solid particle impact”, Wear, 138, 33-46, (1990).
4. ASM Handbook, “Friction, lubrication and wear tech.”, vol.18, ASM international, U.S. (1992).
5. ASTM E23-07, “Standard test methods for notch bar impact testing of metallic materials”, West Conshohocken, PA, (2011).
6. ASTM E8M-09, “Standard test methods for tension testing of metallic materials”, West Conshohocken, PA, (2011).
7. ASTM G32-10, “Standard test methods for cavitation erosion using vibratory apparatus”, West Conshohocken, PA, (2011).
8. ASTM G40-10, “Standard terminology relating to wear and erosion”, West Conshohocken, PA, (2010).
9. ASTM G76-07, “Standard Test Method for Conducting Erosion Tests by Solid Particle Impingement Using Gas Jets”, West Conshohocken, PA, (2011).
10. Avellan F., Farhat M., “Shock pressure generated by cavitation vortex collapse”, Proc. of the 3rd International Symposium on Cavitation Noise and Erosion in Fluid systems, FED-vol. 88, ASME Winter Annual Meeting, San Francisco, CA, 119-125, (1989).
11. Bakare M.S., Voisey K.T., Chokethawai K., McCartney D.G., “Corrosion behaviour of crystalline and amorphous forms of the glass forming alloy Fe43Cr16-Mo16C15B10”, J. Alloys Compd.,527, 210-218, (2012).
12. Balachandran G., Bhatia M.L., Ballal N.B., Rao P.K., “Some theoretical aspects on designing nickel fee high nitrogen austenitic stainless steels”, ISIJ International, 41, 1018-1027, (2001).

13. Baldev Raj, Mudali, K., Vasudevan M., Shankar P., "Current status on AISI types 304 LN and 316 LN austenitic stainless steels", Special Issue on High Nitrogen Steels Part A, Trans. Ind. Inst. for Metals, 55, 131-147, (2002).
14. Baligidad R.G., Satya Prasad V.V., Rao A.S., "Effect of Ti, W,Mn, Mo and Si on microstructure and mechanical properties on Fe-10.5wt% Al alloys", Material Science and Technology, 23, 613-620, (2007).
15. Barber J., Mellor B.G., Wood R.J.K., "The development of sub-surface damage during high energy solid particle erosion of a thermally sprayed WC-Co-Cr coating", Wear, 259,125-134, (2005).
16. Barbezat G., Nicoll A.R., Sickinger A., "Abrasion, erosion and scuffing resistance of carbide and oxide ceramic thermal sprayed coatings for different applications", Wear, 162-164, 529-537, (1993).
17. Basak A., Roy D.K., Dutta, G.L., "Adhesive wear characteristics of cast nitrogenated stainless steel", Wear, 184, 241-244, (1995).
18. Berger L.M., "Application of hardmetals as thermal spray coatings Int. Journal of Refractory Metals and Hard Materials" 49, 350-364, (2015).
19. Bitter J.G.A., "A study of erosion phenomena: Part I", Wear, 6, 5-21, (1963a).
20. Bitter J.G.A.," A study of erosion phenomena: Part II", Wear, 6, 169-190, (1963b).
21. Bolelli G., Borner T., Milanti A., Lusvarghi L., Laurila J., Koivuluoto H., "Tribological behavior of HVOF- and HVAF-sprayed composite coatings based on Fe-alloyþWC–12%", Co. Surf. Coat. Technol., 248, 104-112, (2014).
22. Bose S.C., Singh K., Ray A.K., Ghosh R.N., "Effect of thermal ageing on mechanical properties and microstructures of a standard G-X 12 CrMoVWNbN 1011 grade of cast steel for turbine casing", Material Science Engineering :A, 476, 257-266 (2008).
23. Brach M.R., "Impact dynamics with applications to solid particle erosion", Int. J. Impact Engg., 7, 37-53, (1988).
24. Bregliozzi G., Schino A.D., Ahmed S.I.U., Kenny J.M. and Haefke H., "Cavitation wear behaviour of austenitic stainless steels with different grain sizes", Wear, 258, 503, (2005).
25. Burnett A.J., Bradley M.S.A., O'Flynn D.J., Deng T., Bingley M.S., "Anomalies in the results obtained from rotating disc accelerator erosion testers: a discussion of possible causes", Wear, 233-235, 275-283, (1999).

26. Burns H., “Manufacture and application of high nitrogen steels”, ISIJ International, 36, 909-914, (1996).
27. Camacho J.R.L., Chavez A.M., Mendez J.V.M., Torres M.V., Hernandez E.A.G., “Solid particle erosion of AISI 304, 316 and 420 stainless steels”, Wear, 301, 398-405, (2013a).
28. Camacho J.R.L., Lewis R., Torres M.V. and Mendez, J.V.M., “A study of cavitation erosion on engineering materials”, Wear, 301, 467-476, (2013b).
29. Chattopadhyay R., “High silt wear of hydro turbine runners”, Wear, 162-164, 1040-1044, (1993).
30. Chauhan A.K., Goel D.B., Prakash S., “Erosion behaviour of hydroturbine steels”, Bull. of Material Science, 31,115-120, (2008).
31. Chauhan A.K., Goel D.B., Prakash S., “Solid particle erosion behaviour of 13Cr-4Ni and 21Cr-4Ni-N steels”, Journal of Alloys and Compounds, 467, 459-464, (2009).
32. Chen Y.M., Mongis J., “Cavitation wear in plain bearing: case study”, Mecanique & Industries, 6, 195-201, (2005).
33. Cheng F.T., Kwok C.T., Man H.C., “Laser surfacing of S31603 stainless steel with engineering ceramics for cavitation erosion resistance”, Surf. Coat. Technol.,139, 14-24, (2001).
34. Christman T., Shewmon P.G., “Erosion of a strong aluminium alloy”, Wear, 52, 57-70, (1979).
35. Cieslak M.J., Ritter A.M., Savage W.F., “Chi-Phase formation during solidification and cooling of CF-8M weld metal”, Welding Journal, 63,133s-139s, (1984).
36. Cojocaru V., Miclosina C.O., “Residual stresses analysis of weld overlays coatings used for the repairs at kaplan turbine runner blades areas damaged by cavitation erosion”, Recent Researches in Environment, Energy planning and Pollution, XVIII, 161-166, (1997).
37. Covert R.A., Tuthill A.H., “Stainless steels: An introduction to their metallurgy and corrosion resistance”, Dairy, Food and Environmental Sanitation, 207, 506-517, (2000).
38. Cui Y., Lundin C.D., “Effect of microfissures on mechanical properties of 308L austenitic stainless steel weld metals”, J. of Material Science, 40, 1281-1283, (2005).

39. Deng T., Bradley M.S.A., Bingley M.S., "An investigation of particle dynamics within a centrifugal accelerator type erosion tester", Wear, 247, 55-65, (2001).
40. Divakar M., Agarwal V.K., Singh S.N., "Effect of the material surface hardness on the erosion of AISI 316", Wear, 259, 110-117, (2005).
41. Dular M., Petkovšek M., "On the mechanisms of cavitation erosion-Coupling high speed videos to damage patterns", Experimental Thermal and Fluid Science 68, 359–370, (2015).
42. Dular M., Stoffel B., Širok B., "Development of a cavitation erosion model", Wear, 261, 642-655, (2006).
43. Eschobar J.D., Velasquez E., Santos T.F.A., Ramirez A.J., Lopez D., "Improvement of cavitation erosion resistance of a duplex stainless steel through friction stir processing (FSP), Wear, 297, 998-1005, (2013).
44. Evans A.G., Wilshaw T.R., "Quasi-static particle damage in brittle solids - I: observations, analysis and its applications", Acta Metall., 24, 939-956, (1976).
45. Finnie I., "Erosion of surfaces by solid particles", Wear, 3, 87-103, (1960).
46. Finnie I., "The mechanism of erosion of ductile metals", Proc. of 3rd U.S. National congress of Applied Mechanics, 527-532, (1958).
47. Foley T., Lavy A., "The erosion of heat-treated steels", Wear, 91, 45-64, (1983).
48. Folkhard E., "Welding Metallurgy of Stainless Steels", Springer-Verlag, Wien, (1984).
49. Friedrich K., "Erosive wear of polymer surfaces by steel blasting. Journal of Material Science", 21, 3317-3332, (1986).
50. Gadhikar A.A., Sharma A., Goel D.B., Sharma C.P., "Effect of carbide resistance of steel", Bulletin Material Science, 37,315, (2014).
51. Gahr K.H.Z., "Modelling of two-body abrasive wear", Wear, 124, 87-103, (1988).
52. Ganesh Kumar J., Ganesan V., Laha K., Mathew M.D., "Time dependent design curves for a high nitrogen grade of 316LN stainless steel for fast reactor applications", Nuclear Engineering and Design, 265, 949-956, (2013).
53. Gee M.G., Gee R.H., McNaught I., "Stepwise erosion as a method for determining the mechanisms of wear in gas borne particulate erosion", Wear, 255, 44-54, (2003).

54. Geng J., Tsakiropoulos P., Shao G., “A study of the effect of Hf and Sn addition on the microstructure of Nb/Nb_5Si_3 based in situ composites”, Intermetallics, 15, 69-76, (2007).
55. Gill T.P.S., Gnanamoorthy, J.B. “A method for quantitative analysis of delta-ferrite, sigma and $M_{23}C_6$ carbide phases in heat treated type 316 stainless steel weldments”, Journal of Material Science, 17, 1513-1518, (1982).
56. Goel D.B., “Metallurgy of erosion of underwater parts in hydro electric projects”, Proc. Of 3rd Inter. conference on silting problems in hydro power projects, New Delhi, 27-28, Feb. (2008).
57. Goel D.B., Sharma M.K., “Present state of damages and their repair welding in Indian hydroelectric projects”, Workshop on Silt damages to equipments stations remedial messures, CBIP proceeding, New Delhi, 137-146, (1996a).
58. Goel D.B., Sharma M.K., Misra P.S., “Compilation of data on repair welding of runner blades to avoid erosion due to silt”, Water and Energy (CBIP), New Delhi, 4, 1-10, (1993).
59. Goel D.B., Sharma M.K., Misra P.S., “Damage of hydroelectric power equipments in himalyan region and role of metallurgy providing remedial measures”, 3rd international conference on power development in Afro-Asian countries, Kathmandu (Nepal), 1, 546-556, (1996b).
60. Goretta K.C., Arroyo R.C., Wu C.T., Routbort J.L., “Erosion of work-hardened copper, nickel, and 304 stainless steel”, Wear, 147, 145-154, (1991).
61. Goretta K.C., Thompson A.C., Routbort J.L., “Erosion of heat-treated AISI 4140 steel”, Materials Science and Engineering A, 161, 7-10, (1993).
62. Hajian M., Zadeh A.A., Nejad S.S.R., Assadi H., Hadav S.M.M, Chung K., Shokouhimehr M., “Improvement in cavitation erosion resistance of AISI 316L stainless steel by friction stir processing”, Appl. Surf. Sci., 308, 184-192, (2014).
63. Hajiannia I., Shamanian M., Kasiri M., “Microstructure and mechanical properties of AISI 347 stainless steel/A335 low alloy steel dissimilar joint produced by gas tungsten arc welding”, Materials and Design, 50, 566-573, (2013).
64. Hammitt F.G., De M.K., “Cavitation damage prediction”, 52, 243-262, (1979).

65. Hanninen H., Romu J., Ilola R., Jervo J., Laitinen A., “Effects of processing and manufacturing of high nitrogen-containing stainless steels on their mechanical, corrosion and wear properties”, J. of Mater. Proc. Tech., 117, 424-430, (2001).
66. Harris S.D., Nag N.R., “Kinetics of niobium carbide precipitation in a low carbon austenitic steel”, J. of Material Science, 10, 1137-1148, (1975).
67. Hart D., Whale D., “A review of cavitation erosion resistant weld surfacing alloys for hydroturbines”, Eutectic Australia Ptv. Ltd. Sydney, (2007).
68. Hattori S., Kishimoto M., “Prediction of cavitation erosion on stainless steel components in centrifugal pumps”, Wear, 265, 1870-1874, (2008).
69. Head W.J., Harr M.E., “The development of a model to predict the erosion of materials by natural contaminants”, Wear, 15, 1-46, (1970).
70. Heathcock C.J., Ball A., Protheroe B.E., “Cavitation erosion of cobalt-based stellite alloys, cemented carbides and surface-treated low alloy steels”, Wear, 74, 11-26, (1981).
71. Heathcock C.J., Protheroe B.E., “Cavitation erosion of stainless steels”, Wear, 81, 311-327, (1982).
72. Hertzman S., “The influence of nitrogen on microstructure and properties of highly alloyed stainless steel welds”, ISIJ International, 41, 580-589, (2001).
73. Hertzman S., Jarl M., “Thermodynamic analysis of the Fe-Cr-N system”, Metall. Trans., 18A, 1745-1752, (1987).
74. Hodgson P.D., Microstructure modelling for property prediction and control, J. Mat. Proc. Tech. 60 (1996) 27-33.
75. Hutchings I.M., “A model for the erosion of metals by spherical particles at normal incidence”, Wear, 70, 269-281, (1981).
76. Hutchings I.M., “Ductile-brittle transitions and wear maps for the erosion and abrasion of brittle materials”, J. Phys. D: Appl. Phys. 25, 212-221, (1992).
77. Hutchings I.M., “Some comments on the theoretical treatment of erosive particle impact”, Proc. of the Annual Industrial Pollution Conference, 1-36, (1979).
78. Hutchings I.M., “Tribology: Friction and wear of engineering materials”, 1st published in Great Britain, 171-197, (1992).
79. Hutchings I.M., Levy A.V., “Thermal effects in the erosion of ductile metals”, Wear, 131, 105-121, (1989).

80. Hutchings I.M., Winter R.E., “Particle erosion of ductile metals: A mechanism of material removal”, Wear, 27, 121-128, (1974).
81. Inoue H., “Formation mechanism of vermicular and lacy ferrite in austenitic stainless steel weld metals”, Sci. Tech. Weld Join., 5, 385-396, (2000).
82. Jiang Z., Guan Z., Lian J., “Effects of microstructural variables on the deformation behaviour of dual-phase steel”, Materials Science and Engineering: A, 190, 55-64, (1995).
83. Jin H., Zheng F., Li S., Hang C., “The role of sand particles on the rapid destruction of the cavitation zone of hydraulic turbines”, Wear, 112, 199-205, (1986).
84. Karimi A., “Cavitation erosion of a duplex stainless steel”, Materials Science and Engineering, 86, 191-203, (1987).
85. Karimi A., “Ripple formation in solid-liquid erosion”, Wear, 156, 33-47, (1992).
86. Karimi A., Avellan F., “Comparison of erosion mechanisms in different types of cavitation”, Wear, 113, 305-322, (1986).
87. Karimi A., Martin J.L., “Cavitation erosion of materials”, Int. Met. Rev., 31, 1-26, (1984).
88. Katada Y., “Current research activities on high nitrogen steel in Japan”, Material Science Forum, 539-543, 114-118, (2007).
89. Khaple S., Baligidad R.G., Sankar M., Satya Prasad V.V., “Structure and properties of Fe(3-7wt.%) Al-0.5wt.%C alloys”, Materials Science and Engineering: A, 527, 7452-7456, (2010).
90. Kim K.N., Kim H.W., Shin G.S., Park M.C., Kim J.K., Kim S.J., “Effects of Strain-Induced Martensitic Transformation on the Solid Particle Erosion Behavior of Fe-Cr-C-Ni/Mn Austenitic Alloys”, Tribo. lett., 48, 417-424, (2012).
91. Kishor B., Chaudhari G.P., Nath S.K., “Cavitation erosion of thermomechanically processed 13/4 martensitic stainless steel”, Wear, 319, 150-159, (2014).
92. Klueh R.L., Maziasz P.J., Lee E.H., “Manganese as an austenite stabilizer in Fe-Cr-Mn-C steels”, Material Science Engineering, 102, 115-124,(1988).
93. Kokawa H., Shimada M., Sato Y.S., “Grain boundary structure and precipitation in sensitized austenitic stainless steel”, JOM, 57, 34-37, (2002).
94. Krella A., “The influence of TiN coatings properties on cavitation erosion resistance”, Surf. Coat. Technol., 204, 263-270, (2009).

95. Krella A., Czyzniewski A., “Cavitation erosion resistance of Cr–N coating deposited on stainless steel”, Wear, 260, 1324-1332, (2006).

96. Kumar M., “Effect of Welding parameters on the structures, properties and silt erosion of 13/4 martensitic stainless steel”, Ph.D. Thesis, University of Roorkee, (1996).

97. Kwok C.T., Man H.C., Cheng F.T., “Cavitation erosion and damage mechanisms of alloys with duplex structures”, Materials Science and Engineering: A, 242, 108-120, (1998).

98. Lang Y.P., Qu H.P., Chen H.T., Weng Y.P., “Research progress and development tendency of nitrogen alloyed austenitic stainless steels”, J. of iron and steel research, international, 22(2), 91-98, (2015).

99. Laxminarayanan A.K., Shamungan K., Balasubramanium V., “Effect of welding process on tensile and impact properties, hardness and microstructure of AISI 409Mo joint by duplex stainless steel filler metal”, J. of Iron and Steel Research Inter., 16, 66-72,(2009).

100. Levin B.F., Dupont J.N., Marder A.R., “Solid particle erosion resistance of ductile wrought superalloys and their weld overlay coatings”, J. of Materials Science, 3, 2153-2163, (1998).

101. Levin B.F., Vecchio K.S., DuPont J.N., Marder A.R., “Modeling solid-particle erosion of ductile alloys”, Metall. Mat.Trans. A, 30A, 1763-1774, (1999).

102. Levy A.V., “The solid particle erosion behaviour of steel as a function of microstructure”, Wear, 68, 269-287, (1981).

103. Li S., “Cavitation enhancement of silt erosion-An envisaged micromodel”, Wear, 260, 1145-1150, (2006).

104. Lindsley B.A., Marder A.R., “The effect of velocity on the solid particle erosion rate of alloys”, Wear, 225-229, 510-516, (1999).

105. Lippold J.C., Kteki D.J., “Welding metallurgy and weldability of stainless steel”, Newjercy: John Wiley and sons, (2005).

106. Liu W., Zheng Y.G., Liu C.S., Yaoz M., Ke W., “Cavitation erosion behaviour of Cr-Mn-N stainless steels in comparison with 0Cr13Ni5Mo stainless steel”, Wear, 254, 713-722, (2003).

107. Liu W.H., Shieu F.S., Tien Hsiao W.T., “Enhancement of wear and corrosion resistance of iron-based hard coatings deposited by high-velocity oxygen fuel (HVOF) thermal spraying”, Surface & Coatings Technology, 249, 24-41, (2014).
108. Lopez D., Falleiros N.A. Tschiptschin A.P., “Corrosion-erosion behaviour of austenitic and martensitic high nitrogen stainless steels”, Wear, 263, 347-354, (2007).
109. Malakondaiah G., Srinivas M., Rao P.R., “Ultrahigh-strength low-alloy steels with enhanced fracture toughness”, Progress in Material Science, 42, 209-242, (1997).
110. Mann B.S., “Boronizing of cast martensitic chromium nickel stainless steel and its abrasion and cavitation-erosion behaviour”, Wear, 208 125-131, (1997).
111. Mann B.S., “Erosion visualization and characteristics of a two dimensional diffusion treated martensitic stainless steel hydrofoil”, Wear, 217, 56-61, (1998).
112. Mann B.S., “High-Energy particle impact wear resistance of hard coatings and their application in hydroturbines”, Wear, 237, 140-146, (2000).
113. Mann B.S., Reddy D.M., Ramadass N., Somasundaram R., “Ceramics and coatings to prevent wear of hydro turbine components”, Proc. All India Seminar on Metallurgical Problems in Power project; The Institution of Engineers (India), UP State Centre, Lucknow, 152-158, (1987).
114. Marshall D.B., Lawn B.R. Evans A.G., “Elastic/Plastic Indentation Damage in Ceramics: The Lateral Crack System”, J. of the Amer. Cera. Soc., 65, 561-566, (1982).
115. Matthews S.,“Development of high carbide dissolution/low carbon loss Cr_3C_2-NiCr coatings by shrouded plasma spraying”, Surface and Coatings Technology, 258, 886-900, (2014a).
116. Matthews, S., “Shrouded plasma spray of Ni-20Cr coatings utilizing internal shroud film cooling”, Surface and Coatings Technology, 249, 56-74, (2014b).
117. Mazumdar D., Evans J.W., “A model for stimating exposed plume eye area in steel refining ladles covered with thin slag”, Metallurgical and Materials Transactions B, 35B, 400-404, (2004).
118. Mazumdar D., Gutharie I.L., “Modelling energy dissipation in slag covered steel bath in steelmaking ladle”, Metallurgical and Materials Transactions B, 41B, 976-989, (2010).
119. McCaul C., “CA6NM for sulfide service”, Materials News Letter 6, 1-5, (2007).

120. Meng H.C., Ludema K.C., "Wear models and prediction equations: their form and content", Wear, 181-183, 443-457, (1995).

121. Meng H.C., Ludema K.C., "Wear models and prediction equations: their form and content", Wear, 181-183, 443-457, (1995).

122. Morrison C.T., Scattergood R.O., Routbort J.L., "Erosion of 304 stainless steel", Wear, 111, 1-13, (1986).

123. Mudali U.K., "Nitrogen-A boon to metals industry", Materials Manufacturing Processes 19, 1-5, (2004).

124. Mullner P., Solenthaler C., Uggowitzer P.J., Spiedel M.O., "Brittle fracture in austenitic steel", Acta. Metall. 42, 2211-2217, (1994).

125. Muralikrishna A., Bagui S., Mazumdar D., "Modelling and measurement of intermixing time in a water of a four strand steelmaking tundish system", Trans. Ind. Inst. of metals, 66, 281-295, (2013).

126. Naidu B.S.K., "Silting problems in hydro power plants", Proc. of the Second International Conference on Silting Problems in Hydro Power Plants, Bangkok, 12-21, (2001a).

127. Naidu B.S.K., "Uprating and refurbishment of silt affected hydro power plants, Hydro power an Indian perspective", CBS Publishers and distributors, 289-311, (2001b).

128. Naim M., Bahadur S., "Effect of microstructure and mechanical properties on the erosion of 18 Ni (250) maraging steel", Wear, 112, 217-234, (1986).

129. Naim M., Bahadur S., "Work hardening in erosion due to single particle impacts", Proc. Int. Conf on Wear of Materials, Ed. Ludena, K.C., New York, 340-345, (1985).

130. Naveena V.D., Vijayanand V.D., Ganesan V., Laha K., Mathew M.D., "Application of impression creep technique for development of creep resistant austenitic stainless steel", Procedia Engineering, 55, 585-590, (2013).

131. Ness E., Zibbell R., "Abrasion and erosion of hard materials related to wear in the abrasive water jet", Wear, 196, 120-125, (1996).

132. Neville A., Hu X., "Mechanical and electrochemical interactions during liquid– solid impingement on high-alloy stainless steels", Wear, 251, 1284-1294, (2001).

133. Ninham A., "The effect of mechanical properties on erosion", Wear, 121, 307-324, (1988).

134. O'Flynn D.J., Bingley M.S., Bradley M.S.A., Burnett A. J., "A model to predict the solid particle erosion rate of metals and its assessment using heat-treated steels", Wear, 248, 162-177, (2001).
135. Ogawa M., Hiraoka K., Katada Y., Sagara M., Tsukamoto S., "Chromium nitride precipitation behaviour in weld heat affected zone of high nitrogen steel", ISIJ International, 42,1391-1398, (2002).
136. Ogawa T., Suzuki K., Zaizen T., "The weldability of nitrogen-containing austenitic stainless steel:part II - porosity, cracking and creep properties", Welding Journal, 64, 213s-23s, (1984).
137. Okada T., Iwai Y., Yamamoto A., "A study of cavitation erosion of cast iron", Wear, 84, 297-312, (1983).
138. Okagawa R.D., Dixon R.D., Olson D.L., "The influence of nitrogen from welding on stainless steel weld metal microstructures", Welding Journal, 62, 204s-209s, (1983).
139. Oliver W.C., Pharr G.M., "An improved technique for determining hardness and elastic modulus using load and displacement sensing indentation experiments", J. Mater. Res., 7, 1564-1583, (1992).
140. Padilha A.F., Rios P.R., "Decomposition of austenite in austenitic stainless steels", ISIJ International, 42, 325-337, (2002).
141. Panthee A., Thapa B., Neopane H.P., "Quality control in welding repair of Pelton runner", Renewable Energy, 79, 96-102, (2015).
142. Panwar S., Kumar S., Goel D.B., "Effect of heat treatment on erosive wear of 13/4 martensitic stainless steel", Sixteenth National Convention of Mechanical Engineers and All India Seminar on Future Trends in Mechanical Engineering Research and Development, Department of Mech. and Ind. Eng., University of Roorkee, Roorkee , Sept. 29-30, (2000).
143. Peckner, D., Bernstein I.M., "Handbook of stainless steels", Mc-Graw-Hill Book Company, USA, (1977).
144. Philipp A., Lauterborn W., "Cavitation erosion by single laser-produced bubbles", J. Fluid Mechanics, 361, 75-116, (1998).
145. Piatti G., Vedani M., "Relation between tensile properties and microstructure in type 316 stainless steel SA weld metal", J. of Materials Science, 25, 4285-4297, (1990).

146. Pickering F.B., "Physical Metallurgy and Design of Steels", 1st Edition, Applied Sci. Pub., London, 226-241, (1978).
147. Preece C.R., Brunton J.H., "A comparison of liquid impact erosion and cavitation erosion", Wear, 60, 269-284, (1980).
148. Pugsley V.A., Allen C., "Microstructure/property relationships in the cavitation erosion of tungsten carbide-cobalt", Wear, 233-235, 93-103, (1999).
149. Qiu N., Wang L., Wu S., Likhachev D.S., "Research on cavitation erosion and wear resistance performance of coatings", Engineering Failure Analysis, 55, 208-223, (2015).
150. Raju K., Harsha A.P., Ojha S.N., "Evolution of microstructure and its effect on wear and mechanical properties of spray cast Ai-12Si alloys", Materials Science and Engineering A, 528, 7723-7728, (2011).
151. Raju K., Ojha S.N., "Effect of spray forming on the microstructure and wear properties of Al-Si alloys", Procedia Materials Science, 5, 345-354, (2014).
152. Rao P.V., "Evaluation of epoxy resins in flow cavitation erosion", Wear, 122, 77-96, (1988).
153. Rao P.V., Buckley D.H., "Angular particle impingement studies of thermoplastic materials at normal incidence", ASLE Transactions, 29, 283-298, (1986).
154. Richman R.H., McNaughton W.P., "Correlation cavitation erosion behaviour with mechanical properties of metal", Wear, 140, 63-82, (1990).
155. Ritter, A.M., "Sigma-phase formation in Nitronic-50 and Nitronic-50W stainless steels". J. Materials Science, 23, 3348-3356, (1988).
156. Roy S., Nataraj B.R., Suwas S., Kumar S., Chattopadhyay K., "Accumulative roll bonding of aluminum alloys 2219/5086 laminates: Microstructural evolution and tensile properties", Materials & Design, 36, 529-539, (2012).
157. Rudrakshi G.B., Srivastava V.C., Ojha S.N., "Microstructural development in spray formed Al-3.5Cu-10Si-20Pb alloy and its comparative wear behaviour in different environmental conditions", Materials Science and Engineering: A, 457, 100-108, (2007).
158. S.C. Li, "Cavitation of Hydraulic Machinery", Imperial College Press, (2000).

159. Sakhujja V.S., Paul T.C., Dhillon G.S., “Combating sediment problems in hydropower plants”, Proc. All India Seminar on Metallurgical Problems in Power project; The Institution of Engineers (India), UP State Centre, Lucknow, 94-103, (1987).
160. Sankaranarayanan S., PranavNayak U,Sabat R.K., Suws S., Almajid A., Gupta M., “Nano-ZnO particle addition to monolithic magnesium for enhanced tensile and compressive response”, J. of Alloys and Compounds, 615, 211-219, (2014).
161. Santa J.F., Blanco J.A., Giraldo J.E., Toro A., “Cavitation erosion of martensitic and austenitic stainless steel welded coatings”, Wear, 271, 1445-1453, (2011).
162. Sargent G.A., Saigal D., “Erosion of low-carbon steel by coal particles”, ASLE Transactions, 29, 256-266, (1986).
163. Satya Prasad V.V., Rao A.S., Prakash U., Baligidad R.G., “Electroslag cladding of low alloy steel with stainless steel”, Science & Technology of welding and Joining, 72, 102-107, (2007).
164. Schino A. D., Kenny J.M., Mecozzi M.G., Barteri M., “Development of high nitrogen, low nickel, 18%Cr austenitic stainless steels”, J. of Material Science, 35, 4803-4808, (2002).
165. Schino A.D., Salvatori I., Kenny J.M., “Effect of grain refinement on strength and corrosion resistance of AISI 304 stainless steel”, in: Proceedings of the 1st Inter. Conference on Austenitic Stainless Steel, Tsukuba, Japan, 327, (2002).
166. Schramm R.E., Reed R.P., “Stacking fault energies of seven commercial austenitic stainless steels”, Metall. Mat. Trans., A, 6A, 1345-1351, (1975).
167. Selokar A., Prakash U., Goel D.B., Chaurasia A., “Erosion Behaviour of Fe-Alloys for Underwater Components of Hydroelectric Power Plant”, Trans. Ind. Inst. Met., 6,425, (2013).
168. Semenov S.Y., Cetegen B.M., “Experiments and modeling of the deposition of nano-structured alumina-titania coatings by detonation waves”, Materials Science and Engineering A, 335, 67-81, (2002).
169. Shah S.M., Bahadur S., Verhoeven J.D., “Erosion behavior of high silicon bainitic structures: II: High silicon steels”, Wear, 113, 279-290, (1986b).
170. Shah S.M., Verhoeven J.D., Bahadur S., “Erosion behavior of high silicon bainitic structures: I: Austempered ductile cast iron”, Wear, 113, 267-278, (1986a).

171. Shankar V., Gill T.P.S., Mannan S.L., Sundaresan S., “Solidification cracking in austenitic stainless steel welds”, Sadhana, 28, 359–382, (2003b).

172. Shankar, V., Gill, T.P.S., Mannan, S.L., Sundaresan S., “Effect of nitrogen addition on microstructure and fusion zone cracking in type 316L stainless steel weld metals”, Material Science and Engineering A, 343, 170-181, (2003a).

173. Sharma A., Kumar A., Tyagi R., “Erosive wear analysis of medium carbon dual phase steel under dry ambient condition”,Wear, 334-335, 91-98, (2015).

174. Sheldon G.L., Finnie I., “The mechanism of material removal in the erosive cutting of brittle materials”, Trans. ASME 88, B, 393-400, (1966).

175. Sheldon G.L., Kanhere A., “An investigation of impingement erosion using single particles”, Wear, 21, 195-209, (1972).

176. Shuji H., Keisuke T., Kengo K., Hiroshi T., “Cavitation erosion of silver plated coatings considering thermodynamic effect”, Wear, 300, 136-142, (2013).

177. Shuji H., Takamoto I., “Cavitation erosion resistance of plastics”, Wear, 271, 1103-1108, (2011).

178. Sidky B.S., Hocking M.G., “Reviewing of organic coatings and coating processes for reducing wear and corrosion”, British Corrosion J., 34, 171-183, (1999).

179. Simoneau R., “The optimum protection of hydraulic turbines against cavitation erosion”, 12th IAHR Symposium, Stirling, UK, 297-301, (1984).

180. Soussan A., Degallaix S., “Work-hardening behaviour of nitrogen-alloyed austenitic stainless steels”, Material Science Engineering, A, 142, 169-176, (1991).

181. Speidel M.O., “High nitrogen steels”, Proc. of the 2nd International Conf. on High-Nitrogen Steels, HNS 90, Aachen, Germany, 128-131, (1990).

182. Srinivasan V.S., Nagesha A., Valsan M., Rao K.B.S., Mannan S.L., Sastry D.H., “Effect of hold-time on low cycle fatigue behaviour of nitrogen bearing 316L stainless steel”, International J. Pressure Vessels and Piping 76, 863-870 (1999).

183. Stachowiak G.W., Batchelor A.W., “Abrasive, erosive and cavitation wear”, Engg. Tribology (3rd Edition), 501-551, (2006).

184. Stack M.M., Abdulrahman G.H., “Mapping erosion–corrosion of carbon steel in oil exploration conditions: some new approaches to characterizing mechanisms and synergies”, Tribology International, 43, 1268-1277, (2010).

185. Stack M.M., Pungwiwat N., “Slurry erosion of metallics, polymers, and ceramics: particle size effects”, Material Science Technology, 15, 337-344, (1999).

186. Sugiyama K., Harada K., Hattori S., “Influence of impact angle of solid particles on erosion by slurry jet”, Wear, 265,713-720, (1988).

187. Sumita M., Hanawa T., Teoh S.H., “Development of nitrogen-containing nickel-free austenitic stainless steels for metallic biomaterials”, Material Science Engineering:C, 24, 753-760, (2004).

188. Sundararajan G., “An analysis of the erosion-oxidation interaction mechanisms”, Wear, 145, 251-282, (1991).

189. Sundararajan G., “An analysis of the localization of deformation and weight loss during single-particle normal impact”, Wear, 84, 217-235, (1983a).

190. Sundararajan G., “The solid particle erosion of metallic materials: The rationalization of the influence of material variables”, Wear, 186-187, 129-144, (1995).

191. Sundararajan G., Shewmon P.G., “A new model for the erosion of metals at normal incidence”, Wear, 84, 237-258, (1983b).

192. Sundararajan G., Shewmon P.G., “The oblique impact of a hard ball against ductile, semi-infinite target materials-experiment and analysis”, International J. Impact Engg., 6, 3-22, (1987).

193. Suresh K.S. Geetha M., Richard C., Landoulsi J., Ramasawmi H., Suwas S., Asokamani R., “Effect of equal channel angular extrusion on wear and corrosion behaviour of the orthopedic Ti–13Nb–13Zr alloy in simulated body fluid”, Materials Science and Engineering:C, 32, 763-771, (2012).

194. Tabrett C.P., Sare I.R., Ghomashchi M.R., “Microstructure-property relationships in high chromium white iron alloys”, Int. Mater. Rev, 41, 59-82, (1996).

195. Telling R.H., Field J.E., “The erosion of diamond, sapphire and zinc sulphide by quartz particles”, Wear, 233-235, 666-673, (1999).

196. Thapa B.S., Dahlhaug O.G. , Thapa B., “Sediment erosion in hydro turbines and its effect on the flow around guide vanes of Francis turbine”, Renewable and Sustainable Energy Reviews, 49, 1100-1113, (2015).

197. Thiruvengadam A., “A unified theory of cavitation damage”, Trans. ASME J. Basic Eng. 85, 365-376, (1963).

198. Tillman C.J., Edmonds D.V., “Alloy carbide precipitation and aging during high temprrature isothermal decomposition of Fe-Mo-C alloy steel”, Metal Technology, 456-461, (1974).

199. Tilly G.P., “A two stage mechanism of ductile erosion”, Wear, 23, 87-96, (1973).

200. Trethewey K.R., Haley T.J., Clark C.C., “Effect of ultrasonically induced cavitation on corrosion behaviour of a copper-manganese-aluminum alloy”, British Corrosion J., 23, 55-60, (1988).

201. Uggovitzor P., Magdowski R., Speidel M.O., “Nickel fee high nitrogen austenitic steels”, ISIJ International, 36, 901-908, (1996).

202. Vanderschaeve, F., Taillard, R., Foct, J., “Discontinuous precipitation of Cr_2N in a high nitrogen, chromium-manganese austenitic stainless steel”, J. of Material Science, 30, 6035-6046, (1995).

203. Verma M.C., “Silt friendly design of turbine and other under water components”, Proc. of the 1st International Conference on Silting Problems in Hydro Power Plants, CBIP New Delhi IV, 1-19, (1999).

204. Vijayanand V.D. , Laha K., Parameswaran P., Ganesan V., Mathew M.D., “Microstructural evolution during creep of 316LN stainless steel multi-pass weld joints”, Materials Science and Engineering: A, 607, 138-144, (2014).

205. Wang B.Q., Geng G.Q., Levy A.V., “Effect of microstructure on the erosion-corrosion of steel”, Wear, 151, 351-364, (1991).

206. Wang Y., “Friction and wear performances of detonation-gun and plasma-sprayed ceramic and cermet hard coatings under dry friction”, Wear, 161, 69-78, (1993).

207. Watanabe S., Furukawa A., “Theoretical investigations on thermodynamic effect of cavitation”, Turbomachinery, 36(3), 26-33, (2006).

208. Wheeler D.W., Wood R.J.K., “Solid particle erosion of diamond coatings under non-normal impact angles”, Wear, 250, 795-801, (2001).

209. Winter R.E. Hutchings I.M., “Solid particle erosion studies using single angular particles”, Wear, 29, 181-194, (1974).

210. Winter R.E. Hutchings I.M., “The role of adiabatic shear in solid particle erosion”, Wear, 34, 141-148, (1975).

211. Woo, I. and Kikuchi, Y., “Weldability of high nitrogen stainless steel”, ISIJ International, 42, 1334-1343, (2002).

212. Wood R.J.K. “The sand erosion performance of coatings”, Materials & Design, 20, 179-191, (1999).
213. Wood R.J.K., Hutton S.P., “The synergistic effect of erosion and corrosion—trends in published results”, Wear, 140, 387-394, (1990).
214. Wu Y., Lin P., Xie G., Hu J., Cao M., “Formation of amorphous and nanocrystalline phases in high velocity oxy-fuel thermally sprayed a Fe–Cr–Si–B–Mn alloy”, Mater. Sci. Eng. A, 430, 34-39, (2006).
215. Xi Z.T., Zhou Q.D. “Influence of retained austenite on the wear resistance of high chromium cast iron under various impact loads”, Wear, 162-164, 83-88, (1993).
216. Xu, Q., Gabbitas, B., Matthews, S., “Titanium compacts with controllable porosity by slip casting of binary powder mixtures”, Powder Technology, 266, 396-406, (2014).
217. Zhang X.F., Fang L., “The effect of stacking fault energy on the cavitation erosion resistance of alpha- phase aluminum bronzes”, Wear, 253, 1105-1110, (2002).
218. Zhao K., Gu C.Q., Shen F.S., Lou B.Z., “Study on mechanism of combined action of abrasion and cavitation erosion on some engineering steels”, Wear, 162-164, 811-819, (1993).
219. Zheng Y., Yao Z., Wei X., Ke W., “The synergistic effect between erosion and corrosion in acidic slurry medium”, Wear, 186-187, 555-561, (1995).
220. Zheng Z.B., Zheng Y.G., Sun W.H., Wang J.Q., “Effect of heat treatment on the structure, cavitation erosion and erosion–corrosion behavior of Fe-based amorphous coatings” Tribology International, 90, 393-403, (2015).
221. Zhou R., Lu D.H., Jiang Y.H., Li Q.N., “Mechanical properties and erosion wear resistance of polyurethane matrix composites”, Wear, 259, 676-683, (2005).
222. Zhou Z., Wang L., He D.Y., Wang F.C., Liu Y.B., “Microstructure and wear resistance of Fe-based amorphous metallic coatings prepared by HVOF thermal spraying”, J. Therm Spray Technol., 19, 1287-1293, (2010).
223. Zifu L., Tsakiropoulos P., “Study of the effects of Ge addition on the microstructure of Nb-18Si in situ composites”, Intermetallics, 18, 1072-1078, (2010).
224. Zifu L., Tsakiropoulos P., “The microstructures of Nb-18Si-5Ge-5Al and Nb-24Ti-18Si-5Ge-5Al in situ composites”, J. of Alloys and Compounds, 550, 553-560, (2013).